

POLITECNICO DI TORINO
Department of Mechanical and Aerospace Engineering



MASTER DEGREE THESIS

Advanced Finite Element Method for the Vibro-Acoustic response of plate-cavity systems

Author:

Raffaele PANZELLA
s251537

Supervisors:

Prof. Erasmo CARRERA
Prof.ssa Maria CINEFRA
Prof. Enrico ZAPPINO

April 2020

POLITECNICO DI TORINO

Abstract

Department of Mechanical and Aerospace Engineering

Master Degree Thesis

Advanced Finite Element Method for the Vibro-Acoustic response of plate-cavity systemsby Raffaele PANZELLA
s251537

Aerospace vehicles are subject to broadband, sometimes severe, vibroacoustic and structure-borne excitations of various origin, which can danger the availability of the payload on board and the electronic equipment, and consequently the unsuccessful of the entire mission. It is therefore important for the modern industry the development of analytical and numerical tools that can accurately predict the vibroacoustic response within structures of various geometries and subject to a combination of vibroacoustic excitations in order to mitigate unwanted phenomena able to compromise the whole mission. Nowadays, A lot of research has been conducted on the correctly modelling of wave propagation characteristics within representing the reactivity of the structure in noise field. As sake of simplicity, we will deal a simple test, *coupled plate-cavity*, where numerical modelling techniques risen are typically based on deterministic approaches. The plate structure is often modelled by the finite element method and the Kirchhoff/Mindlin are mostly assumed to describe the through-the-thickness variation of the resultant displacement field. These simple assumptions of modelling the plate clearly reduce the required computational effort, but can also introduce *huge errors* in the prediction of the plate dynamic response and consequently affect the surrounding acoustic pressure field, where noise is risen. In this work, a **powerful notation** has been used: *Carrera's Unified Formulation*, whose permits to obtain a wide class of refined plate theories (LW) with a unique formulation, providing an optimal element to completely describe the complex risen effects due to plate layouts and for higher frequency ranges.

This work was conducted through the use of *Actran Software*, in order to conduct research in Vibro-Acoustic field. *Structural Vibroacoustic* interaction is modelled and analysed using the finite element method coupling (interfaces), to solve the structure-acoustic coupled interaction for the noise radiation problem in a plate-cavity system. The important keywords are the complete understanding of the generation of noise, its radiation in operating structure and the mitigation of the negative effect in order to improve the functionality of the system. Structures are generally characterized by the use of composite materials of various configurations/complexity in term of thicknesses, as well as geometries. Acoustic load and high frequency vibration can strictly and disadvantageously affect structures that represents a significant issue in spacecraft structures. Because of the extensive geometric complexity of structures, the usage of Finite Element (FE) modelling is frequently inevitable within the aerospace industry. The use of such models is limited mainly because of the immensity computation time required for calculations.

Acknowledgements

I would like to express my sincere gratitude to my thesis supervisor, *Maria Cinefra*. Her valuable advices and patient guidance were major contributors to the achievement of my objectives through this dissertation. I appreciate her availability, although the distance, insightful assistance and expertise shared.

I would like to express my deep gratitude to Professor, *Erasmus Carrera* and *Enrico Zappino*, and their research group, *MUL*². Their advices were fundamental for the successful development of this project.

I address my acknowledgements to all the *commission members* of the thesis for their participation as well as for the interest and time dispensed to this work.

I would also like to extend my thanks to *MSC software* for their help in offering me the resource in running programs. I wish to thank *my family* for supporting me in these years, throughout all the bad and the good times, encouragement through my study.

Last but not least, I would like to express my thankfulness to all of my friends, who stood by me throughout these years.

Contents

Abstract	iii
Contents	vii
List of Figures	xi
Physical Constants	xv
1 Introduction	1
2 Sound-Structure Interaction Fundamentals	3
2.1 Structural Waves Vibrating against an Acoustic Fluid	3
2.2 Structural Vibrations Induced by Acoustic Pressure Waves	6
3 Acoustics	9
3.1 Introduction of Acoustics	9
3.2 Wave Equation in Fluid	10
3.3 Wave Equation	10
3.4 Energy and Intensity	11
3.4.1 Losses	12
3.5 Impedance	13
4 Actran	15
4.1 Actran Software	15
4.2 Direct Frequency Response	18
4.3 Examples of Application	18
4.3.1 Virtual Kundt's Tube	18
Sound propagation in porous materials	21
4.3.2 Radiation of a Horn Speaker	23
4.3.3 Acoustic Transmission through a Muffler	25
4.3.4 Diffuse Sound Field on Antenna for <i>Spacecraft</i> Application	28
5 Vibroacoustic Modelling Techniques	35
5.1 Introduction	35
5.2 Governing equations	36
5.3 The Variational Formulation	38
5.4 The Numerical Approximation	39
5.5 The Finite Element Method	41
Criterion of Building a Mesh	42
Nodal approximation of the variable	44
Assembling and Imposition of constraints	45
5.6 Generalized Hooke's law	46
Monoclinic materials	47
Orthotropic materials	48

	Isotropic materials	49
5.7	Unified Finite Element Model	50
	Condensed notation for Mechanical Problems	51
5.8	Structural Hypothesis Through-the-thickness for primary variables	53
5.8.1	Equivalent Solid Layer (<i>ESL</i>) Approach	54
5.8.2	Layer Wise (<i>LW</i>) Approach	55
5.8.3	Applying the Finite Element Approximation	58
5.9	Derivation of Fundamental Matrices	59
5.9.1	Structural Stiffness Matrix	59
5.9.2	Structural External Loads	59
5.9.3	Fluid-Structure Coupling Matrix	60
5.9.4	Structural Mass Matrix	61
5.9.5	Fluid Stiffness and Mass Matrices	61
5.10	Final Form of the Coupled Equations	61
5.11	Acoustic Coupling	63
5.12	Drawback: Limitations due to the patch size	64
6	Weak Coupling Interaction	65
6.1	Classical Plate Theory (<i>CLPT</i>)	66
	Out-of-plane Displacement of Plates	66
6.2	Boundary Condition	68
	Boundary Condition: Simply Supported	68
	Boundary Condition: Clamped	68
6.3	Cubic Cavity	69
6.3.1	Structural Validation	69
	Vibration Analysis	71
	Orthotropic Material plate	73
6.3.2	Coupled Fluid-Structure Cavity	76
6.3.3	Weak Coupling Interaction	77
	Isotropic Plate Coupled increasing the thickness plate	79
	Isotropic Plate Coupled changing the boundary condition	82
	Orthotropic Material plate	85
	Appendix - Loss of Reality: Shifting Mode	88
6.3.4	Resume: Weak coupling Effect	89
7	Strong Coupling Interaction	91
7.0.1	The Locking Phenomenon in finite element method	95
7.0.2	Isotropic Plate strongly Coupled increasing the thickness plate	96
7.0.3	Orthotropic Plate strongly Coupled with <i>Simply Supported</i> and <i>Clamped</i> edges BC with different lamination $[0^\circ/90^\circ/0^\circ]$ and $[90^\circ/0^\circ/90^\circ]$	97
7.0.4	Resume: Strong coupling Effect	100
8	Numerical Model Validation	101
8.1	Vibro-Acoustic Response of a Rectangular Cavity (Water Filled) backed by a Isotropic panel	101
8.1.1	Water Coupled Cavity	102
8.2	Sandwich Composite Plate	107
8.3	Vibro-Acoustic Response of a Cubic Cavity backed by a Multi-layered panel	110
8.4	Mesh Variation Effect	112

Air Cavity	114
Water Cavity	115
8.5 Numerical Model Validation	116
9 Conclusion and Further Developments	119
9.0.1 Conclusion	119
9.0.2 Further Developments	121
10 Matlab® Sources Used	123
11 Bibliography	127

List of Figures

2.1	Bending and acoustic wavenumber-frequency plot	4
2.2	AT the Coincidence	4
2.3	AFTER the Coincidence	4
2.4	Effects of stiffening on plate coincidence frequencies	5
2.5	Blocked pressure field acting on a plate	6
2.6	Blocked pressure field acting on a plate	8
3.1	Noise: Small Fluctuation of Pressure	11
4.1	ActranVI Windows	16
4.2	Actran Windows	16
4.3	1st Summary of Actran Analysis	17
4.4	2nd Summary of Actran Analysis	17
4.5	Kundt's Tube	18
4.6	Kundt's Tube Mesh	19
4.7	Sound Pressure Level in Kundt's Tube	19
4.8	Absorption Coefficient in Kundt's tube	20
4.9	Admittance of FOAM	20
4.10	Evolution of Pressure Field inside the Kundt's Tube	22
4.11	Mesh of a Horn Speaker	23
4.12	Acoustic Radiation Field of Horn	24
4.13	Directivity of the Horn: plane XZ / plane YZ	24
4.14	Mesh of a Muffler	25
4.15	Muffler Acoustic Modes	27
4.16	Mesh of the Antenna	28
4.17	Objects within the Reverberant Room with Diffuse Sound Field	28
4.18	Location of six accelerometers	29
4.19	Normal Acceleration [g ² /Hz] in logarithmical scale	30
4.20	Normal Acceleration [g ² /Hz] in linear scale	30
4.21	Reference map for Stress field	31
4.22	Stress as a function of frequency	32
4.23	Element Force as a function of frequency	32
4.24	Stress Field for 20 Hz	33
4.25	Stress field for 220 Hz	33
5.1	Continuum discretized with <i>Finite Element</i> for FEM	35
5.2	Continuum coupled system (<i>fluid and structure</i>) General domain	36
5.3	(a) Entire Acoustic Cavity (b) Finite Elements Mesh 3D	39
5.4	The seven steps of the FEM	41
5.5	Bidimensional mesh.	43
5.6	Connectivity table	43
5.7	Two types of geometrical discretization of the one-dimensional problem	44

5.8	Definition of the <i>PLATE</i> Reference System (x, y, z) and Material one (1, 2, 3)	51
5.9	(ESL) Approach	54
5.10	LW model	55
5.11	Three layered structure with the internal layer in assembling Equivalent Single Layer (ESL) assembly procedures.	56
5.12	Three layered structure with the internal layer in assembling Layer-Ways (LW) assembly procedures.	57
6.1	Undeformed and deformed geometry in thickness direction under Kirchhoff hypothesis	66
6.2	Actran Visualization of Simply Supported edges plate	68
6.3	Actran Visualization of Clamped edges plate	68
6.4	Simply Supported edges (at left); Clamped edges (at right)	69
6.5	Displacement at (0.25m, 0.35m) for <i>Isotropic</i> plate with layer-wise 2 considering <i>Simply Supported edges</i>	70
6.6	Displacement at (0.25m, 0.35m) for <i>Isotropic</i> plate with different layer-wise considering <i>Clamped edges</i>	70
6.7	49 [Hz]	72
6.8	123 [Hz]	72
6.9	197 [Hz]	72
6.10	246 [Hz]	72
6.11	Displacement at (0.25m, 0.35m) for <i>Orthotropic</i> plate LW2 , lamination $[0^\circ/90^\circ/0^\circ]$, considering <i>Simply Supported edges</i>	73
6.12	Displacement at (0.25m, 0.35m) for <i>Orthotropic</i> plate LW2 , lamination $[90^\circ/0^\circ/90^\circ]$, considering <i>Simply Supported edges</i>	74
6.13	Displacement at (0.25m, 0.35m) for <i>Orthotropic</i> plate LW2 , lamination $[0^\circ/90^\circ/0^\circ]$, considering <i>Clamped edges</i>	75
6.14	Displacement at (0.25m, 0.35m) for <i>Orthotropic</i> plate LW2 , lamination $[90^\circ/0^\circ/90^\circ]$, considering <i>Clamped edges</i>	75
6.15	Plate backed <i>Cubic Cavity</i> system.	76
6.16	Coupled FE/FE model: Plate backed by a rigid walled cavity.	77
6.17	Actran Solution (FRF) in point B(0.75m, 0.75m, 0.75m)[left] and C(0.35m, 0.70m, 0.65m) [right] for Isotropic plates	77
6.18	Fluid Node Pressure in point B(0.75m, 0.75m, 0.75m) [left] and C(0.35m, 0.70m, 0.65m) [right] for Isotropic plates	78
6.19	Coupled plate with <i>Thickness</i> = $10 t_{ref}$ using LW3	79
6.20	Coupled plate with <i>Thickness</i> = $20 t_{ref}$ using LW3	80
6.21	Coupled plate with <i>Thickness</i> = $30 t_{ref}$ using LW3	80
6.22	Clamped solution: Acoustic pressure in B (left); and Acoustic pressure in C (right)	82
6.23	(2,2) mode Natural frequency comparison: Simply supported	83
6.24	(2,2) mode Natural frequency comparison: Clamped	83
6.25	Fluid Node Pressure in point B(0.75m, 0.75m, 0.75m); [left] and C(0.35m, 0.70m, 0.65m) [right] for Orthotropic plates, <i>weakly</i> coupled, for the lamination $[0^\circ/90^\circ/0^\circ]$, simply supported edges	85
6.26	Fluid Node Pressure in point B(0.75m, 0.75m, 0.75m); [left] and C(0.35m, 0.70m, 0.65m) [right] for Orthotropic plates, <i>weakly</i> coupled, for the lamination $[90^\circ/0^\circ/90^\circ]$, simply supported edges	85

6.27	Fluid Node Pressure in point B(0.75m, 0.75m, 0.75m); [left] and C(0.35m, 0.70m, 0.65m) [right] for Orthotropic plates, <i>weakly</i> coupled, for the lamination $[0^\circ/90^\circ/0^\circ]$, clamped edges	86
6.28	Fluid Node Pressure in point B(0.75m, 0.75m, 0.75m); [left] and C(0.35m, 0.70m, 0.65m) [right] for Orthotropic plates, <i>weakly</i> coupled, for the lamination $[90^\circ/0^\circ/90^\circ]$, clamped edges	86
6.29	Fluid Node Pressure in point B(0.75m, 0.75m, 0.75m); [left] and C(0.35m, 0.70m, 0.65m) [right] for Orthotropic plates, <i>weakly</i> coupled, for the lamination $[0^\circ/90^\circ/0^\circ]$, simply supported edges	87
6.30	Relative Difference from LW1 and LW2 theories, the resulting solution are highly comparable	87
6.31	LD1 at the left without the central node, while LD2 at the right with the central node	88
6.32	Comparison: FRF Pressure response (top) and Plate Dynamic Response (bottom)	89
6.33	1 st Cavity Mode at 171 [Hz]	90
6.34	2 nd Cavity Mode at 242 [Hz]	90
6.35	3 rd Cavity Mode at 297 [Hz]	90
7.1	Fluid Node Pressure in point B(0.75m, 0.75m, 0.75m) [left] and C(0.35m, 0.70m, 0.65m) [right] for Isotropic plates for Simply supported edges, using LW2 Mul solution.	92
7.2	Fluid Node Pressure in point B(0.75m, 0.75m, 0.75m) [left] and C(0.35m, 0.70m, 0.65m) [right] for Isotropic plates for Simply supported edges, using LW3 Mul solution.	92
7.3	Fluid Node Pressure in point B(0.75m, 0.75m, 0.75m) for Isotropic plates for <i>Clamped edges</i> for LW2 and Actran for Strong Coupling	93
7.4	Fluid Node Pressure in point C(0.35m, 0.70m, 0.65m) for Isotropic plates for <i>Clamped edges</i> for LW2 and Actran for Strong Coupling	94
7.5	Fluid Node Pressure in point B(0.75m, 0.75m, 0.75m) for Isotropic plate, considering considering MUL2 LW1 with element 1 and 2 and Actran	95
7.6	Fluid Node Pressure in point B(0.75m, 0.75m, 0.75m) for Isotropic plate, considering thickness $x10 t_{ref}$ for LW3 MUL2 and Actran for Strong Coupling	96
7.7	Fluid Node Pressure in point B(0.75m, 0.75m, 0.75m) for Isotropic plate, considering thickness $x20 t_{ref}$ for LW3 MUL2 and Actran for Strong Coupling	96
7.8	Fluid Node Pressure in point B(0.75m, 0.75m, 0.75m) for Isotropic plate, considering thickness $x30 t_{ref}$ for LW3 MUL2 and Actran for Strong Coupling	97
7.9	Fluid Node Pressure in point B(0.75m, 0.75m, 0.75m); [left] and C(0.35m, 0.70m, 0.65m) [right] for Orthotropic plates, <i>strongly</i> coupled, for the lamination $[0^\circ/90^\circ/0^\circ]$, simply supported edges	98
7.10	Fluid Node Pressure in point B(0.75m, 0.75m, 0.75m); [left] and C(0.35m, 0.70m, 0.65m) [right] for Orthotropic plates, <i>strongly</i> coupled, for the lamination $[90^\circ/0^\circ/90^\circ]$, simply supported edges	98
7.11	Fluid Node Pressure in point B(0.75m, 0.75m, 0.75m); [left] and C(0.35m, 0.70m, 0.65m) [right] for Orthotropic plates, <i>strongly</i> coupled, for the lamination $[0^\circ/90^\circ/0^\circ]$, clamped edges	99

7.12	Fluid Node Pressure in point B(0.75m, 0.75m, 0.75m); [left] and C(0.35m, 0.70m, 0.65m) [right] for Orthotropic plates, <i>strongly</i> coupled, for the lamination $[90^\circ/0^\circ/90^\circ]$, clamped edges	99
8.1	Plate backed rectangular cavity (water filled) system. Excitation location: $A = (0.0435 [m], 0.28 [m], 0.14075 [m])$; Measurement location(s): $A = (0.0435 [m], 0.28 [m], 0.14075 [m])$, $B = (0.1305 [m], 0.175 [m], 0.07 [m])$	101
8.2	Displacement at $(4.35 [cm], 0.28 [m])$ for <i>Isotropic</i> plate LW2 considering <i>Simply Supported edges</i>	103
8.3	Displacement at $(4.35 [cm], 0.28 [m])$ for <i>Isotropic</i> plate LW2 considering <i>Clamped</i>	103
8.4	Fluid Node Pressure in point B; (left) Actran and Mul2 (LW2) solution, (right) literature	103
8.5	Fluid Node Pressure in point B using Actran and Mul2 (LW3)	104
8.6	Plate (coupled) Displacement in point A; (left) Actran and Mul2 (LW2) solution, (right) literature	104
8.7	Plate (coupled) Displacement in point A; Actran and Mul2 (LW3) solution	105
8.8	Fluid Node Pressure at B for <i>Isotropic</i> plate LW2 considering <i>Clamped</i>	105
8.9	Example of Sandwich plate: Face Sheet and Core	107
8.10	Sandwich Plate (Air coupled); Fluid node pressure in B (left); Fluid node pressure in C (right) with the relative Actran solution	108
8.11	Sandwich Plate (Water coupled); Fluid node pressure in B (left); Fluid node pressure in C (right) with the relative Actran solution	108
8.12	Sandwich Plate: Face Sheet and Core	109
8.13	Multi-layered Plate	110
8.14	Multi-layered (nine-ply) Plate (Air coupled): Fluid node pressure in B with the relative Actran solution	111
8.15	Multi-layered (nine-ply) Plate (Water coupled): Fluid node pressure in B with the relative Actran solution	111
8.16	Patch size limit at the spatial wavelength frequency	112
8.17	Mesh 20x20 elements, Cubic Cavity, Orthotropic Material Excitation Location in $A = (0.25, 0.35m, 1m)$; Measurement Location in $B = (0.35m, 0.7m, 0.65m)$	113
8.18	Fluid Node Pressure at B for <i>Orthotropic</i> plate LW2 considering <i>Simply Supported</i> for Air filled cavity	114
8.19	Fluid Node Pressure at B for <i>Orthotropic</i> plate LW2 considering <i>Simply Supported</i> for Air filled cavity	115
8.20	Test case: MUL2 LW2 vs 20x20 mesh structure in Actran	117
8.21	Test case: MUL2 LW2 vs 80x80 mesh structure in Actran	118

Physical Constants

Speed of Light

$$c_0 = 2.997\,924\,58 \times 10^8 \text{ m s}^{-1}$$

Reference Pressure [in Air]

$$p_{ref} = 0.000\,02 \text{ Pa}$$

Reference Pressure [in Water]

$$p_{ref} = 0.000\,001 \text{ Pa}$$

Reference Intensity [Energy per Surface]

$$I_{ref} = 0.000\,000\,000\,001 \text{ W m}^{-1} \text{ m}^{-2}$$

Density of air (at standard conditions)

$$\rho_0 = 1.225 \text{ [Kg/m}^3\text{]}$$

Speed of Sound in air (at standard conditions)

$$c_0 = 343 \text{ [m/s]}$$

Characteristic impedance of air (at standard conditions)

$$Z_0 = 412 \text{ [s/m}^3\text{]}$$

Shear modulus

$$\mathbf{E} / [2(1+\nu)] = G$$

M = Mass Matrix

K = Stiffness Matrix

E = Young's modulus

ν = Poisson's ratio

f = Frequency [Hz]

SWL = Sound Power Level

SPL = Sound Pressure Level

IL = Intensity Level

dB scale of a quantity q (Reference value: q_{ref})

$$L_q [dB] = 20 \text{Log} \left(\frac{q}{q_{ref}} \right)$$

Partial derivative with respect to x_i

$$(\cdot)_{,i} = \partial(\cdot) / \partial x_i$$

Superscript indicating the reference to an element

$$(\cdot)^e = \text{ref. element}$$

Einstein Notation for sum

$$a_k = \sum_{k=1}^N a_k$$

*To my Family, who believed in me and taught me the
truthfulness and always to strive for the best...*

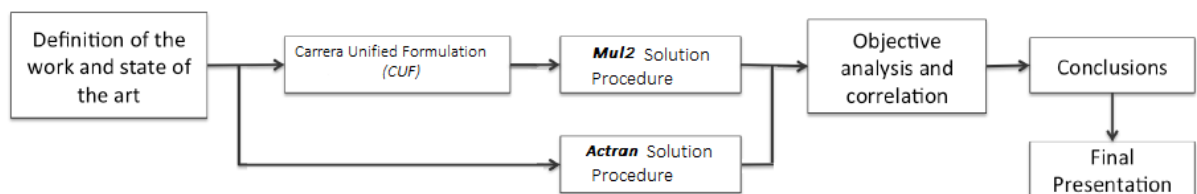
Chapter 1

Introduction

When structure is in contact with a fluid, the the vibro acoustic coupling interaction influences the structural vibration and the fluid pressure, in the same time. The loading on the plate, due to the acoustic pressure distribution on the fluid/structure interface, influences the induced vibration on the plate structure, whilst the acoustic pressure inside the fluid volume is itself affected by the structural behaviour, the **mutual interaction** is presented alongside this work, and that represents the main aim of this dissertation.

We will deal a simple test, coupled plate-cavity, where numerical modelling techniques risen are typically based on deterministic approaches. The plate structure is often modelled by the finite element method and the Kirchhoff/Mindlin are mostly assumed to describe the through-the-thickness variation of the resultant displacement field.

In general, the methodology of the project can be observed in the following figure.



Methodology and procedure of the project

In the first chapter, we deeply explain the fluid structure interaction through the noise transmission of acoustic waves, whose principles are shown in the following chapter.

In chapter 4, the powerful actran software is shown through the determination of noise frequency function. In chapter 5, The Vibroacoustic Modelling Techniques are explained throughout the *Carrera Unified Formulation (CUF)* and the fluid - structure

coupling. In chapter 8, Numerical Tests are introduced, considering different configuration in order to the powerful advanced layer wise theory in MUL^2 for Acoustics Noise Interaction. In the following, the relative correlation of the resulting solution is introduced. Obviously, since MUL^2 is based on a more advanced theory, we can obtain more precise solution using less computational effort in terms of finite elements.

For a detailed outline, Please refer to the index page in vii.

In the following, we are treating the low-frequency range, in which all the system components are small considered to the relative wavelength, and due to the long structural wavelength, shape functions can be selected by low order polynomial, but whenever the excitation frequencies increase, the global response is sensitive to minor structural modification, this behaviour is associated considered shorter structural wavelength, resulting in a more complex system.

Finally, The conclusion and further developments are reported.

The whole organ will bring knowledge of interaction phenomenon

Chapter 2

Sound-Structure Interaction Fundamentals

The aim of this chapter is based on understanding concept of *linear* sound-structure interaction. *The normal velocity in the structure and on the fluid particle boundary along the fluid-structure interaction must be the same.*

This means that when a structure vibrates against a fluid, the component of the vibration normal to the structural surface *must be identical* to the corresponding particle velocity in the neighbouring fluid. This concept must be kept on mind along this chapter. This simple equality allows us to **couple** the equations that define *structural* and *fluid motion* at the fluid-structure interface.

Another concept is important, that the **normal particle velocity** is *identical* onto the structure and fluid boundary, but the *tangential particle velocity* is **not** the same, defining the "*slip condition*" between the material wall and fluid, typical in Fluid dynamic.

This concept is implemented in Actran software through the using f interfaces and coupling surfaces. Remember that, as sake of simplicity, we are assuming the Fluid Linearity, so that fluid properties do not depend on the fluctuating pressure amplitude or phase.

2.1 Structural Waves Vibrating against an Acoustic Fluid

The Structural motion normal to an object's material wall induces an equal motion in a neighbouring fluid, we consider just transversely vibrating. We are going to understand how structures radiate sound in free field.

The Sound radiated by structural waves may be considered in wave-number space, and examine wave types on frequency-wave-number plot diagrams. This shows a frequency dependent behaviour. At *low frequencies*, the *structural* wave-numbers (or speed wave) are **higher** than those in the *acoustic* fluid ones, corresponding to subsonic structural waves. These transversal waves radiate **no sound** at all; due to the particle velocity in the fluid normal to the structure's surface must *match* those of the structure ones. At low frequencies, acoustic waves are faster than structural ones, so their wavelengths are longer. This means that the structure simply can not induce a propagating wave in the fluid itself. Remember that for frequency below the coincidence, no sound is radiated [26].

As matter of facts, Let us assume the following behaviour described in the following figure.

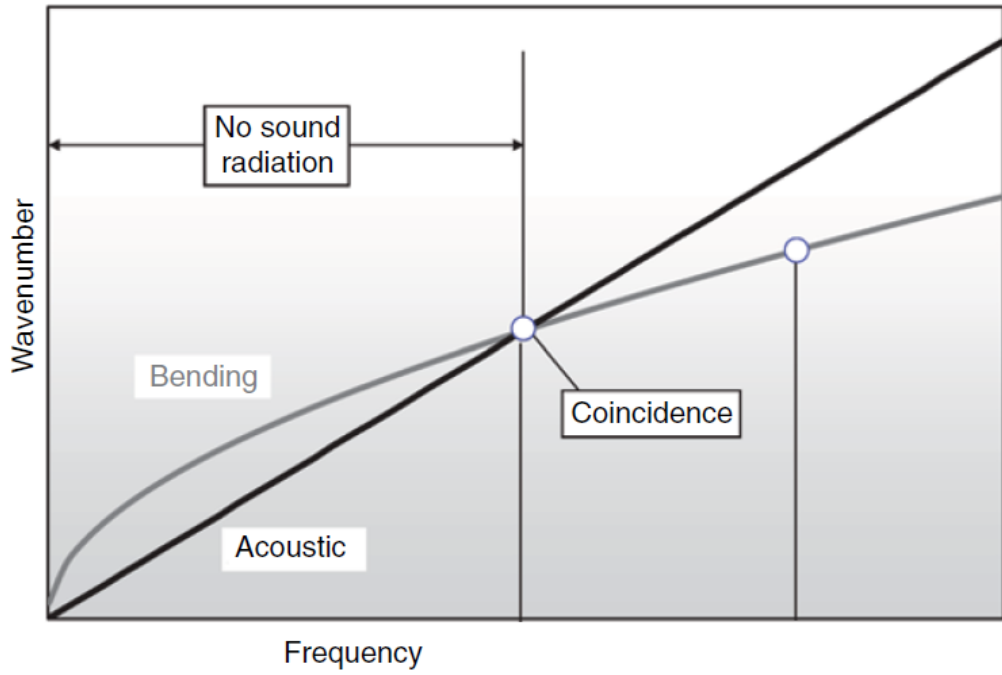
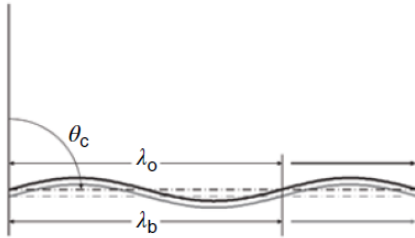
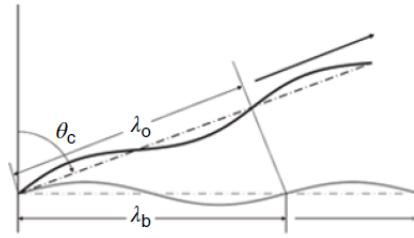


FIGURE 2.1: Bending and acoustic wavenumber-frequency plot

The frequency at which the transversal and acoustic waves have the same wavenumber is called the *coincidence frequency*, where the transversal waves now radiate sound in the free field, as shown in the figure (2.1) in the middle, as in ref (2.2)

FIGURE 2.2:
AT the Coin-
cidenceFIGURE 2.3:
AFTER the
Coincidence

At frequencies above coincidence, the transversal waves continue to speed up, and the sound radiated by the transversal waves propagates in a preferred direction which is computed comparing the flexural wave to the shorter acoustic wave, as in ref (2.3) [34].

The angle of radiant noise is computed as follow

$$\theta_c = \arcsin \left(\frac{c_o}{c_B} \right) \quad (2.1)$$

where c_B is the transversal wave speed. It is also possible to compute the infinite plate's coincidence frequency by setting the flexural and acoustic wave speeds equal to each other, for thin plate

$$c_0 = c_B = \left(\frac{D\omega_c^2}{\rho h} \right)^{\frac{1}{4}} \quad (2.2)$$

$$\omega_c^2 = c_0^4 \frac{\rho h}{D} \quad (2.3)$$

where h is *thickness of thin plate*

$$D = \frac{Eh^3}{12(1-\nu^2)} \quad (2.4)$$

The position of coincidence frequency is very important. It may be useful to vary it with the plate parameters, executing the *Parametric Study*. For instance, increasing a plate's elastic moduli (Young's Modulus E) stiffens the plate itself, speeds up the transversal waves, and lowers in the same time the plate's coincidence frequency; so increasing radiation efficiency. Conversely, increasing a plate's density increases its mass, slowing down the transversal waves, and raises the plate's coincidence frequency, so reducing the radiation efficiency.

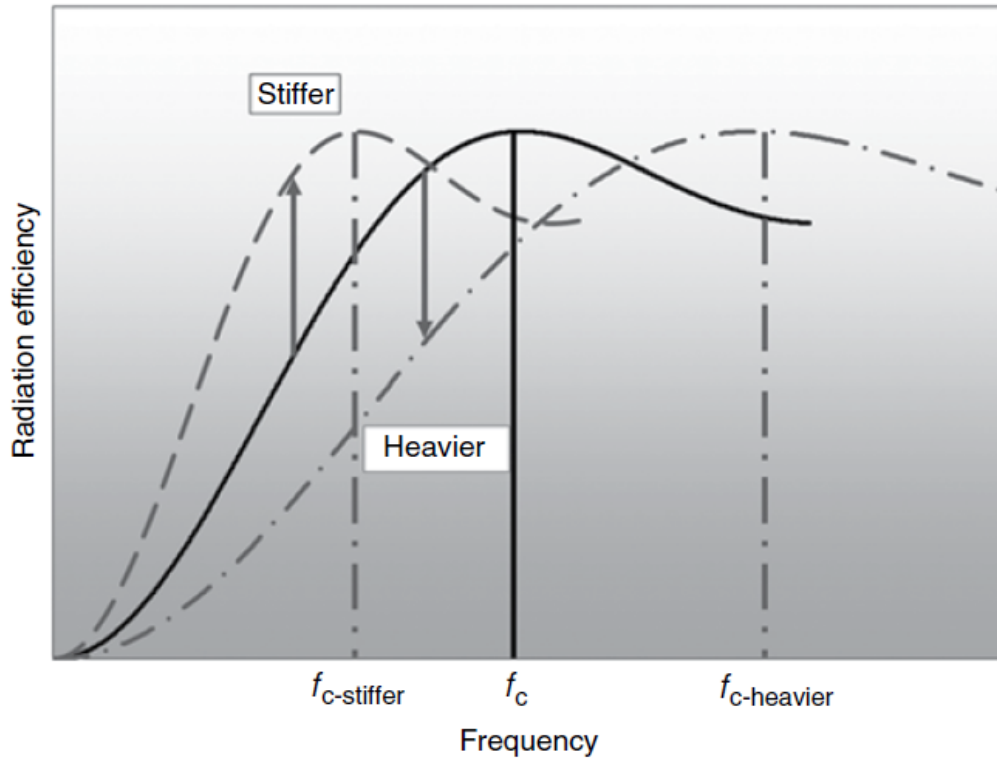


FIGURE 2.4: Effects of stiffening on plate coincidence frequencies

The figure above shows that stiffening a thin plate reduces the coincidence frequency, and adding mass increases it. This obviously influences the noise radiation into the free space around, answering to most noise control problems to simply add

mass to a plate while reducing its stiffness of themselves. But do not forget that we are dealing with light structure.

In space Industry, all new structures are lightweight and stiff, like carbon-fiber composites reinforced with ribbed. These kind of structures typically have *low coincidence frequencies*, and therefore radiate *sound very well*. This is valid only for **infinite thin plate**, if our plate is considered infinite, such that there were no reflections from any of the plate boundaries.

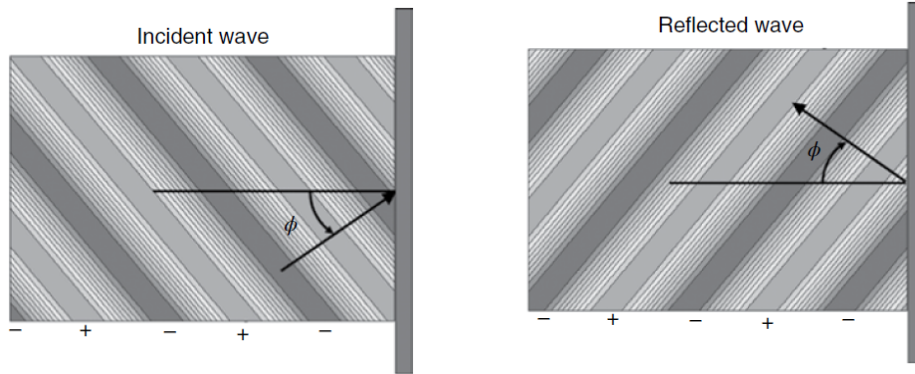
Considering finite dimension, the discontinuities at the boundaries "scatter" the energy in transversal waves into many wave-numbers, some of them supersonic, so that a finite plate radiates sound below its coincidence frequency.

2.2 Structural Vibrations Induced by Acoustic Pressure Waves

In Spacecraft industry, vibrations induced in structures by impinging acoustic waves can be so high that the structures may present failures and fail the mission. The physics that explain this phenomenon are the same as those that explain how a vibrating structure radiates sound, in the previous chapter. Let us clear this idea.

Consider the classical problem of a *flat infinite plate* that is impinging by an incoming acoustic wave. There are **three pressure waves** next to the structural surface; the *incident wave*, a *reflected wave*, and a *wave re-radiated* by the structure itself, which has been forced into vibration by the incident and reflected waves.

For instance, the following images show the incident and reflected waves for a 30° angle of incident from the direction normal to the plate itself.



The sum of the incident and reflected waves forms a "*blocked*" pressure on the surface, and if the surface is rigid, the blocked pressure field is, in fact, the total pressure.

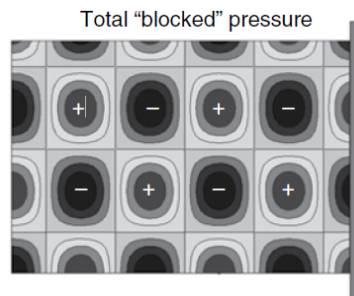


FIGURE 2.5: Blocked pressure field acting on a plate

Since in this case the structure is flexible and vibrates, it radiates a third pressure wave, which sums with the blocked one to form the overall pressure field. The standing wave pattern propagates in the direction parallel to the surface at a speed $c_0 \sin(\phi)$, where ϕ is the angle of incidence.

The fluid impedance depends on the pressure wave's angle of incidence and the fluid's characteristic impedance

$$z_{fluid} = \frac{\rho_0 c_0}{\sqrt{1 - (\sin \phi_{incident})^2}} \quad (2.5)$$

while the infinite plate's impedance is as follows

$$z_{plane} = D(k_0 \sin \phi_{incident})^4 \frac{\eta}{\omega} - i \frac{D(k_0 \sin \phi_{incident})^4 - \rho h \omega^2}{\omega} \quad (2.6)$$

where η is the structural loss factor and h is the plate thickness.

According to the infinite plate theory, the plate vibration may be used to estimate caused by the blocked pressure field:

$$v_n = \frac{2p_{incident}}{z_{fluid} + z_{plate}} \quad (2.7)$$

The equation shows that the plate vibrates most when its structural impedance is minimized. This occurs when annulling the imaginary part of z_{plane} , as in ref (2.6). Since $k_0 = \omega / c_0$

$$D(k_0 \sin \phi_{incident})^4 = \rho h \omega^2 \quad (2.8)$$

We obtain that

$$\omega_{co} = \sqrt{\frac{\rho h}{D}} \frac{c_0^2}{(\sin \phi_{incident})^2} \quad (2.9)$$

This represent the most critical frequency of the system due to the severe level of vibration induced by acoustic field on the structure.

It's possible to provide a derivation of the sound power transmission coefficient τ through an infinite plate (by Fahy and Gardonio). We provide it here

$$\tau = \frac{[2\rho_0 c_0 / \sin \phi]^2}{(2\rho_0 c_0 / \sin \phi + (D/\omega)\eta(k_0 \sin \phi)^4)^2 + (\omega \rho h - (D/\omega)(k_0 \sin \phi)^4)^2} \quad (2.10)$$

where η represents the damping (assumed a priori) and ρ represents the surface mass density (of the infinite plate).

$$\text{Transmission Loss Plot} = 10 \log_{10}(1/\tau) \quad (2.11)$$

The analysis of typical transmission loss plots can reveal some important features. As sake of clarity, let's give an example

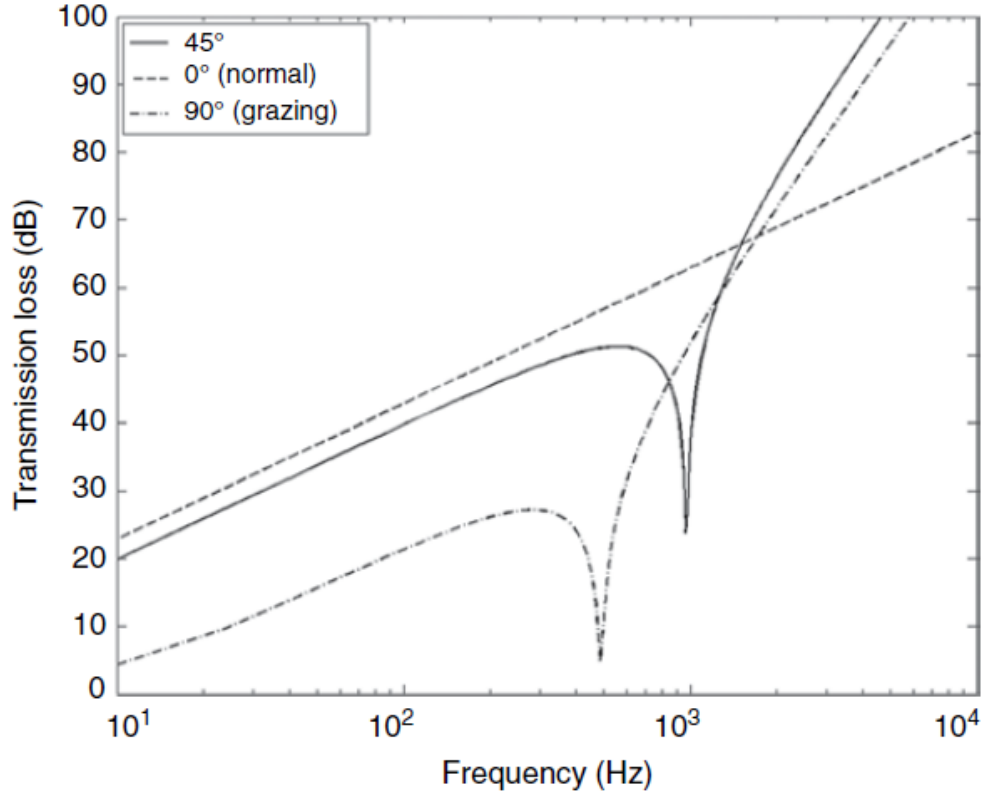


FIGURE 2.6: Blocked pressure field acting on a plate

For acoustic waves **not** normally incident on the plate, sharp apex appears in the transmission loss plot; while considering different the perpendicular one, a strait line is going to appear, as shown in figure (2.6). The apexes are at the coincidence frequencies of the plate. The coincidence frequencies depend not only on the geometry of the plate, but also on the angle of incidence on which the sound waves are acting; while the angle of incidence changes, the coincidence frequency and the frequency of the transmission loss apex change as well. This is useful for designing the interaction noise/structure.

At *low frequencies*, the mass term determines the transmission loss, which increases with the *square* of frequency (6 dB/octave).

At *high frequencies*, above the coincidence frequency apex, plate stiffness is dominant, and the transmission loss increases (more than the previous case) with the *sixth power* of frequency (18 dB/octave).

Chapter 3

Acoustics

3.1 Introduction of Acoustics

Sound waves might be considered as compressional oscillatory perturbations that propagate in a fluid. The waves involve molecules of the fluid moving backward and forward in the direction of propagation, accompanied by changes in the local pressure, density and temperature.

The *Sound Pressure*, the difference between the instantaneous value of the local pressure and the static pressure, is the quantity that can be heard. Since the pressure changes associated with a sound wave can be **very small** if compared with ambient pressure: for instance the human hear can perceive as sound pressure variation in a particular limited range, whereas the ambient pressure at sea level is about $1[atm] = 101\,325\,Pa$.

As matter of fact, the *Sound Pressure Level* (SPL) is introduced. SPL is actually defined the ratio of the absolute, Sound Pressure and a reference level (usually defined as the *Threshold of Hearing*), the lowest intensity sound perceived by humans; it's measured in logarithmical scale and its unity is *DeciBel* (dB).

$$SPL = 10 \log_{10} \frac{p_{rms}^2(t)}{p_{ref}^2} = 20 \log \frac{p_{rms}(t)}{p_{ref}} \quad (3.1)$$

where p_{ref} is the lowest level perceived by humans, approximately in air $p_{ref} = 10^{-12}[Pa]$ and the local pressure level, measured in *root mean square*

$$p_{rms}^2 = \frac{1}{T} \int_0^T p'^2(t) dt \quad (3.2)$$

It is important to note that these pressure perturbations are *small* (Ex. for 120dB, relative perturbations $(p_{rms}/p_0 = 2 \cdot 10^4)$). A mathematical description of the wave motion in a fluid can be obtained through the combination of equations expressing:

1. Conservation of mass
2. Local longitudinal force caused by a difference in the local pressure is balanced by the inertia of the medium
3. Sound is very nearly an adiabatic phenomenon, so there is no flow of heat.

The most important property of sound is that it could be treated by the linearization of the Navier Stokes equations due to small perturbation and they usually carry a tiny fraction of the total energy in the flow.

It is important to understand the mechanisms of flow induced noise generation in order to mitigate its production. The mechanisms of noise production depends on the associated flow field which in turn depends on flow parameters like Reynolds number, the type of boundary layer and the geometry of the object in the flow itself.

Vibrating structures radiate noise. The *Radiated power* is determined by the acoustical coupling between the *Vibrating Structure* and the surrounding fluid. The resulting acoustic field induced by the vibrating structure is also influenced by reflecting surfaces (constituting the structure itself) and variations, for example, temperature and velocity in the fluid. For example, the noise generated by piece of spacecraft is reflected on other pieces constituting the structure. In addition to reflection effects, the measured noise is influenced by a certain noise attenuation in air. Temperature can influence the direction of the propagation of the sound waves and the recorded noise level. *Two field* of measurement can be found:

Indoor measurements, the acoustical field induced by a source in a closed room depends on the acoustical characteristics of the room as well the distance to the source;

Outdoor measurements, the acoustical field induced is mainly created by the reflection and air attenuation.

The Governing Equation of the wave propagation in fluids is now introduced. Noise radiation from elementary sources as well as the effects of reflecting boundaries is discussed later on. The observation that most acoustic phenomena involve perturbations that are several orders of magnitude *smaller* than the equilibrium values of the medium makes it possible to *simplify* the mathematical description by neglecting higher-order terms.

3.2 Wave Equation in Fluid

Supposing an ideal non-viscous fluid is at rest; the ambient temperature T_0 , pressure p_0 , and density ρ_0 are constant with respect time and space. Let's introduce a disturbance caused by a vibrating solid. It will produce a wave motion in the fluid, which in turn will cause pressure local fluctuations, as previously stated, in *small perturbation*. Equation governing are based on the principles of conservation of mass and momentum as well as the equation of state for a perfect gas.

3.3 Wave Equation

The combination of these equations linearized gives the **Wave Equation** that is the *basic* partial differential equation governing the spatial and time dependence of the *acoustic wave transmission*.

$$\nabla^2 p' = \frac{1}{c^2} \frac{\partial^2 p'}{\partial t^2} \quad (3.3)$$

where p' is the fluctuating component of the pressure.

Noise Transmission is generated by the (small) fluctuation of pressure p' and related density, radiating through a medium (air, water).

The *main aim* of an acoustic study is, firstly, to understand the mechanisms of noise production, then identify the location and main sources of noise and accurately compute far-field acoustic pressure fluctuations and directivity in order to mitigate.

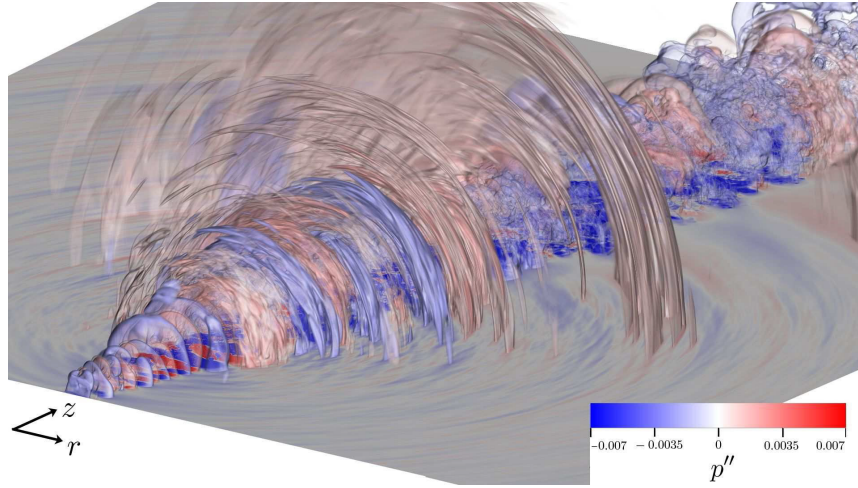


FIGURE 3.1: Noise: Small Fluctuation of Pressure

3.4 Energy and Intensity

The fluid volume Ω has *Energy*, as containing kinetic energy.

$$T = \int_{\Omega} \frac{\rho_0}{2} |V|^2 d\Omega = \int_{\Omega} \frac{\rho_0}{2} |\nabla \Phi|^2 d\Omega \quad (3.4)$$

Potential energy is stored in a fluid when the fluid is compressed, that's equal to the work carried out to compress the gas to the volume V to a new volume $\Omega - \Delta\Omega$. The Work (W) stored during the compression may be calculated as follows

$$W = - \int p d\Omega = \frac{p^2 \Omega}{\rho_0 c^2} \quad (3.5)$$

In Acoustics Problem, another concept is important: *The Intensity*.

The **Intensity**, better the intensity vector, resulting from a wave motion in the fluid is defined as

$$I = p \cdot v \quad [W/m^2] \quad (3.6)$$

where p is the pressure and v the particle velocity vector in the fluid. Using complex notations and assuming a time dependence in the form $\exp(i\omega t)$

$$I = \operatorname{Re} \left(\frac{p \cdot v}{2} \right) = -\operatorname{Re}[i\omega\rho_0\Phi |\nabla\Phi|] \quad (3.7)$$

The **intensity vector** is set to equal the real part, that's the active intensity. The imaginary part of the intensity vector is the reactive intensity.

As shown in figure, In the case of Spherical Propagation wave, The intensity will decrease with the radially distance from the source, not because for any process of power-decay itself (the intensity will remain the same); but due to the increase of the area. Since the area will increase with the distance, and the power is the same, the overall result is the decrease of the intensity $[W/m^2]$, this concept will be explained deeply in the next section, as in 3.7.

Intensity, as well, is measured in logarithmical scale. We define the **Intensity Level** as

$$IL = 10 \log_{10} \left(\frac{I}{10^{-12} [W/m^2]} \right) = 10 \log_{10} I + 120 \text{ dB}. \quad (3.8)$$

where $I_{ref} = 10^{-12} [W/m^2]$ is the reference intensity, that is energy over surface.

3.4.1 Losses

When sound is radiated over large distances in infinite space or in a flow through narrow openings or close to boundaries, the losses can no longer be neglected.

In infinite space, the losses are due to a number of mechanisms in the fluid itself. In air the losses are caused by viscosity, heat conduction, molecules diffusion, heat radiation, and molecular losses. The effect of viscosity in the equation of motion in a fluid leading up to the *complete* Navier-Stokes equation set.

The dissipation effect is caused by the presence of water molecules [for instance: Humid Air], and due to the presence of wall in motion field, cause the viscosity produces large velocity gradient, so the energy is dissipated.

For losses in air, the humidity or number of water molecules per volume of the gas is an important parameter. In addition to humidity, the losses are functions of temperature, atmospheric pressure, and frequency.

The losses, if small, can be included in the wave equation by letting the *compressibility be a complex quantity*. Following this idea. the bulk modulus K may be written as $K = K_0(1 + i\delta)$, introducing δ as the loss factor in the fluid.

So the effect of dissipation is given considering the imaginary part of velocity, in fact, for small losses the speed of sound in the fluid is obtained

$$c = \sqrt{\frac{1}{k\rho_0}} = \sqrt{K_0(1 + i\delta)/\rho_0} \approx c_0(1 + i\delta/2) \quad (3.9)$$

The corresponding wave number k for noise wave radiating in fluid is expressed as

$$k = \omega/c = \omega/[c_0[1 + i\delta/2]] \approx k_0(1 - i\delta/2) \quad (3.10)$$

3.5 Impedance

The ratio between the complex amplitude of the pressure and the complex amplitude of the *normal* velocity in a given location is called **impedance**

$$Z = \frac{\hat{p}}{\hat{u}_n} \quad (3.11)$$

where Z is the impedance and \hat{u}_n represents the normal component on the surface (pointing outside). The impedance is the result of the ratio between two complex, and itself is complex. The real part of Z is called Resistance and its imaginary part Reactance. The inverse $1/Z$ is known as *Admittance*.

$$Z = \text{complex number} = \text{Resistance} + j(\text{Reactance}) \quad (3.12)$$

$$\frac{1}{Z} \mapsto \text{Admittance} \quad (3.13)$$

The characteristic impedance is inherent to the propagation medium throughout it propagates, and it depends tightly on the material properties. Notice that when $\text{Re}(Z) > 0$ the surface is *passive* and **absorbs energy**, useful for the representation of *Material losses*, but when $\text{Re}(Z) < 0$ the surface is *active* and **produces energy**.

Chapter 4

Actran

In Cooperation With



4.1 Actran Software

Actran is a complete acoustics, vibro-acoustics and aero-acoustics simulation software, based on the finite and infinite element method through the linearization of Navier Stokes Equation for Acoustics.

Actran offers different calculation procedures

1. *Direct Frequency Response* for the computation of the acoustic, vibro-acoustic or aero-acoustic response of a system in the frequency domain and in physical coordinates. This will be deeply treated, as in 4.2.
2. *Time Response* for the computation of the acoustic, vibro-acoustic response of a system in the time domain in physical coordinates.
3. *Modal Frequency Response* for the computation of the vibro-acoustic response of a system using a preliminary representation of the structure and the cavity in the modal space.
4. *Green Analysis* for the computation of the radiation of a vibrating system using the Green theorem for acoustics.
5. *Pellicular Analysis* for the computation of the radiation of a system using pellicular modes.
6. *Modal Extraction* for computing the modes of an uncoupled and closed acoustic or undamped structural model.
7. *Compressible Flow Analysis* for computing a compressible and irrotational flow field on an acoustic domain.

In most cases, The acoustic phenomena can be assumed to be linear. As a consequence, Actran solves **linear equations**, as shown in the previous chapter 2.

Actran is divided in two different part:

1. *ActranVI* is used for projecting the Vibroacoustics Model, imposing the Boundary Condition, Part, Component.
2. *ACTRAN* is used for running the computation, it's the *solver*.

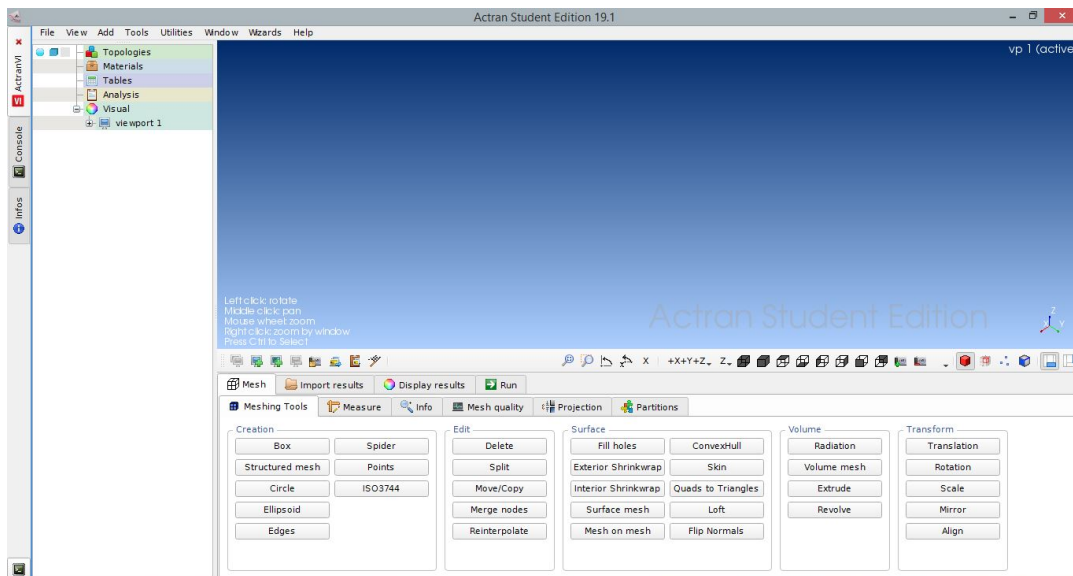


FIGURE 4.1: ActranVI Windows

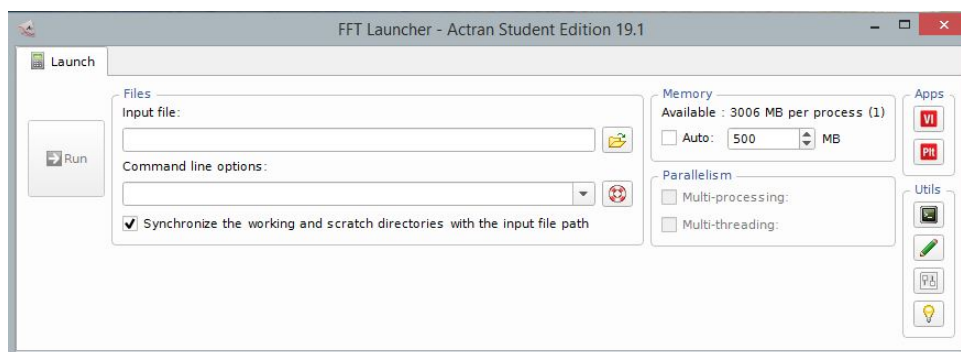


FIGURE 4.2: Actran Windows

An Actran model contains different kinds of information such as the description of the finite elements (FE), the material properties, the parameters of the analysis itself.

Each piece of data belongs to one of the 6 categories shown below

1. **Domain and Element Set / Topology.** An element set is a collection of finite elements, while a domain is a collection of element sets.
2. **Material.** A material describes the physical properties of a material.
3. **Component.** A component characterizes the numerical properties and the physical interpretation of a domain of finite elements.
4. **Boundary Condition.** A boundary condition characterizes a boundary condition or an excitation on the finite elements.
5. **Analysis Parameter.** An analysis parameter is any other parameter influencing the computation of the model.
6. **Fields and Tables.**

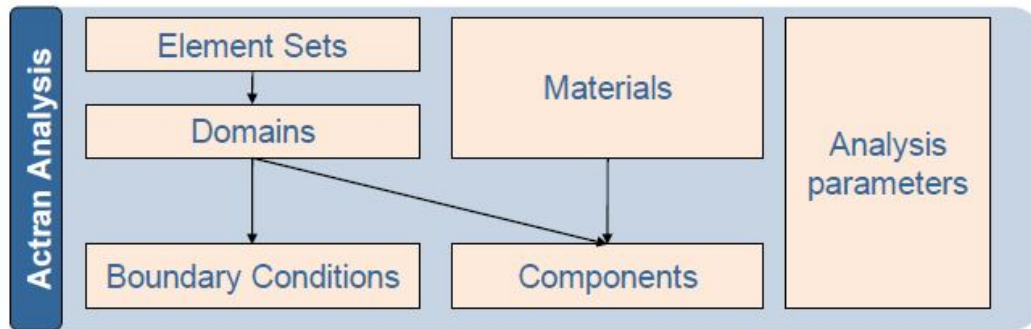


FIGURE 4.3: 1st Summary of Actran Analysis

When using the software, The first step is to import the mesh, defining the element properties. We divide the whole model into different elements; after that, we can unify the *elements*, previously defined, into a different *Domain*, building a particular piece of the model.

The next important step is associate the material for each domain, building the *components*, we have to decide the Analysis to make, in this latest step, the Boundary Conditions and the components are the input.

Obviously, the objectives are different according to the analysis chosen. The last step is extracting the file (.edat format, in ASCII format) in order to analyse with Actran.

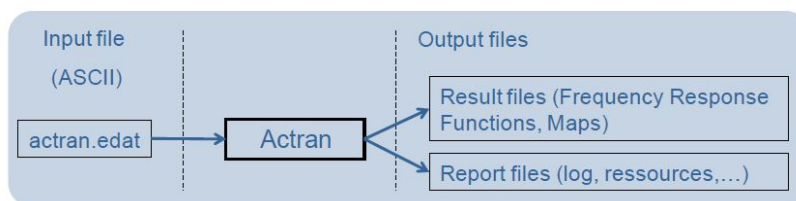


FIGURE 4.4: 2nd Summary of Actran Analysis

Actran reads the file .edat and solves the computation in order to give the results of the analysis. This is summarized in figures (4.3) and (4.4).

4.2 Direct Frequency Response

The *direct frequency response* is a computation procedure which is used to compute the response of an acoustic, a vibro-acoustic or aero-acoustic system to a specific excitation in physical coordinates. This is the most common Actran analysis type, and we'll later see important and simple examples of this. This will be used in the second part for the following part.

The following system of equations is set-up and solved for various pulsations $\omega = 2\pi f$

$$(\mathbf{K} + i\omega\mathbf{C} - \omega^2\mathbf{M})x(\omega) = F(\omega) \quad (4.1)$$

yielding values of the unknown vector $x(\omega)$ for every pulsation ω .

We will apply the acoustics theory through four simple examples. Thanks to this, we will easily understand the more complex coupled system, which is the aim of this dissertation.

4.3 Examples of Application

4.3.1 Virtual Kundt's Tube

The Kundt's tube may be considered as a device closed at one extremity by an absorbing material. At the other end of the tube, a sound generator corresponding to a piston produces pure incident sine waves which are more or less reflected due to the presence of the foam.

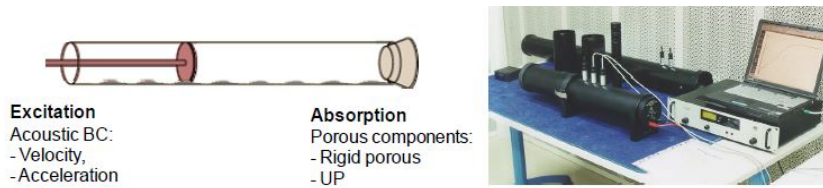


FIGURE 4.5: Kundt's Tube

The *objective* of this training is to *evaluate* the absorption coefficient and the equivalent impedance of an arbitrary **porous material**. In this simple example, we will see the importance of Porous material in acoustics application as Damping material. Calculate the SPL in the center of front face of the foam. The first step is building the mesh as follows

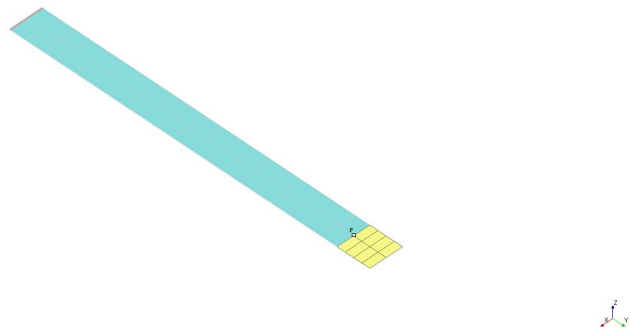


FIGURE 4.6: Kundt's Tube Mesh

in which, the red line is the moving piston, the blue is the air, the acoustics domain, and the final yellow part is the foam to be characterized. The foam Properties are

Foam Properties		
Properties	Value	Unity
Porosity	0.94	
Flow Resistivity	10000	Ns/m^4
Tortuosity	1.06	

After imposing the solver, the computation has been run. From the interpretation of the results.

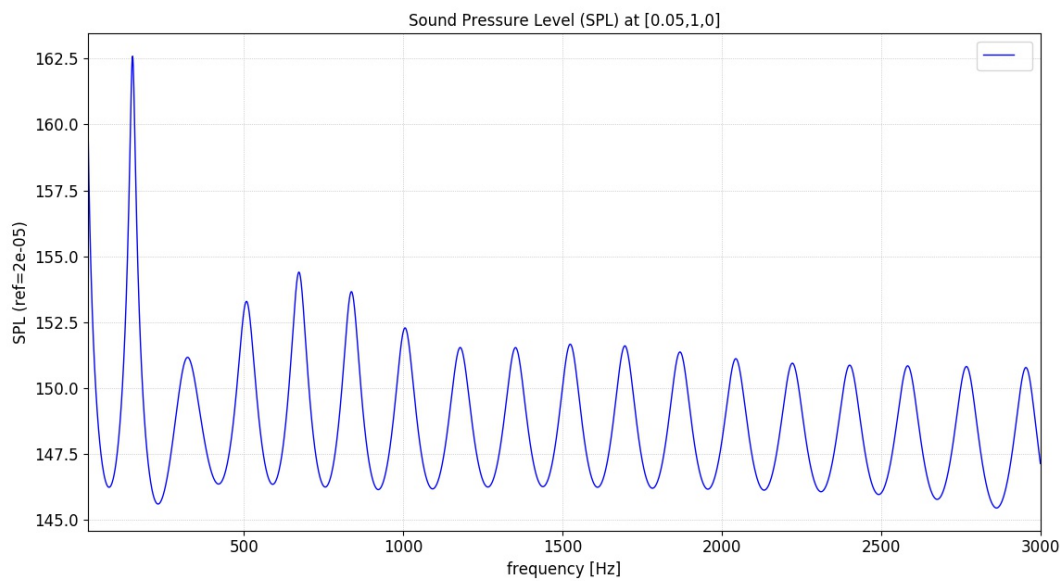


FIGURE 4.7: Sound Pressure Level in Kundt's Tube

in the previous figure, Resonance points are shown, in which sound wave in the tube are in the form of standing waves; the first resonance peak is near 150 [Hz].

The ratio between the reflected incident pressure wave and the incident pressure wave is known, the acoustic impedance of the material can be calculated using the below equations

$$\text{Absorption Coefficient} \rightarrow \alpha = 1 - |R(\omega)|^2 \quad (4.2)$$

$$\text{Reflection Coefficient} \rightarrow R(\omega) = \frac{p_{\text{reflected}}(\omega)}{p_{\text{incident}}(\omega)} \quad (4.3)$$

$$\text{Impedance} \rightarrow Z(\omega) = \rho \cdot c \cdot \frac{1 + R(\omega)}{1 - R(\omega)} \quad (4.4)$$

$$\alpha = 1 - \text{abs} \left(\frac{\frac{p}{v} - \rho \cdot c}{\frac{p}{v} + \rho \cdot c} \right)^2 \quad (4.5)$$

The absorption capability of this foam can be easily plotted as a function of the frequency

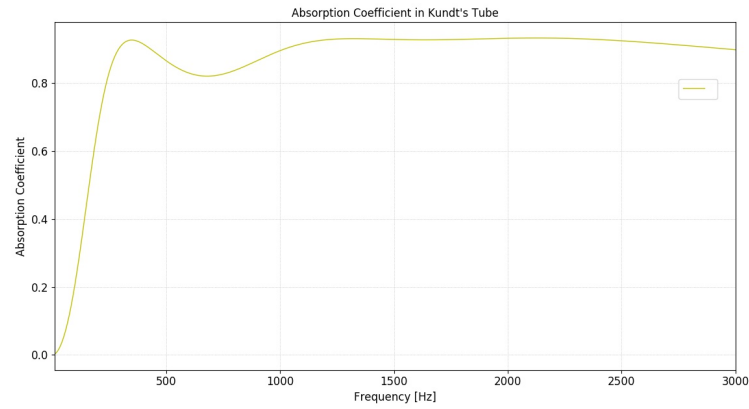


FIGURE 4.8: Absorption Coefficient in Kundt's tube

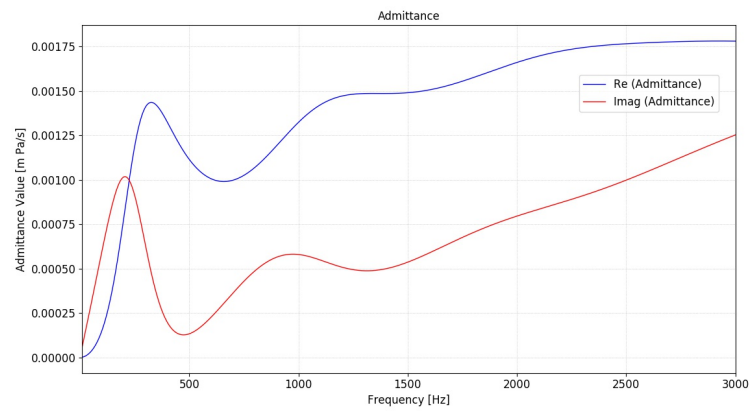


FIGURE 4.9: Admittance of FOAM

Sound propagation in porous materials

The propagation of sound in porous media is an important topic though the geometry of the pores as innovative material for the propagation acoustic wave. The propagation of sound in porous materials can be treated in two different philosophy:

Porous material having rigid frame This approach is optimal for porous materials directly subject to an acoustic field. The elastic part of the porous structure can be neglected, being relevant only for frequencies close to the resonances of the considered system.

Porous material having elastic frame This approach considers the frame with no more relative motion respect to the fluid considering a certain level of elasticity. The simulation of the frame elasticity is really important when studying a complex system for which the vibroacoustic behaviour coupling is fundamental.



The *absorption coefficient* α may be defined as the **ratio** of the *non-reflected sound energy* to the *incident sound energy* on a surface. It can take values between 0 and 1 and it's dimensionless, and $\alpha = 1$ means that all incident sound energy is absorbed in the surface itself, in the foam, in this case.

As shown in figure (4.8), Higher the frequency of the system is, and more incident sound energy is absorbed, presenting higher coefficient.

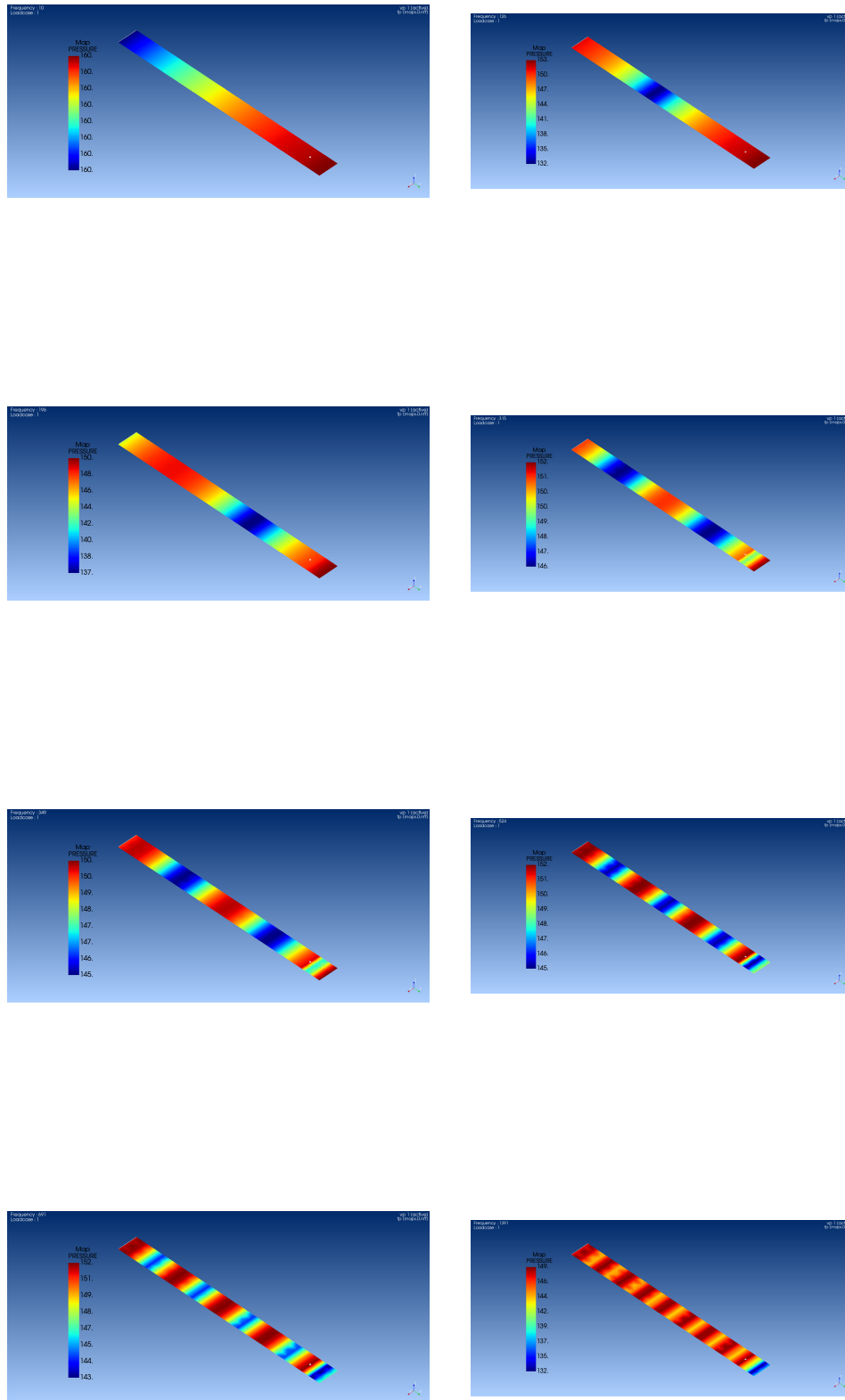


FIGURE 4.10: Evolution of Pressure Field inside the Kundt's Tube

4.3.2 Radiation of a Horn Speaker

A *horn loudspeaker* is a loudspeaker element which uses a horn to increase the overall efficiency of the driving element (diaphragm driven by an electromagnet), emitting sound. The horn itself is a passive component which improves the coupling efficiency between the speaker driver and the air. The aim of this is characterizing the acoustic directivity of the speaker at different frequencies. The mesh is therefore presented hereafter

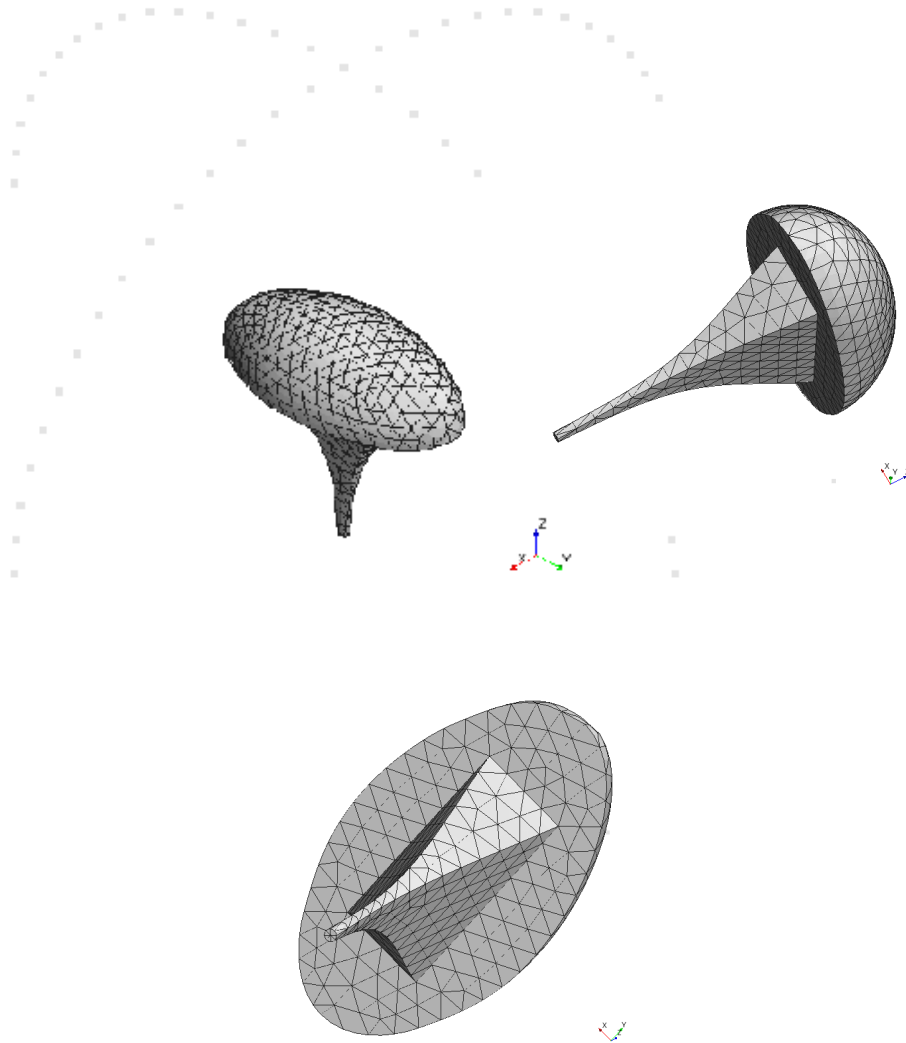


FIGURE 4.11: Mesh of a Horn Speaker

As shown in figure (4.11), the mesh is composed by three different domain:

1. **Acoustic Excitation** (BC) representing the cause of noise.
2. **Infinite Element** (IFE) representing the unbounded free infinite space.
3. **Air Volume** (FE) representing the acoustic computation volume of interest.

We divide the surrounding space in two different plane perpendicular to the acoustic source. The computation holds as follows

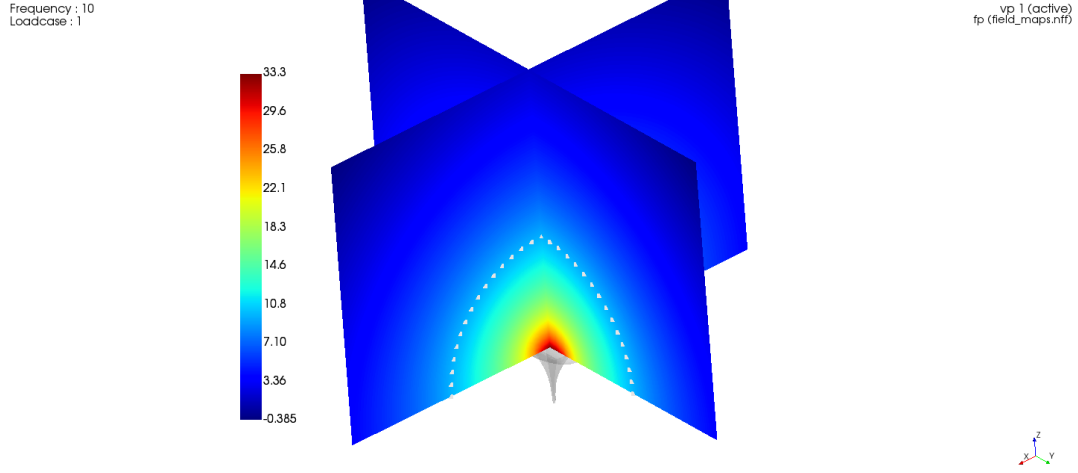


FIGURE 4.12: Acoustic Radiation Field of Horn

In the figure, the acoustic source is emitting and the red color is associated to the emission of the signal (high pressure), and a list of virtual microphones around the horn are inserted in order to characterize the directivity, as previously discussed in section, we are going to analyse the directivity of the source

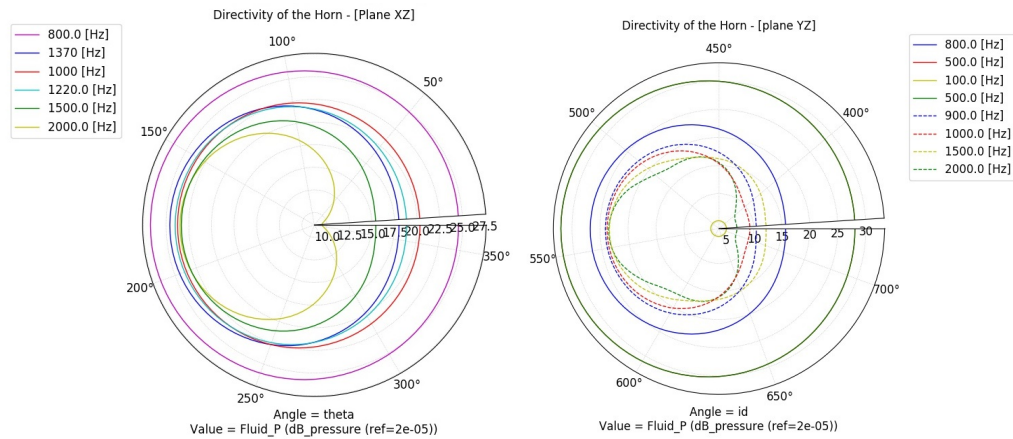


FIGURE 4.13: Directivity of the Horn: plane XZ / plane YZ

The previous figure shows that the directivity of horn is frequency dependent; in fact in the *low frequency regime*, the source is omni-directional and uniform without a preference direction, the resulting curve is a cycle. In *high frequency regime*, the horn becomes directional (inner region), the resulting curve isn't a cycle any more. The behaviour is a frequency function. This may be exploited in different fields.

4.3.3 Acoustic Transmission through a Muffler

The muffler is a closed acoustic cavity. The inlet and outlet sections are supposed to be coupled to semi-infinite ducts in which the sound wave propagates without reflection, assuming connecting with infinite energy tube. The objective of this part is to study the *Transmission Loss* (TL) of a muffler.

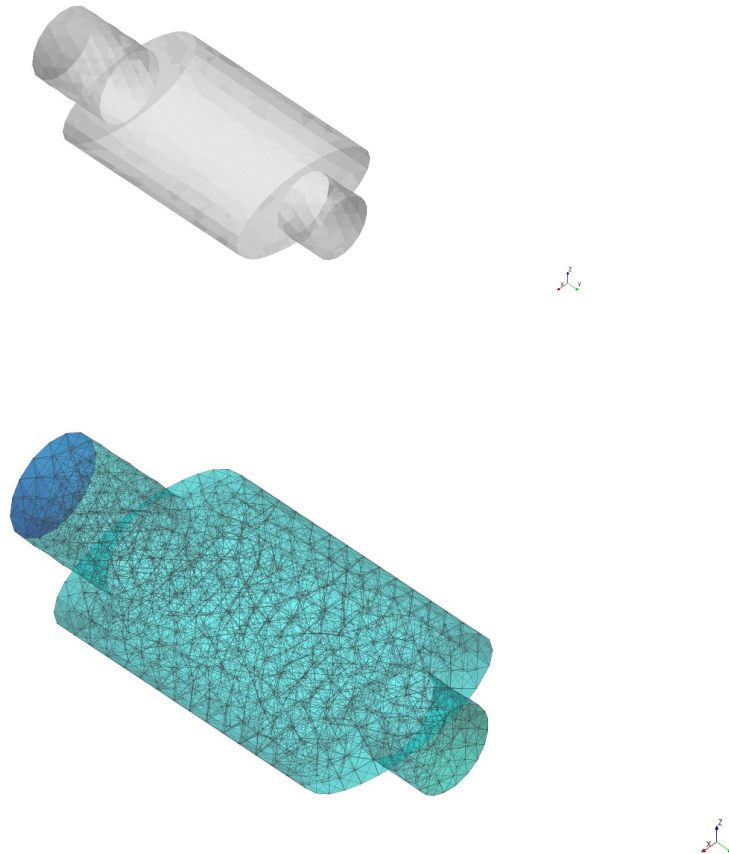


FIGURE 4.14: Mesh of a Muffler

Let's divide the whole model in 3 different element sets are created to support the different domains as follows

1. One **2D** *element set* to model the Inlet modal basis
2. One **2D** *element set* to model the Outlet modal basis infinite space.
3. One **3D** *element set* to model the computational acoustic domain

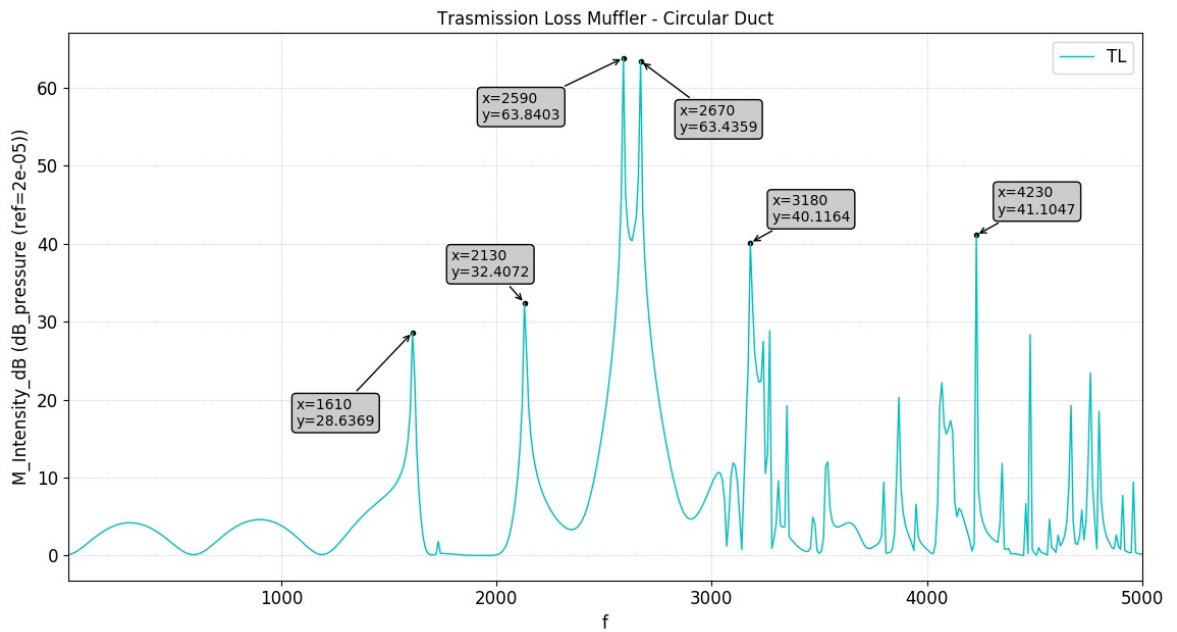
The *transmission loss* (TL) index is an indicator of the acoustic efficiency of the muffler itself. It represents the accumulated decrease in intensity of a waveform energy as a wave propagates outward from a source (the muffler in this case), or such as it propagates through a certain area of the structure. It can be expressed in terms of decibels

$$TL = 10 \log_{10} \frac{W_{in}}{W_t} \quad [dB] \quad (4.6)$$

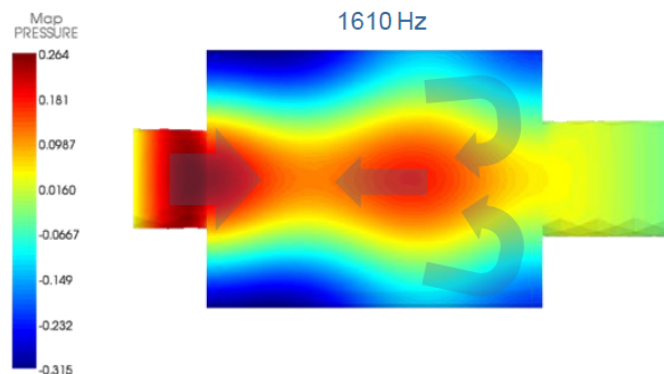
where

1. W_{in} the power of incident wave coming towards a defined area (incident).
2. W_t the power of transmitted wave coming away from the defined area (transmitted).

After having run the computation, plotting the results in the frequency range 0 – 5000[Hz] we obtain



In the muffler, “peaks” and “holes” are presented in the TL curve with important meaning, also note that the maximum point are highlighted. The “Holes” ($TL = 0$) indicates that all the acoustic energy radiates through the outlet of the muffler, while “peaks” show the frequency for which is efficient, that is: Most of the acoustic energy injected is reflected by the cavity and comes back through the inlet section. I’ve selected six different cases. The *First elementary frequency* is 1610 [Hz].



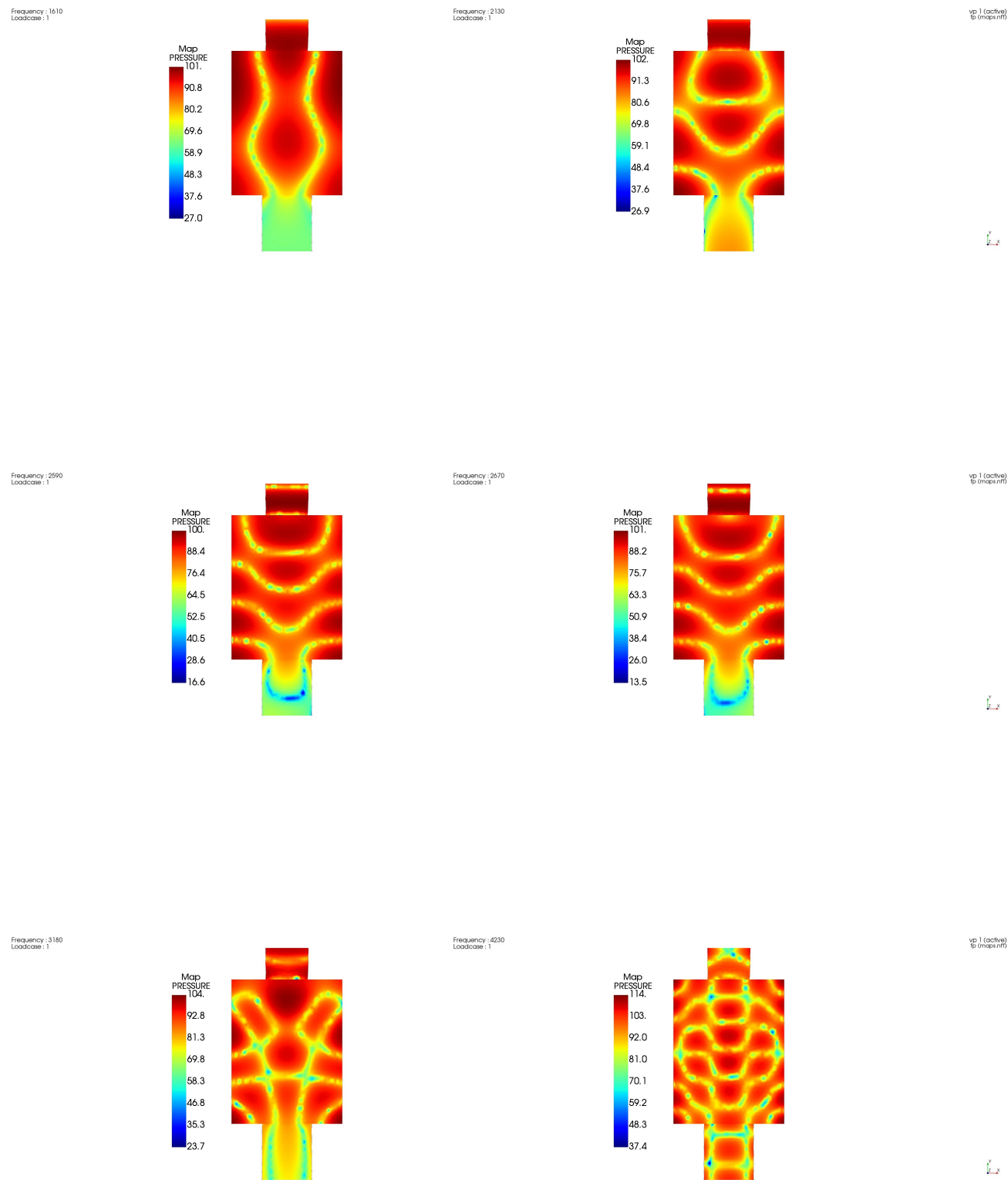


FIGURE 4.15: Muffler Acoustic Modes

4.3.4 Diffuse Sound Field on Antenna for *Spacecraft* Application

During the lift off, Components like antenna carried on launchers are exposed to intense acoustic excitation that can lead to a damage, damaging the communication between spacecraft and Earth; for this reason it's important to deeply study load factor and reaction in spacecraft components like below.

In this case, we will analyse the antenna components below

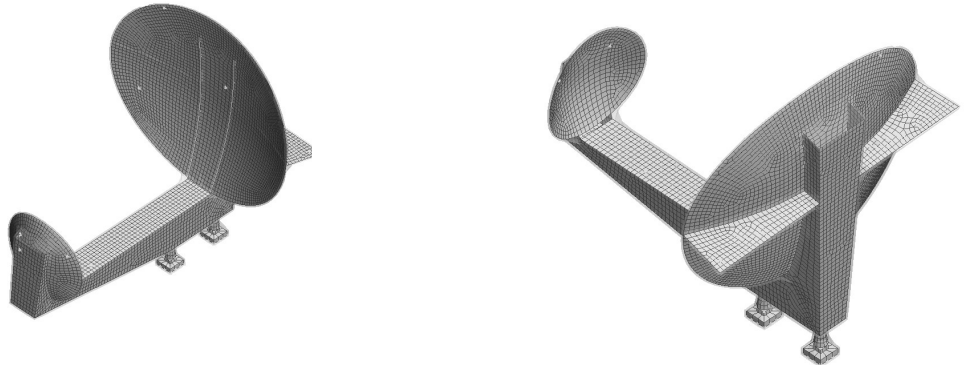


FIGURE 4.16: Mesh of the Antenna

The objective of this part is to evaluate the vibro-acoustic response of a deployable reflector loaded by a Diffuse Sound Field, mounted on a general spacecraft.

On the Structure, accelerometers will be fixed in order to calculate the acceleration, as well as the force and stress acting on them. The general Structure will be loaded by the central structure, are loaded with a *Diffuse Sound Field*, simulating the vibroacoustic effects

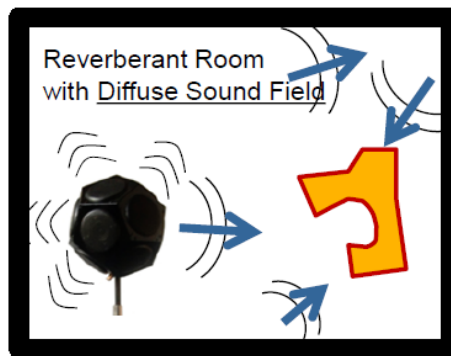


FIGURE 4.17: Objects within the Reverberant Room with Diffuse Sound Field

The object, in this case, an antenna is shaken by a **Diffuse Sound Field** around. That permits us to build diagrams very similar to the envelope diagrams in aeronautical structures.

Diffuse Sound Field is created by considering by 126 PW automatically generated all around the structure itself and equally spread around a reference sphere with sampling *random* phases, based on the statistical data. The results are considered as deterministic ones.

The structural response is measured by 6 *accelerometers* located onto the antenna.

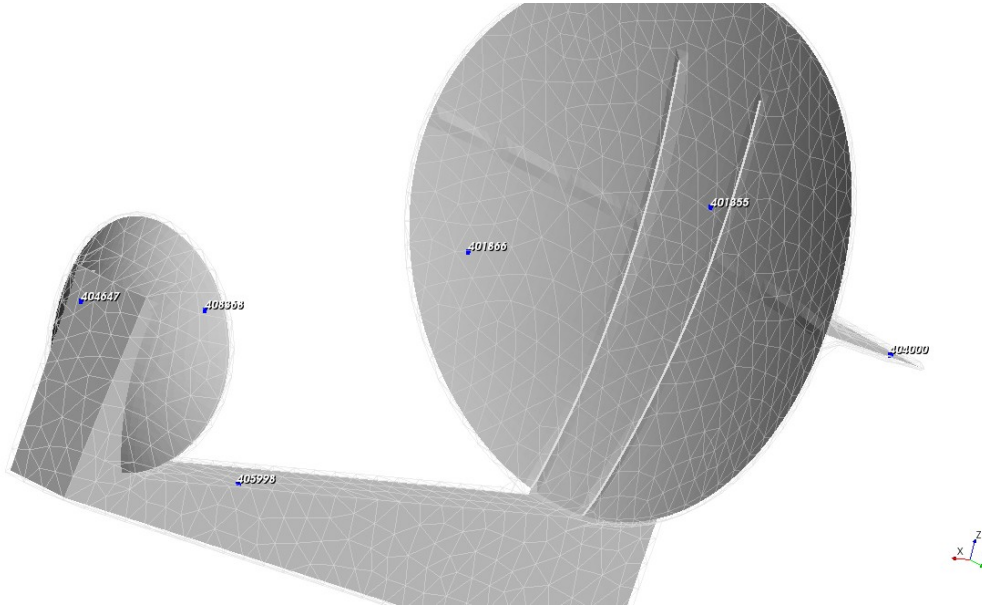


FIGURE 4.18: Location of six accelerometers

Actran is working on structure when loaded with a random excitation (DSF). In order to compute the normal acceleration in $[\frac{g^2}{Hz}]$, the following formula is applied to the normal displacement resulting in

$$a_n = \frac{\omega^4}{g^2} u_n \quad (4.7)$$

In following, we will graph the acceleration for different points in order to understand the most critical point

The behaviour is a function of the frequency. At different frequency, different accelerometers are the most critical. Obviously, the general trend is in increasing the value with increasing the frequency itself.

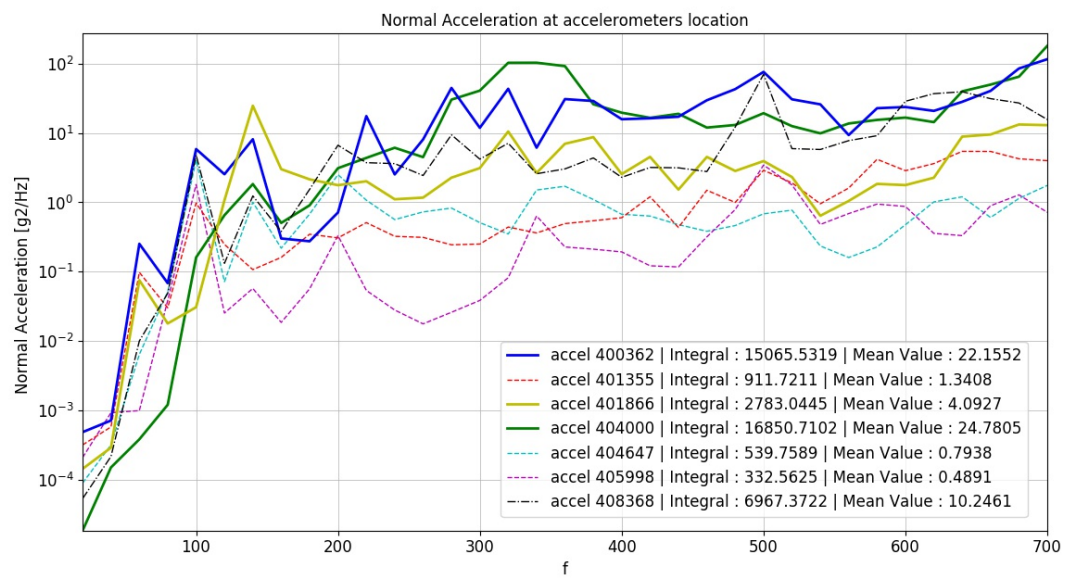


FIGURE 4.19: Normal Acceleration [g2/Hz] in logarithmical scale

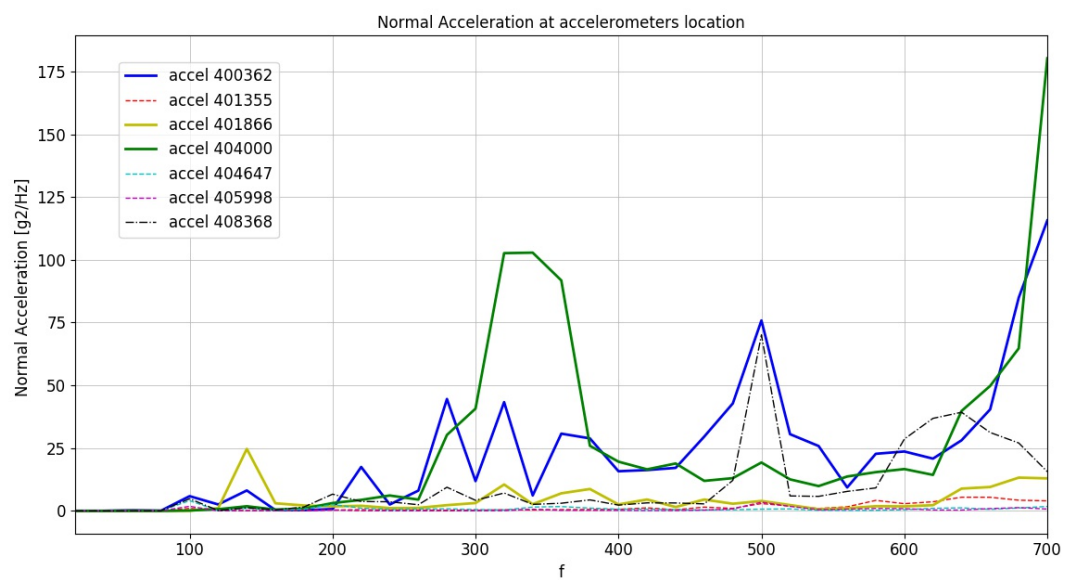


FIGURE 4.20: Normal Acceleration [g2/Hz] in linear scale

As sake of clarity, Let's introduce the mean values in the following table, using Location of six accelerometers, as in ref (4.18)

accelerometer	Number	Mean Value [g^2/Hz]
	400362	22.1552
	401355	1.3408
	401866	4.0927
	404000	24.7805
	404647	0.7938
	405998	0.4891
	408368	10.2461

As shown in the previous table, the accelerometers 404000 and 400362 are the most loaded, and they need to be designed in more deeply attention. In figure (4.18), their location may be verified.

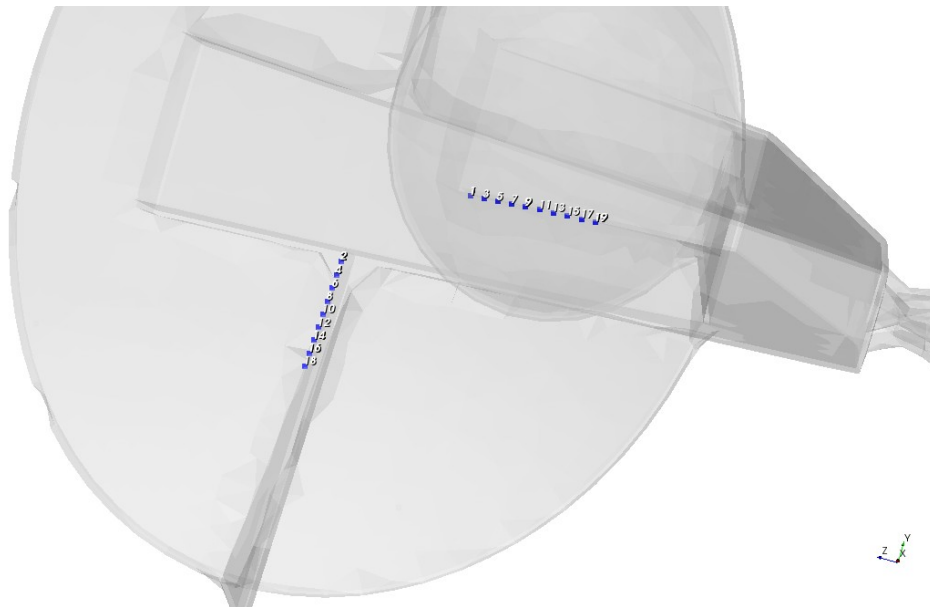


FIGURE 4.21: Reference map for Stress field

In the previous figure, Different points are numbered. According to this picture, it's possible to graph the stress and force acting on the element. After this analysis, a *local strengthening* may be considered in order to make the structure work safely.

We observe that this behaviour is a function of the frequency, so that peaking frequency may be avoided in the working range of the structure, since the antenna is important for communication purpose, and so fundamental for the mission itself.

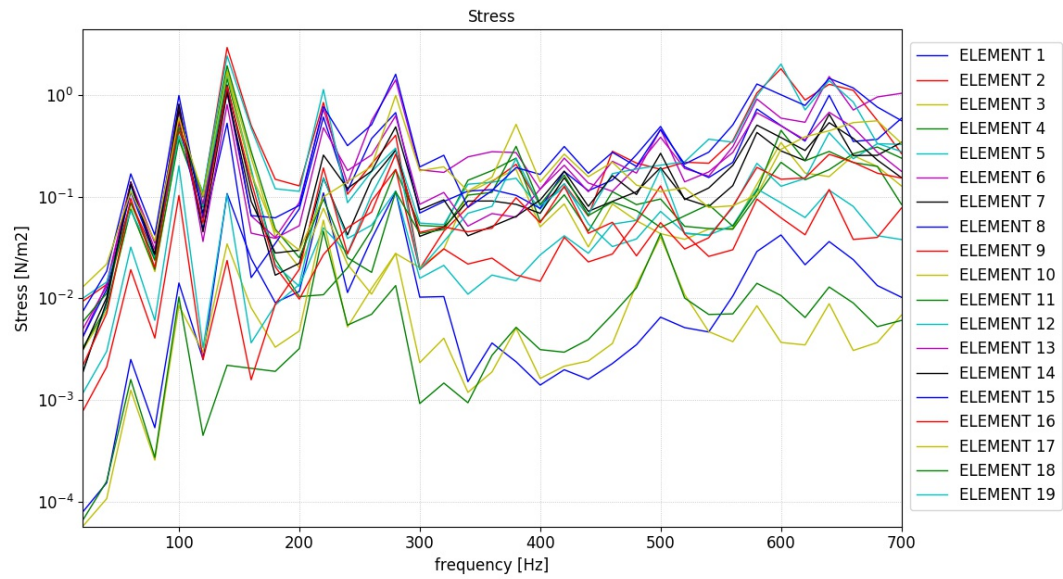


FIGURE 4.22: Stress as a function of frequency

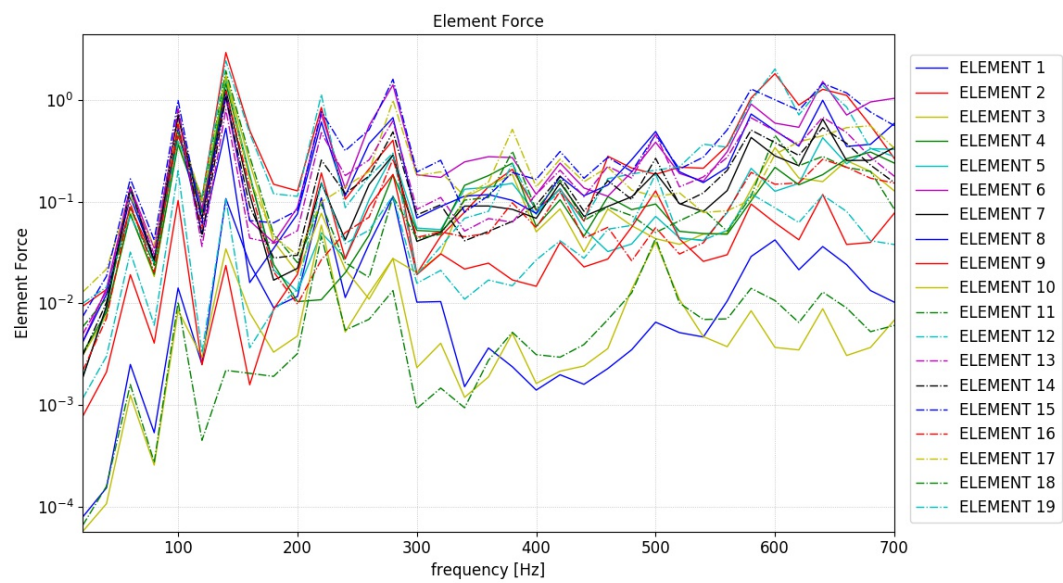


FIGURE 4.23: Element Force as a function of frequency

Frequency : 20
Loadcase : 10000

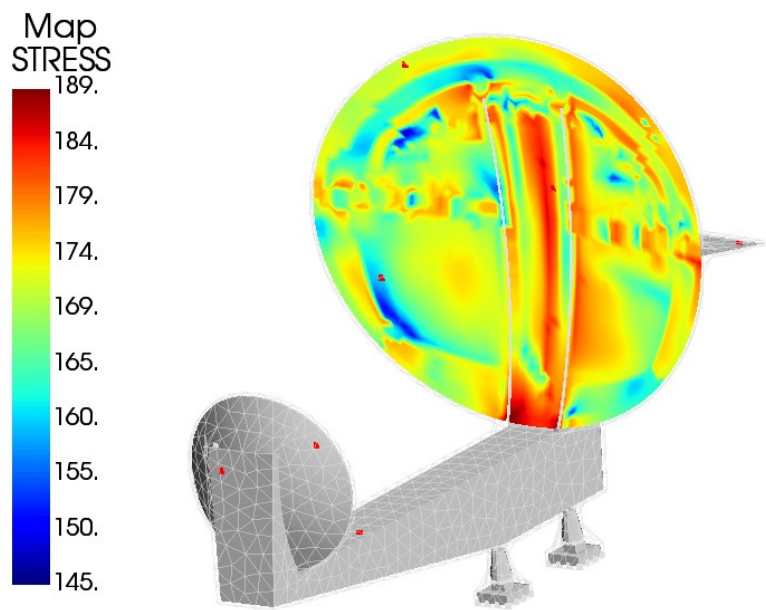


FIGURE 4.24: Stress Field for 20 Hz

Frequency : 220
Loadcase : 10000

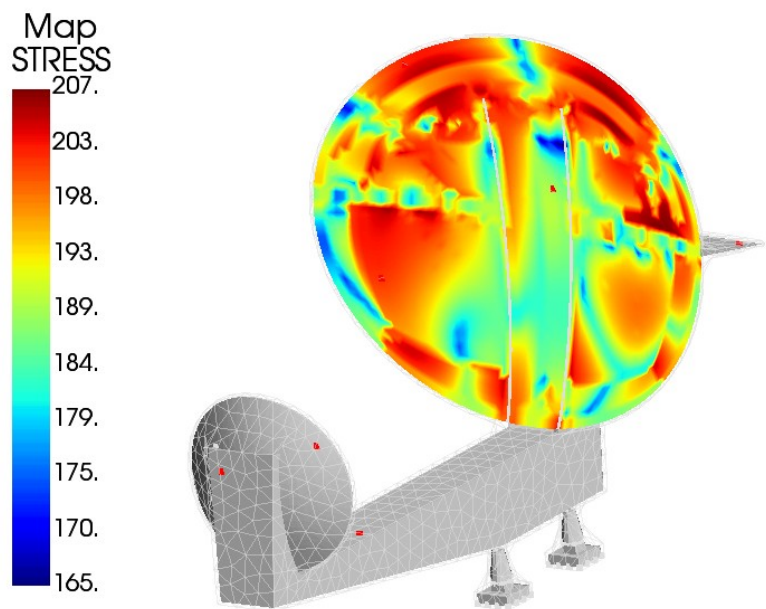


FIGURE 4.25: Stress field for 220 Hz

Chapter 5

Vibroacoustic Modelling Techniques

5.1 Introduction

The Finite Element allows the method to be tailored to the specific application case and field, in this case, different plate cavity structures coupled to surrounding fluid. Firstly we have to determine the frequency range of interest, given the application field; it is possible to combine different materials/thickness to obtain the structure best performance. A important role in the design phase is played by the numerical modelling of coupling surface between fluid and structure.

In this study case, A point load is applied on the plate. Excited structures radiate sound mainly at frequencies corresponding to their structural resonances, condition in which the plate becomes a perfect radiator, so detailfull knowledge of the structure modal behaviour, and modal shapes, plays a fundamental role in the preliminary design step of a vibroacoustic structure.

One of the most **powerful tools** in engineering field problem is the **Finite Element Method (FEM)**. This discretization method is based on the idea that a structure can be approximated by replacing it with an assemblage of discrete elements, constituting the whole structure itself.

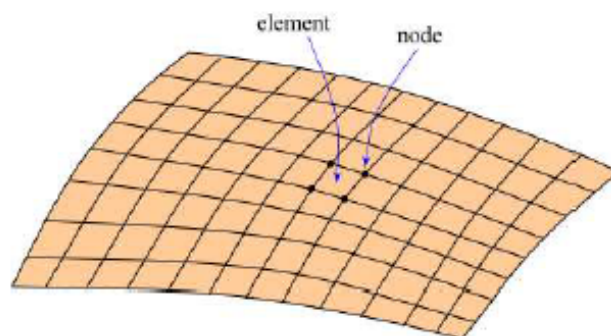


FIGURE 5.1: Continuum discretized with *Finite Element* for FEM

We will deeply verify that the displacement field (within each element) and on its boundaries is expressed as function of the nodes of the elements, using suitable

(respecting precise rule) interpolating functions called "*shape functions*", which permit the explanation of quantities (displacement, stress or strain; as an example) in a certain point (within element) through the determination of quantities at nodal element.

The displacement functions (u, v, w) define the state of strain (and later of stress) within each element defined throughout the mesh. The constitutive law of the structure material (*Hook-Generalized Problem*), it is possible to define the stress state of each element as function of strain. In this way a continuum problem is reduced to a finite number of unknowns, the nodes displacement. This is what happens for the structural problem. Something similar happens for the discretization of the fluid with different element dimension (3D), but something important in this case is introduced, the coupling surface between the structure element and the fluid ones. A restriction is introduced, in fact the planar dimension of the fluid element should be of the *same dimension* of element dimension used to discretize the whole structure plate.

This is just a general introduction of what we will later deeply demonstrate.

5.2 Governing equations

The structure is described by the differential equations of motion for a continuum body assuming small deformation since a linear behaviour of the fluid coupled structure system is here assumed. The structure is coupled to a homogeneous, inviscid and irrotational compressible fluid. As sake of simplicity, Both the fluid and the structure are modelled neglecting the gravity effects (for instance, no gravitational force).

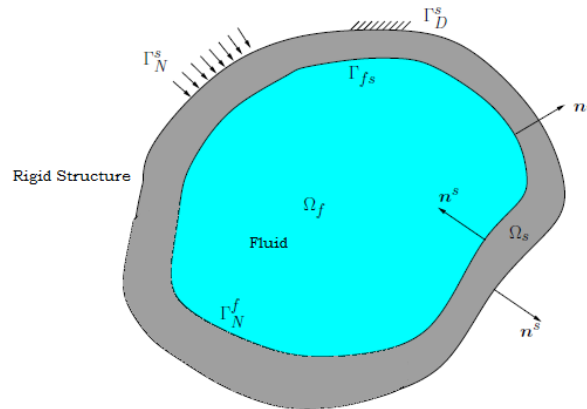


FIGURE 5.2: Continuum coupled system (*fluid and structure*) General domain

Referring at (figure 5.2), the structure occupies the domain Ω_s . The general structure could be subjected to Dirichlet boundary conditions Γ_s^D , which prescribe the applied displacement; and to Neumann boundary conditions Γ_s^N , which prescribe the applied force on the control volume.

The interior fluid domain is denoted by Ω_f and Γ_{fs} is the fluid-structure interface surface. The fluid boundary Γ_N^f describes the rigid walled bounds of the fluid

filled cavity, where the zero normal pressure gradient boundary condition is strictly imposed. Please keep in mind that, in this work, the whole structure is assumed to be rigid, so at this level, the intermediate surface is important for the coupling problem.

As common in structural problem, The linearized deformation tensor is later denoted by ϵ_{ij} and the corresponding stress tensor by σ_{ij} , while the mass density of the structure is denoted by ρ_s , while c_f and ρ_f are the constant speed of sound $[m/s]$ and mass density $[Kg/m^3]$ of the fluid. Finally n_{se} is the unit normal external to general Ω_s and n_{si} is the unit normal internal to general Ω_s , but with the assumption that the interested structure is composed with parallel wall, the following condition $n_{se} = -n_{si}$ is valid, or viceversa.

This problem could be divided in two different subsystem: **Structure** and **Fluid**, described by different set of equation. Let us start with the structure subsystem. The equations that describes the elastic **behaviour of the structure** are

$$\sigma_{ij,j} = \rho_s \frac{\partial^2 s}{\partial t^2} \quad \text{on } \Omega_s \quad (5.1)$$

$$\sigma_{ij} n_j^s = f_i \quad \text{on } \Gamma_N^s \quad (5.2)$$

$$s_i = s_i^{assigned} \quad \text{on } \Gamma_D^s \quad (5.3)$$

$$\sigma_{ij} n_j^s = p n_i^f \quad \text{on } \Gamma_{fs} \quad (5.4)$$

The previous formula represent the resolution set for the structure subsystem, and keep in mind that the Einstein notation is used. The first equation (5.1) describe the Dynamic Structural behaviour (since the derivation in time is presented), while the last one (5.4) represents the equality of stress (force per unit of surface) applied on the structure with the pressure on fluid domain (force per unit of surface), while the middle ones [(5.2) and (5.3)] represent the equation for the boundary condition, for Neumann and Dirichlet respectively.

Finally, The derivation of *fluid domain* equation is introduced. The **acoustic field** inside the cavity, assuming in absence of sound sources, is described by the wave equation and the following boundary conditions

$$p_{,ii} = \frac{1}{c_f^2} \frac{\partial^2 p}{\partial t^2} \quad \text{on } \Omega_f \quad (5.5)$$

$$p_{,i} n_i^f = -\rho_f \frac{\partial^2 s}{\partial t^2} n_i^f \quad \text{on } \Gamma_{fs} \quad (5.6)$$

$$p_{,i} n_i^f = 0 \quad \text{on } \Gamma_D^f \quad (5.7)$$

where the first equation (5.5) represents the globally known "wave equation" for the transmission of signal through a fluid domain. The second one (5.6) is valid when the boundary wall of the structure is elastically modified in order to consider wall deformation, where the normal pressure gradient is related to the motion of the structure on the interface surface, while the last one (5.7) expresses the null normal pressure gradient.

The previous last two set of equation represents the whole general behaviour of system (fluid and structure) coupled written in formal way. Later we will specify them for our numerical case.

The *stress tensor* σ_{ij} are related to the linearized *strain tensor* ϵ_{kl} through the linear constitutive relation

$$\sigma_{ij} = c_{ijkl} \epsilon_{kl} \quad (5.8)$$

where the linearized *strain tensor* ϵ_{kl} and the *displacement* s_k

$$\epsilon_{kl} = \frac{1}{2} (s_{k,l} + s_{l,k}) \quad (5.9)$$

5.3 The Variational Formulation

A generic weak formulation is reached, introducing arbitrary weighting functions which are exactly the field variables (displacement and pressure) which describe the evolution of the coupled system previously introduced; This procedure is equivalent to the *Principle of Virtual Displacement (PVD)* applied on the same system.

We maintain the coupled problem divided, and firstly we consider the structure and later the acoustic domain. The former is obtained by integrating over Ω_s and multiplying the dynamic equilibrium of system by arbitrary time-independent test-function δs_i (or *virtual displacement*).

$$\int_{\Omega_s} \partial \epsilon_{ij} \sigma_{ij} dV + \int_{\Omega_s} \partial s_i \rho_s \frac{\partial^2 s}{\partial t^2} dV = \int_{\partial \Omega_s} \partial s_i \sigma_{ij} n_j^s ds \quad (5.10)$$

where $\partial \epsilon_{ij} = \frac{1}{2} (\partial s_{k,l} + \partial s_{l,k})$. Now distributing the right hand side integrals over the boundaries, and coupling the acoustic fluid, we obtain

$$\int_{\Omega_s} \partial \epsilon_{ij} \sigma_{ij} dV + \int_{\Omega_s} \partial s_i \rho_s \frac{\partial^2 s}{\partial t^2} dV = \int_{\Gamma_N^s} \partial s_i f_i ds + \int_{\Gamma_{fs}} \partial s_i p n_i ds \quad (5.11)$$

This is the **PVD statement** for the mechanical variables including the acoustic coupling term. This formulation exactly satisfy, in a weak formulation, the natural boundary conditions, that is the Neumann type boundary condition, because

the virtual displacement ∂s_i must be chosen according with the essential conditions, Dirichlet type. Everything is in accordance with the *Principle of Virtual Displacement (PVD)* statement.

In the end, multiplying the wave equation of system (equation (5.5)) by ∂p , integrating by parts, and applying Green's formula and using the Neumann boundary condition on the fluid-structure coupled interface surface, we obtain

$$\int_{\Omega_s} \partial p_{,i} p_{,i} dV + \int_{\Omega_f} \frac{1}{c_f^2} \partial p_{,i} \frac{\partial^2 p}{\partial t^2} dV = - \int_{\Gamma_{fs}} \partial p \rho_f \frac{\partial^2 s_i}{\partial t^2} n_i ds \quad (5.12)$$

The fluid-structure coupling appear evident in the terms in the right hand side of the structural and fluid equations (5.11) and (5.12) respectively.

Our procedure was firstly based on the introduction of the *general equation set*, then expressing the *weak form*, through the PVD statement; later we have to proceed with the *numerical approximation*, since our goal is the resolution set.

5.4 The Numerical Approximation

The Finite Elements Method is usually applied for the analysis of sound field in bounded or nearly bounded domains (within small dimension). The basic concept of *FEM in acoustics* is **exactly** the **same** than in pure structural analysis. The domain is divided in elements sharing a common border, so that substantially smaller than the highest frequency of interest. The Acoustic field problem determination is shifted from the original problem of determining the pressure field at any position in the fluid within a domain to determination the pressure values at some discrete position of the domain, nodal (3D element). Within each element the pressure is approximated as a expansion in terms of shape functions. The main **drawback** is related to the *problem size*.

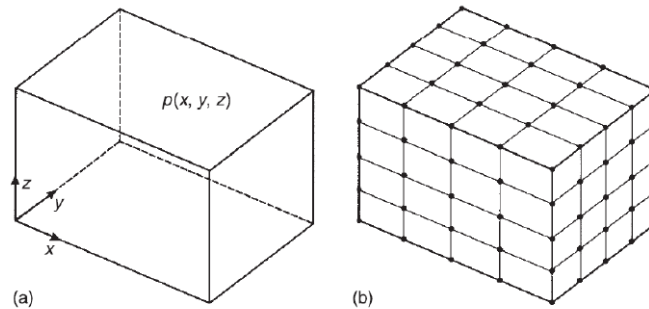


FIGURE 5.3: (a) Entire Acoustic Cavity (b) Finite Elements Mesh 3D

The fluid region is divided in elements and field values are assigned to the elements nodes. The finest is the mesh, and better the solution is captured within the volume. This problem is a function of the frequency, so a particular rule of thumb valid for lower frequency region may not be also valid for higher range and viceversa; this fact complicate everything.

As previously introduced, In order to obtain a numerical solution of the coupled system, in term of displacement (u, v, w) a pressure p ; an approximation of variable set has to be considered, as follows

$$s_i = \mathbf{N}_i^s \mathbf{U} \quad (5.13)$$

$$p = \mathbf{N}^p \mathbf{P} \quad (5.14)$$

where \mathbf{N}_i^s and \mathbf{N}^p are generic column matrices functions of the space coordinates x_i , which interpolates the continuous unknown variables; while \mathbf{U} and \mathbf{P} are the value of displacement (or pressure, respectively) at the nodal position mesh, through the discrete Finite Element Method.

With the introduction of equations (5.13) and (5.14) into equation (5.11) and (5.12), the resultant system of equations leads to the following sub matrices

$$\int_{\Omega_s} \partial \epsilon_{ij} c_{ijkl} \epsilon_{kl} dV = \partial \mathbf{U}^T \mathbf{K}_{ss} \mathbf{U} \quad (5.15)$$

$$\int_{\Omega_s} \partial s_i \rho_s \frac{\partial^2 s}{\partial t^2} dV = \partial \mathbf{U}^T \mathbf{M}_{ss} \mathbf{U} \quad (5.16)$$

$$\int_{\Gamma_N^s} \partial s_i f_i dV = \partial \mathbf{U}^T \mathbf{F}_s \mathbf{U} \quad (5.17)$$

$$\int_{\Gamma_{fs}} \partial s_i p n_i dV = \partial \mathbf{U}^T \mathbf{S}_{sp} \mathbf{P} \quad (5.18)$$

$$\int_{\Omega_f} \partial p_i p_i dV = \partial \mathbf{P}^T \mathbf{H} \mathbf{P} \quad (5.19)$$

$$\frac{1}{c^2} \int_{\Omega_f} \partial p \frac{\partial^2 p}{\partial t^2} dV = \partial \mathbf{P}^T \mathbf{Q} \frac{\partial^2 \mathbf{P}}{\partial t^2} \quad (5.20)$$

$$\rho_f \int_{\Gamma_{fs}} \partial p \frac{\partial^2 s_i}{\partial t^2} n_i ds = \rho_f \partial \mathbf{U}^T \mathbf{S}_{sp}^T \frac{\partial^2 \mathbf{P}}{\partial t^2} \quad (5.21)$$

where M_{ss} and K_{ss} are the *mass* and *stiffness* matrices of the *structure*; while \mathbf{Q} and \mathbf{H} are the *mass* and *stiffness* matrices of the *fluid*; S_{sp} is the fluid structure coupling matrix; F_s and F are the applied mechanical force applied.

It can be arranged as follows

$$\begin{bmatrix} M_{ss} & 0 \\ -\rho_f S_{sp}^T & 0 \end{bmatrix} \begin{bmatrix} \frac{\partial^2 \mathbf{U}}{\partial t^2} \\ \frac{\partial^2 \mathbf{P}}{\partial t^2} \end{bmatrix} + \begin{bmatrix} K_{ss} & S_{sp} \\ 0 & H \end{bmatrix} \begin{bmatrix} \mathbf{U} \\ \mathbf{P} \end{bmatrix} = \begin{bmatrix} F_s \\ 0 \end{bmatrix} \quad (5.22)$$

5.5 The Finite Element Method

The finite element discretization is based on a representation of the geometry and the unknown variables in terms of shape functions and nodal variables.

The analysis of a problem by FEM essentially consists of seven basic steps.

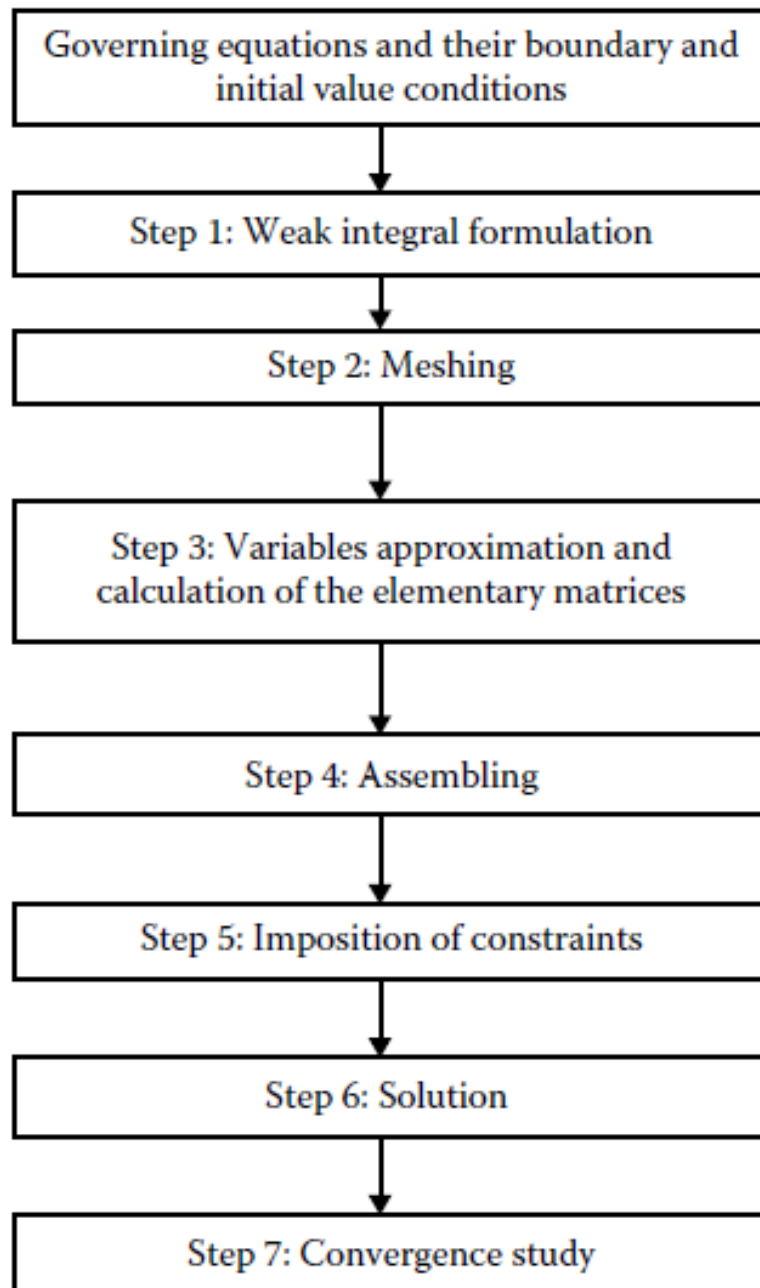


FIGURE 5.4: The seven steps of the FEM

The previous figure (5.4) summarizes the required steps for FEM analysis:

Step 1: Writing the weak (or variational) integral form of the equations governing the problem.

Step 2: Meshing or geometry discretization. It consists in breaking up the geometry of the domain Ω into a set of sub domains Ω_e called “the elements.” The sub domains are usually simple geometrical primitives (for instance, lines, triangles, quadrangles, tetrahedral).

Step 3: Approximation of variables and calculation of elementary matrices. It consists in defining on each sub domain Ω_e an approximate function of the exact desired function. This so-called nodal approximation function must have the following features: First of all, it must only involve the nodal variables attached to nodes located on Ω_e and its boundary; Second of all, it must be continuous on Ω_e . In addition, all nodal approximation functions must satisfy the continuity conditions between different sub domains. The calculation of the elementary matrices consist then in evaluating, on each sub domain Ω_e , the nodal approximation of the integral form, determined in previous step 1.

Step 4: Assembling. In this step, the elementary matrices are combined to form global matrices. In other words, the integral form is evaluated over the entire domain Ω . By doing so, continuity conditions between elements are enforced. *Step 5:* Imposition of boundary conditions or constraints.

Step 6: Invocation of stationary condition. This step will lead to a system of algebraic equations. This system is solved using conventional numerical algorithms.

Step 7: Study of the convergence of the solution; calculation of physical indicators, and interpretation of results.

In the finite elements methods, steps (1) and (2) are part of the *preprocessing* phase, while step (7) is part of the *post processing* phase.

Criterion of Building a Mesh

If we choose a partition of domain Ω constituted of n_e elements Ω_e . The nodes of the elements are numbered sequentially from 1 to n_N where n_N is the total number of nodes.

To define the mesh completely, **two tables** are built: a *table of coordinates* denoted as $XYZ(:, :)$ (denoted as NODES file) and a *connectivity table* referred to as IEN $(:, :)$.

Table of coordinates: Table $XYZ(:, :)$ of dimension $n_d \times n_N$ contains the coordinates of the nodes (n_d is the geometrical dimension of the problem; $n_d = 3$ in the three-dimensional case, the case of our interest; while $n_d = 2$ in the bi-dimensional case). (denoted as CONNECTIVITY file)

Table of Connectivity Dimension $n_{ne} \times n_e$ establishes the correspondence between the local and the global numbering of the nodes, where n_{ne} is the total number of nodes per a single element and n_e represents the total number of elements constituting the mesh.

As sake of simplicity, let me show a brief example of these two previous table for the following easy example; Illustrate these two tables, considering the following two-dimensional (2D for simplicity) mesh.

In this case, $n_d = 2$, $n_e = 6$, $n_{ne} = 4$, $n_N = 12$

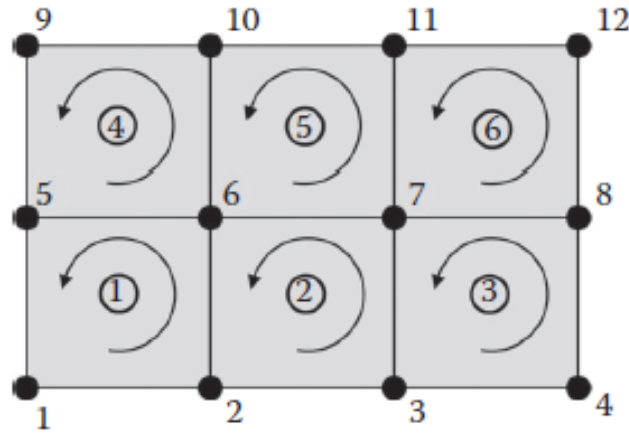


FIGURE 5.5: Bidimensional mesh.

In this simple case

Table of coordinates: $XYZ(1,i) = x_{1,i}$; $XYZ(2,i) = x_{2,i}$ for $i = 1, \dots, n_N$

Connectivity table:

		Element e					
		1	2	3	4	5	6
nodes (local numbering)	1	1	2	3	5	6	7
	2	2	3	4	6	7	8
	3	6	7	8	10	11	12
	4	5	6	7	9	10	11

FIGURE 5.6: Connectivity table

In following numerical test, We will build more complex tables. For example, The acoustic cavity is modelled by using 10x10x10 mesh 3D element; while the plate by using 10x10 mesh 2D element as the coupling surface. Keep in mind that the dimension of element plate and the projection 2D of a 3D mesh **must** have the same dimension for MUL2 program.

Nodal approximation of the variable

Since a general variable must be differentiable as a requirement, we need to select at least a linear approximation in order to evaluate it within the domain and to ensure inter-elements continuity.

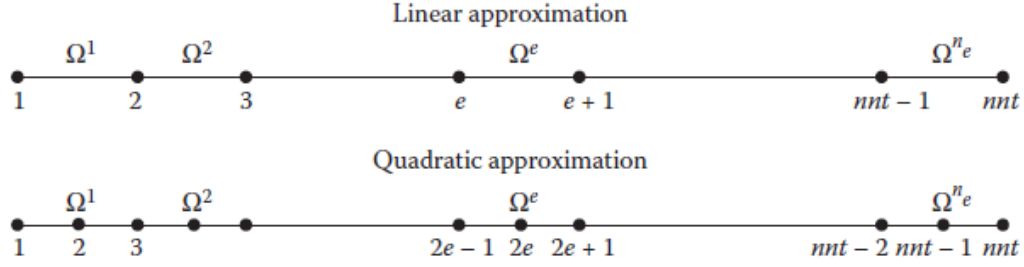


FIGURE 5.7: Two types of geometrical discretization of the one-dimensional problem

In the following test case, This is **very** important because we will discretize the thickness of the plate (normal displacement) as a 1D model; while in plane deformation will be discretized through a 2D model.

For sake of simplicity, here we are going to discuss just two these simple cases, but please keep in mind that it can be used for more order, obtaining more precise results.

The first line represents a two-noded linear element, knowing the values of the normal displacement w_1 and w_2 at the two nodes of the element, we seek to construct a linear approximation of displacement w within the element as follows

$$w(x) = ax + b \quad (5.23)$$

In consequence,

$$w(x_1^e) = w_1 = ax_1 + b \quad \text{and} \quad w(x_2^e) = w_2 = ax_2 + b \quad (5.24)$$

This leads to

$$w(x) = \frac{x_2^e - x}{x_2^e - x_1^e} w_1^e + \frac{x - x_1^e}{x_2^e - x_1^e} w_2^e = \sum_{i=1}^2 N_i^e(x) w_i^e \quad (5.25)$$

The nodal interpolation functions $N_i^e(x)$ must satisfy precise conditions, first of all, they should only involve the nodal variables attached to the nodes of the element. They must be continuous across the element and differentiable as required by the weak integral form. In general, polynomial functions are chosen to construct

nodal interpolation functions since the process is simple and the numerical evaluation of the integrals involved in the weak integral form is easy. When the interpolation functions are polynomials, these polynomials must be complete in order to represent all possible variations of the independent variable.

If we repeat the same procedure as shown for the linear but considering second order, we obtain *Quadratic approximation*

$$w(x) = a + bx + cx^2 \quad (5.26)$$

This is mostly used for discretize thicknesses along plate in the FE application method.

Assembling and Imposition of constraints

The assembly procedure consists in writing this sum in terms of the vectors of nodal unknowns. Doing so requires the continuity of the variable between elements. Later, the imposition of constraints and boundary condition of the problem. By the Structural point of view, two different boundary condition may be imposed.

Simply supported and Clamped

We have introduced in this part the fundamental concepts of FEM. The seven-step-based methodology was introduced and illustrated via several examples. Later we proceed with UFEM (*Unified Finite Element Model*), notation which permits the complete unification for the resolution method.

5.6 Generalized Hooke's law

Constitutive equations characterize the individual material and its reaction to applied loads. In the following, we are considering **just Elastic materials** are considered, for which the constitutive behaviour is only a function of the current state of deformation, neglecting the load history path.

A material body is **homogeneous** if its properties are the same throughout the body, it is called *heterogeneous* if the material properties are a function of position. The material is defined *anisotropic* if it has different material properties in different directions at a given point: the material properties are direction-dependent function. An *isotropic* body has the same material properties in all directions at a point. The material is called hyper-elastic if the work done by the stresses during the deformation depends only on the initial state and the current configuration.

The material is defined as **elastic** if it recovers its original form completely upon removal of the forces causing deformations, making it possible an exact relationship between the state of stress and the state of strain in the current configuration exists. In the following, the most-general constitutive equations of linear elasticity is considered for the case of infinitesimal deformations, known as **generalized Hooke's law**.

Furthermore, we can suppose that the reference configuration has a residual stress state indicated with σ_0 . First of all, we are considering the **most general case**, then we reduce the scalar components

$$\sigma_{ij} = C_{ijkl} \epsilon_{kl} + \sigma_{ij}^0 \quad (5.27)$$

where C_{ijkl} is called *stiffness tensor*. In general, it has 81 scalar components. The number of independent components of C_{ijkl} can be reduced considering both the symmetry of σ_{ij} and the symmetry of ϵ_{kl} . The number of independent material stiffness components (presented in Stiffness tensor) is reduced to 54 for the principle of angular momentum, making the stress tensor is symmetric ($\sigma_{ij} = \sigma_{ji}$) and the tensor C_{ijkl} is symmetric in the first two subscripts. The strain tensor is symmetric too, $\epsilon_{kl} = \epsilon_{lk}$, then C_{ijkl} is symmetric in the last two subscripts kl ; in this way the number of independent material stiffness components is reduced to 36; then If we also assume the material hyper-elastic $C_{ijkl} = C_{klij}$, the last statement permits us to reduce the number of independent material stiffness components from 36 to 21, making it possible the double subscript notation for the material stiffness coefficients

$$\sigma_i = C_{ij} \epsilon_j + \sigma_i^0 \quad (5.28)$$

The subscript notation (5.6) for stresses and strains is called **engineering notation or Voigt notation** relation.

The notation for stresses and strains is

$$\begin{aligned}\sigma_1 &= \sigma_{11}, \sigma_2 = \sigma_{22}, \sigma_3 = \sigma_{33}, \sigma_4 = \sigma_{23}, \sigma_5 = \sigma_{13}, \sigma_6 = \sigma_{12}, \\ \epsilon_1 &= \epsilon_{11}, \epsilon_2 = \epsilon_{22}, \epsilon_3 = \epsilon_{33}, \epsilon_4 = 2\epsilon_{23}, \epsilon_5 = 2\epsilon_{13}, \epsilon_6 = 2\epsilon_{12}, \\ 11 &\rightarrow 1, 22 \rightarrow 2, 33 \rightarrow 3, 23 \rightarrow 4, 13 \rightarrow 5, 12 \rightarrow 6,\end{aligned}$$

In matrix notation, 5.6 can be written

$$\begin{pmatrix} \sigma_1 \\ \sigma_2 \\ \sigma_3 \\ \sigma_4 \\ \sigma_5 \\ \sigma_6 \end{pmatrix} = \begin{bmatrix} C_{11} & C_{12} & C_{13} & C_{14} & C_{15} & C_{16} \\ C_{21} & C_{22} & C_{23} & C_{24} & C_{25} & C_{26} \\ C_{31} & C_{32} & C_{33} & C_{34} & C_{35} & C_{36} \\ C_{41} & C_{42} & C_{43} & C_{44} & C_{45} & C_{46} \\ C_{51} & C_{52} & C_{53} & C_{54} & C_{55} & C_{56} \\ C_{61} & C_{62} & C_{63} & C_{64} & C_{65} & C_{66} \end{bmatrix} \begin{pmatrix} \epsilon_1 \\ \epsilon_2 \\ \epsilon_3 \\ \epsilon_4 \\ \epsilon_5 \\ \epsilon_6 \end{pmatrix} + \begin{pmatrix} \sigma_1^0 \\ \sigma_2^0 \\ \sigma_3^0 \\ \sigma_4^0 \\ \sigma_5^0 \\ \sigma_6^0 \end{pmatrix}$$

So, for the most general elastic material, we have 21 independent stiffness coefficients. The previous equations are also invertible and the strain components can be expressed to stress ones by

$$\epsilon_i = S_{ij}\sigma_j + \epsilon_i^0, \quad \epsilon_i^0 = -S_{ij}\sigma_j^0 \quad (5.29)$$

where S_{ij} are the material compliance parameters, where $[S] = [C]^{-1}$. In the next part of this chapter we consider as reference configuration the stress and strain **free configuration**: $\sigma_j^0 = 0$ and $\epsilon_j^0 = 0$.

Further reduction in the number of independent stiffness parameters comes from the so-called material symmetry, considering the existence **material plane of symmetry**, where points mean present values for every pair of coordinate systems that are mirror images of each other in a certain plane in symmetry. We will discuss about various plane of symmetry and forms of associated stress-strain relations, in particular **monoclinic materials**, **orthotropic materials** and **isotropic materials**.

Monoclinic materials

When the elastic coefficients at a point have the same value for every pair of coordinate systems which are the mirror images of each other with respect to a plane material is called a *monoclinic material*. So the independent parameters are $21 - 8 = 13$.

$$C_{14} = C_{15} = C_{24} = C_{25} = C_{34} = C_{35} = C_{46} = C_{56} = 0 \quad (5.30)$$

In matrix notation, for **Monoclinic materials**, 5.6 can be written

$$\begin{Bmatrix} \sigma_1 \\ \sigma_2 \\ \sigma_3 \\ \sigma_4 \\ \sigma_5 \\ \sigma_6 \end{Bmatrix} = \begin{bmatrix} C_{11} & C_{12} & C_{13} & 0 & 0 & C_{16} \\ C_{12} & C_{22} & C_{23} & 0 & 0 & C_{26} \\ C_{13} & C_{23} & C_{33} & 0 & 0 & C_{36} \\ 0 & 0 & 0 & C_{44} & C_{45} & 0 \\ 0 & 0 & 0 & C_{45} & C_{55} & 0 \\ C_{16} & C_{26} & C_{36} & 0 & 0 & C_{66} \end{bmatrix} \begin{Bmatrix} \epsilon_1 \\ \epsilon_2 \\ \epsilon_3 \\ \epsilon_4 \\ \epsilon_5 \\ \epsilon_6 \end{Bmatrix}$$

So the independent parameters are $21 - 8 = 13$.

Orthotropic materials

In *orthotropic materials* three mutually orthogonal planes of symmetry exist, so the number of independent elastic coefficients is reduced from 13 to 9. In matrix notation, for **Orthotropic materials**, 5.6 can be written

$$\begin{Bmatrix} \sigma_1 \\ \sigma_2 \\ \sigma_3 \\ \sigma_4 \\ \sigma_5 \\ \sigma_6 \end{Bmatrix} = \begin{bmatrix} C_{11} & C_{12} & C_{13} & 0 & 0 & 0 \\ C_{12} & C_{22} & C_{23} & 0 & 0 & 0 \\ C_{13} & C_{23} & C_{33} & 0 & 0 & 0 \\ 0 & 0 & 0 & C_{44} & 0 & 0 \\ 0 & 0 & 0 & 0 & C_{55} & 0 \\ 0 & 0 & 0 & 0 & 0 & C_{66} \end{bmatrix} \begin{Bmatrix} \epsilon_1 \\ \epsilon_2 \\ \epsilon_3 \\ \epsilon_4 \\ \epsilon_5 \\ \epsilon_6 \end{Bmatrix}$$

So the independent parameters are 9. The material properties are expressed in terms of the engineering constants such as *Young's modulus* E , *shear modulus* G and *Poisson's ratios* ν .

The material coefficients and engineering constants are expressed in the following

$$\begin{aligned} C_{11} &= \frac{1 - \nu_{23}\nu_{23}}{E_2 E_3 \Delta}, \quad C_{12} = \frac{\nu_{21} + \nu_{31}\nu_{23}}{E_2 E_3 \Delta} = \frac{\nu_{12} + \nu_{32}\nu_{13}}{E_1 E_3 \Delta} \\ C_{13} &= \frac{\nu_{31} + \nu_{21}\nu_{32}}{E_2 E_3 \Delta} = \frac{\nu_{13} + \nu_{12}\nu_{23}}{E_1 E_2 \Delta} \\ C_{22} &= \frac{1 - \nu_{13}\nu_{31}}{E_1 E_3 \Delta}, \quad C_{23} = \frac{\nu_{32} + \nu_{12}\nu_{31}}{E_1 E_3 \Delta} = \frac{\nu_{23} + \nu_{21}\nu_{13}}{E_1 E_3 \Delta} \\ C_{33} &= \frac{1 - \nu_{12}\nu_{21}}{E_1 E_2 \Delta}, \quad C_{44} = G_{23}, \quad C_{55} = G_{31}, \quad C_{66} = G_{12} \\ \Delta &= \frac{1 - \nu_{12}\nu_{21} - \nu_{23}\nu_{32} - \nu_{31}\nu_{13} - 2\nu_{21}\nu_{32}\nu_{13}}{E_1 E_2 E_3} \end{aligned}$$

Isotropic materials

When there is no **preferred directions** in the material, thus infinite number of planes of material symmetry are considered. Such materials are called **isotropic** and the number of independent elastic coefficients are reduced from 9 to 2.

In matrix notation, for **Isotropic materials**, 5.6 can be written

$$\begin{Bmatrix} \sigma_1 \\ \sigma_2 \\ \sigma_3 \\ \sigma_4 \\ \sigma_5 \\ \sigma_6 \end{Bmatrix} = \Lambda \begin{bmatrix} 1-\nu & \nu & \nu & 0 & 0 & 0 \\ \nu & 1-\nu & \nu & 0 & 0 & 0 \\ \nu & \nu & 1-\nu & 0 & 0 & 0 \\ 0 & 0 & 0 & \frac{1}{2}(1-2\nu) & 0 & 0 \\ 0 & 0 & 0 & 0 & \frac{1}{2}(1-2\nu) & 0 \\ 0 & 0 & 0 & 0 & 0 & \frac{1}{2}(1-2\nu) \end{bmatrix} \begin{Bmatrix} \epsilon_1 \\ \epsilon_2 \\ \epsilon_3 \\ \epsilon_4 \\ \epsilon_5 \\ \epsilon_6 \end{Bmatrix}$$

where

$$G = \frac{E}{2(1+\nu)} \quad (5.31)$$

An Alternative stress-strain relations can be written in a compact form by using 2 different independent constants known as **Lamè constants** λ and μ . The relations between the Lamè constants λ and μ and engineering constants E , G and are obtained as in the following

$$E = \frac{\mu(3\lambda + 2\mu)}{(\lambda + \mu)} \quad \nu = \frac{\lambda}{2(\mu + \lambda)} \quad G = \mu$$

5.7 Unified Finite Element Model

The formulation of the structural coupled acoustic problem in terms of structural displacements unknown s_i and acoustic pressure p previously presented (in general form) will be specified for generic laminated plates made of orthotropic materials in contact with an acoustic cavity.

Throughout the *Constitutive equation*

$$\sigma = C^* \epsilon \quad (5.32)$$

where

$$\sigma^T = [\sigma_{11} \quad \sigma_{22} \quad \sigma_{33} \quad \sigma_{23} \quad \sigma_{13} \quad \sigma_{12}] \quad (5.33)$$

$$\epsilon^T = [\epsilon_{11} \quad \epsilon_{22} \quad \epsilon_{33} \quad \epsilon_{23} \quad \epsilon_{13} \quad \epsilon_{12}] \quad (5.34)$$

$$C^* = \begin{bmatrix} C_{11} & C_{12} & C_{13} & 0 & 0 & 0 \\ C_{12} & C_{22} & C_{23} & 0 & 0 & 0 \\ C_{13} & C_{23} & C_{33} & 0 & 0 & 0 \\ 0 & 0 & 0 & C_{44} & 0 & 0 \\ 0 & 0 & 0 & 0 & C_{55} & 0 \\ 0 & 0 & 0 & 0 & 0 & C_{66} \end{bmatrix} \quad (5.35)$$

where the symmetric matrix C^* (material reference frame) grouped the 21 independent elastic material properties, reduced by energetic consideration. Further reduction in the number of independent material parameters comes from the material symmetry, for example, material parameters can exhibit *symmetry properties* about specific directions (for instance, the existence material planes of symmetry), and the structure of the matrix C is modified consequently. Just two different independent parameter exists: E (Young's modulus), and ν (Poisson's Modulus)

$$G = \frac{E}{2(1 + \nu)} \quad (5.36)$$

We consider two different type of material: Isotropic and Orthotropic. The former, when no preferred directions exist in the material properties, infinite number of planes of material symmetry are considered, the number of independent parameters reduces from 9 to 2; while for the latter, three mutually orthogonal planes of symmetry exist, then the number of independent elastic, reducing the independent elastic coefficient from 21 to 9.

The constitutive equations with the material matrices described above are referred to the principal material directions (*Local Reference System*), indicated with pedices 1, 2 and 3. It is necessary to describe the same relations in the plate reference

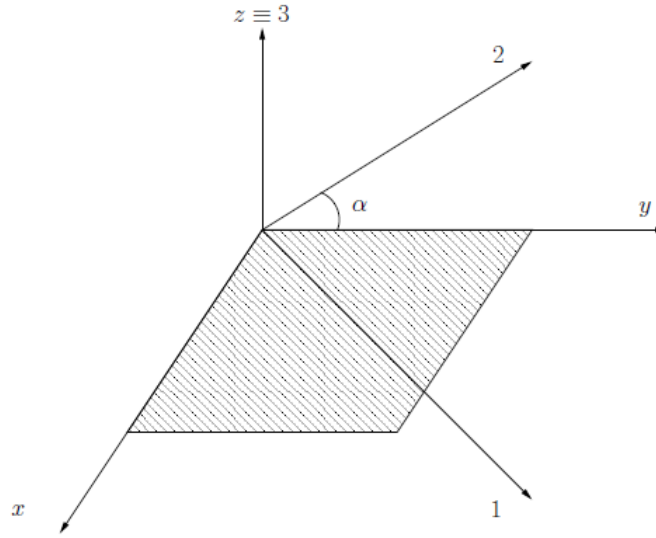


FIGURE 5.8: Definition of the *PLATE* Reference System (x, y, z) and Material one $(1, 2, 3)$

system (*Laminate Reference System*)(x, y, z). They are different because different ply may be oriented in different direction α , that is because different layers may exhibit different material symmetry directions.

Indicating with α the angle between the in plane material coordinates $(1, 2)$ and the plate coordinates (x, y) , we can define the rotation matrix

$$R = \begin{bmatrix} \cos^2\alpha & \sin^2\alpha & 0 & 0 & 0 & -\sin 2\alpha \\ \sin^2\alpha & \cos^2\alpha & 0 & 0 & 0 & \sin 2\alpha \\ 0 & 0 & 1 & 0 & 0 & 0 \\ 0 & 0 & 0 & \cos\alpha & -\sin\alpha & 0 \\ 0 & 0 & 0 & \sin\alpha & \cos\alpha & 0 \\ \frac{-\sin 2\alpha}{2} & \frac{\sin 2\alpha}{2} & 0 & 0 & 0 & \cos^2\alpha - \sin^2\alpha \end{bmatrix} \quad (5.37)$$

Therefore, The constitutive equation in the rotation reference (plate reference frame) holds as follows

$$C = R^T C^* R \quad (5.38)$$

Condensed notation for Mechanical Problems

In this section, we proceed to the rearrangement in a more suitable form of the formula previously explained. In this way, a compact form for the Mechanical PVD is introduced.

First of all, let us introduce the vector U_k containing the unknowns of the composite plate in terms of displacement s_k as follows

$$U_k = [s_k] = [u_k \ v_k \ w_k]^T \quad (5.39)$$

where the superscript $(.)_k$ indicates that the variables refer to the k th layer of the plate. Please keep in mind that we are going to separate the initial 3D structural problem, into the resolution of two of different dimension: **2D** for the in-plane displacement (*planar*); while **1D** for the out-plane displacement (*normal*).

$$\epsilon^T = \begin{bmatrix} \epsilon_{11} \\ \epsilon_{22} \\ \epsilon_{12} \\ \epsilon_{33} \\ \epsilon_{13} \\ \epsilon_{23} \end{bmatrix} = \begin{bmatrix} \epsilon_{planar} \\ \epsilon_{normal} \end{bmatrix} \quad (5.40)$$

$$\sigma^T = \begin{bmatrix} \sigma_{planar} \\ \sigma_{normal} \end{bmatrix} = [C] [\epsilon_{planar} \ \epsilon_{normal}]^T \quad (5.41)$$

$$\sigma^T = \begin{bmatrix} \sigma_{11} \\ \sigma_{22} \\ \sigma_{12} \\ \sigma_{33} \\ \sigma_{13} \\ \sigma_{23} \end{bmatrix} = \begin{bmatrix} \sigma_{planar} \\ \sigma_{normal} \end{bmatrix} \quad (5.42)$$

Defining the following differential matrix, we can rewrite

$$D = \begin{bmatrix} \frac{\partial}{\partial x} & 0 & 0 & 0 \\ 0 & \frac{\partial}{\partial y} & 0 & 0 \\ \frac{\partial}{\partial y} & \frac{\partial}{\partial x} & 0 & 0 \\ 0 & 0 & 0 & -\frac{\partial}{\partial x} \\ 0 & 0 & 0 & -\frac{\partial}{\partial y} \\ 0 & 0 & \frac{\partial}{\partial z} & 0 \\ \frac{\partial}{\partial z} & 0 & \frac{\partial}{\partial x} & 0 \\ 0 & \frac{\partial}{\partial z} & \frac{\partial}{\partial y} & 0 \\ 0 & 0 & 0 & -\frac{\partial}{\partial z} \end{bmatrix} \quad (5.43)$$

We have

$$\Psi^k = D U^k \quad (5.44)$$

$$S^k = C^k \Psi^k = C^k D U^k \quad (5.45)$$

This matrix formalism for the treatment of the structural variables permits to rewrite the variational formulation (previously introduced) in a more compact form that is useful for the introduction of the UF and for the next numerical approximation by FE method. From the coupling structure-fluid, we had

$$\int_{(\Omega_s)^k} \partial \Psi_k^T S^k dV = \int_{(\Omega_s)^k} \partial (U^k)^T f_m^k dV + \int_{\Gamma_{sf}} \partial (U_{assigned}^k)^T f_{sf} ds \quad (5.46)$$

$$\int_{\Omega_f} \partial p_{,i} p_{,i} dV = - \int_{\Omega_f} \frac{1}{c_f^2} \partial p \frac{\partial^2 p}{\partial t^2} dV - \int_{\Gamma_{fs}} \partial p f_{fs} ds \quad (5.47)$$

where

$$f_m^k = \begin{bmatrix} -\rho_s \frac{\partial^2 s}{\partial t^2} \\ 0 \end{bmatrix} \quad (5.48)$$

$$f_{sf} = p \begin{bmatrix} n \\ 0 \end{bmatrix} \quad (5.49)$$

$$f_{fs} = \rho_f [n^t 0] \frac{\partial^2 U^k}{\partial t^2} \quad (5.50)$$

are, respectively, the mechanical inertial load and, the fluid-structure mutual loads. It can be highlighted that the first term of the **first** equation of system is the *internal work* associated with the generic orthotropic layer k, while the right hand side terms are the *external work* done for the structural variable U at layer k, including the inertia of the structure and the fluid loading acting only on the displacement field s. In the **second** equation, the left hand side term is the *internal work* of the acoustic cavity, while the acoustic inertial loading and the fluid-structure coupling term are on the right side. It is shown that the fluid-structure coupling term refers only to the structural variables at layer k and then no summation has to be applied for this term; indeed, only the lamina in contact with the enclosed fluid modifies the boundary condition of the acoustic field.

5.8 Structural Hypothesis Through-the-thickness for primary variables

As previously introduced, we divide the dependence of the 3D initial problem throughout the application of a 2D model which permits to express the unknown variables as a set of thickness function depending only on the thickness coordinate z, and the correspondent coefficients depending on the in-plane plate coordinates x and y, expressed in the plate reference frame [4]. The generic variable $g(x, y, z, t)$ and its variation $\partial g(x, y, z)$ may be written as follows

$$g(x, y, z, t) = F_\tau(z) g_\tau(x, y, t) \quad (5.51)$$

$$\partial g(x, y, z) = F_\tau(z) \partial g_\tau(x, y) \quad (5.52)$$

with

$$\tau = 1, \dots, N. \quad (5.53)$$

The summing convention with repeated index τ is assumed. The order of expansion goes from 1 to higher order values N and the models can be **ESL** (*Equivalent Single Layer*) or **LW** (*Layers Ways*). In the former the expansion variables are assumed for the whole plate, and a Taylor expansion centered on the mid-plane is employed as thickness functions, with z that varies from $-h/2$ and $h/2$, where h is the whole plate thickness. In LW philosophy, In the latter the variable is considered independent in each layer and Lagrange polynomials are assumed as thickness functions, where z is defined in the local thickness coordinate for the k -th layer and goes from -1 (assumed, the bottom of layer k) to 1 (assumed, the top of layer k); different from the previous.

5.8.1 Equivalent Solid Layer (ESL) Approach

This group of theories arises from the basic Kirchhoff plate theory. The composite structure is considered as an integral equivalent layer. ESL gives sufficiently accurate global laminate response but they are inadequate if stresses at ply level are required. In addition, they may lead to inaccurate results in case of high anisotropy or localized loads.

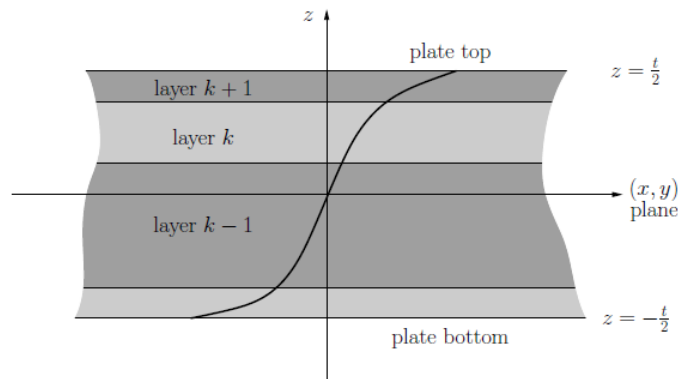


FIGURE 5.9: (ESL) Approach

the thickness expansion for s is obtained via Taylor polynomials, then for each scalar displacement component

$$s(x, y, z, t) = F_0 s_0 + F_1 s_1 + \dots + F_N s_N = F_\tau(z) s(x, y, t) \quad (5.54)$$

$$F_\tau = z^\tau \quad (5.55)$$

Therefore the independent variables become the mid-plane displacements u_0, v_0 and w_0 and their high order derivatives.

5.8.2 Layer Wise (LW) Approach

The composite structure is thought composed of independent layers. This approach may be considered mandatory for a full (and complete) 3D description of the stress-strain state in laminates. The description of the cross sectional deformation of each layer may be inaccurate and normally the continuity of transverse shear stresses among layers is not satisfied a priori [4].

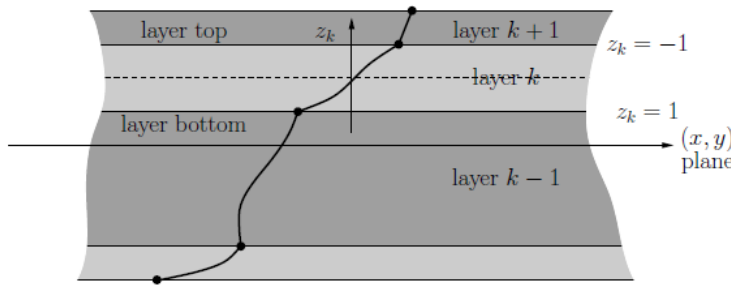


FIGURE 5.10: LW model

Applying this theory, we obtain

$$s^k(x, y, z_k, t) = F_\tau(z_k) s_\tau^k(z, y, t) \quad (5.56)$$

Each layer of a multi-layered structure is described as an independent plate. The displacement s_k is described for each layer, satisfying naturally the continuity piece-function form of displacement. The variables at top and bottom of each layer permit to satisfy the displacement continuity at the layer interfaces. LW description of the plate allows easily to an accurate 3D description of the boundary conditions and the relative applied stress.

Using the **condensed structural variable** U previously introduced

$$U^k(x, y, z, t) = F_\tau(z) U_\tau^k(x, y, t) \quad (5.57)$$

Please keep in mind that, when ESL description is employed, z indicates the whole plate thickness coordinate, whereas for LW assumption, z indicates the k th lamina local thickness coordinate.

Starting from the fundamental nucleus, the general stiffness matrix of the considered multilayer is obtained by expanding via the index r in case of FGM layers, via the indexes τ and s for the order of expansion in the thickness direction and via the index k for the multilayer assembling for both equivalent single layer (ESL) and LayerWise (LW).

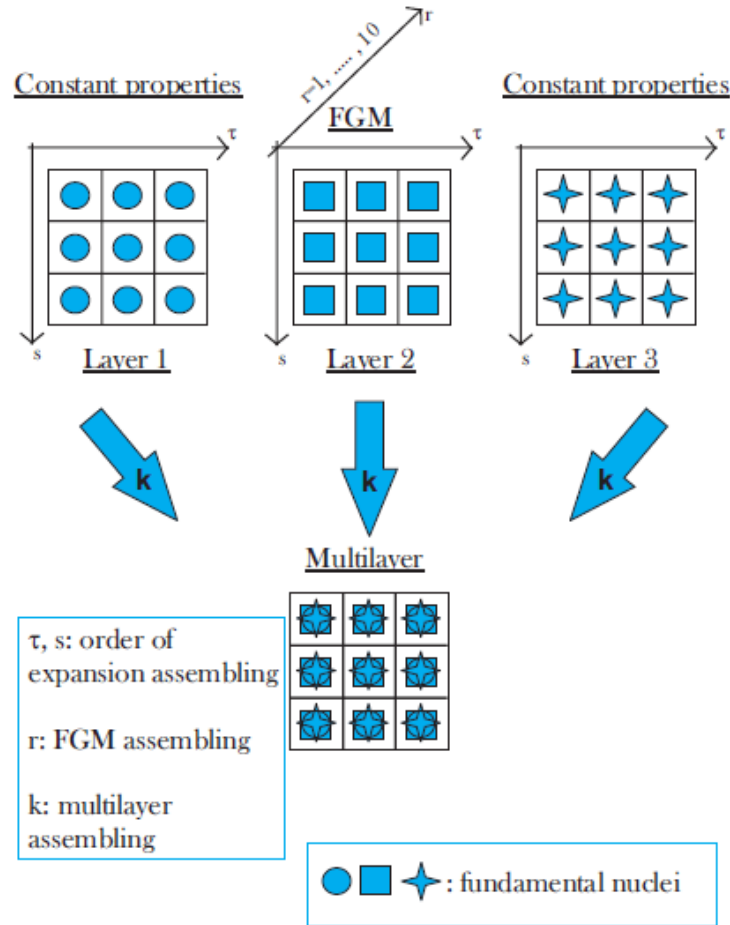


FIGURE 5.11: Three layered structure with the internal layer in assembling Equivalent Single Layer (ESL) assembly procedures.

For composite structures in ESL (Equivalent Single Layer) theory for layer expansion, all the layers accumulate (see 5.11) but in layer-wise approach all the layers expand like finite element assemblage with considering the continuity condition between the layers (see 5.12). In the latter point of view, The assembly procedure leads to a bigger matrix and thus a huge calculation time needed. Actran is based on ESL, while MUL2 results on LW, This points out the fact that the latter presents more accurate results than the one reached in Actran, although the less computational time.

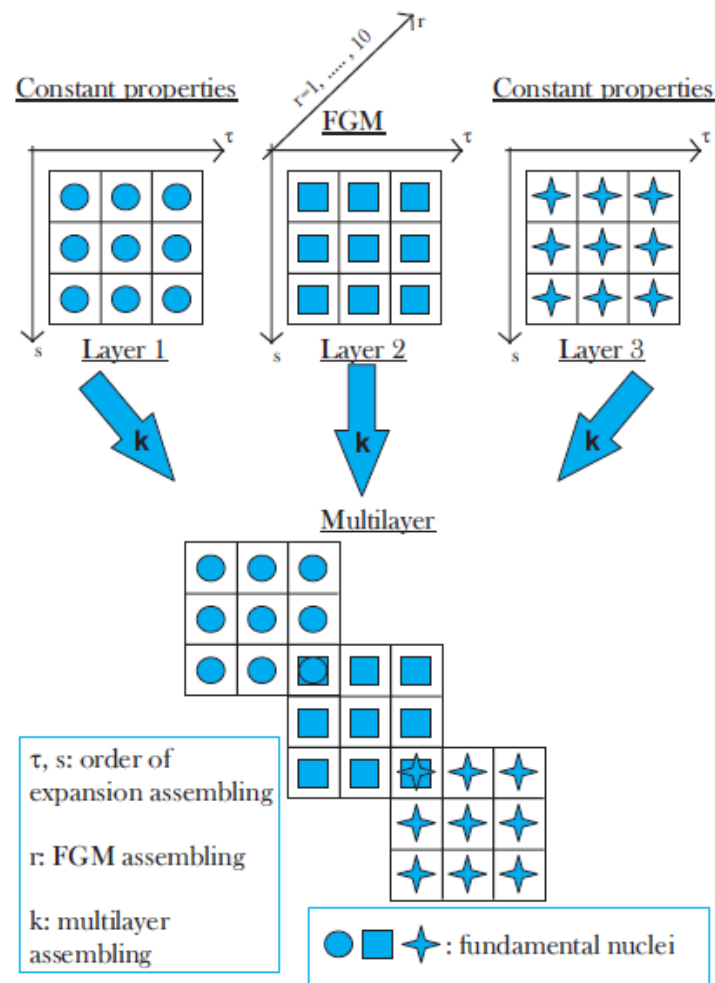


FIGURE 5.12: Three layered structure with the internal layer in assembling LayerWays (LW) assembly procedures.

5.8.3 Applying the Finite Element Approximation

We have largely talked about the main featured of FEM method. Now we are going to apply the previous rule, the structure coupled to fluid. In the FE implementation, the unknowns can be expressed in terms of their nodal values via appropriate shape functions N_i . Thus for the structural variable U^k and for the fluid scalar variable p we have

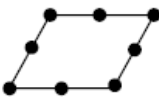
$$U_\tau^k(x, y, t) = N_i^s(x, y) Q_\tau^k(t) \quad (5.58)$$

$$p(x, y, z, t) = N_i^p(x, y, z) P_i(t) \quad (5.59)$$

where $i = 1, \dots, N^s : n$ for structure variables, with N_n^s denotes the number of nodes of the considered 2D structural element, and $i = 1, \dots, N_n^p$ for fluid variable, with N_n^p denotes the number of nodes of the considered 3D acoustic element. Q contains the FE nodal values of the thickness expansion coefficients provided by UF model for the plate subsystem. Finally, substituting

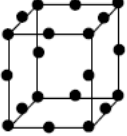
$$U^k(x, y, z, t) = F_\tau(z) N_i^s(x, y) Q_\tau^k(t) \quad (5.60)$$

In the Numerical test case of this dissertation, we will assume the following element For The *structural plate* discretization, and *the coupling surface*, QUAD9 element (with nine nodes) is used

Plate element types		
Element type	Element shape	Node number
QUAD		4 8 9

For The *Acoustic Domain* discretization, HEX27 element (with 27 nodes) is used

Acoustic element types

Element type	Element shape	Node number
HEXA		8 20 27

5.9 Derivation of Fundamental Matrices

In the following, the structural mass \mathbf{M} and stiffness matrix \mathbf{K} , the loads vector \mathbf{F} and the fluid coupling matrix \mathbf{S} are obtained in terms of *fundamental nuclei*, which are independent from the order of the considered expansion in the thickness direction.

5.9.1 Structural Stiffness Matrix

Let us consider the left hand side term of the first equation (5.61)

$$\int_{(\Omega_s)^k} \partial \Psi_k^T S^k dV = \int_{(\Omega_s)^k} [\partial U^k]^T [D]^t [C^k] [D] [U^k] dV \quad (5.61)$$

Substituting equation (5.60), we are going to obtain

$$\int_{(\Omega_s)^k} [\partial U^k]^T [D]^t [C^k] [D] [U^k] dV = [Q_s^k] \int_{(\Omega_s)^k} N_j(x, y) F_s(z) [D] [C^k] [D] F_\tau(z) N_i(x, y) dV [Q_\tau^k(t)] \quad (5.62)$$

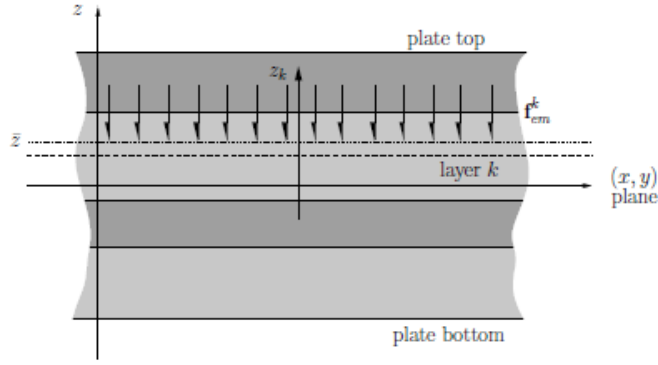
$$\int_{(\Omega_s)^k} [\partial U^k]^T [D]^t [C^k] [D] [U^k] dV = [\partial Q_{sj}^k]^T K^{sj\tau} Q_{sj}^k \quad (5.63)$$

where the 3 x 3 stiffness nucleus $K^{\tau sij}$.

5.9.2 Structural External Loads

Let us consider now the generalized Mechanical Load f_m^k applied on the layer k_{th} , as shown in following figure

From right hand side of the first equation (5.61), we define the work done by f_m as



$$\int_{\Gamma^k} [\partial U^k]^T f_m^k ds \quad (5.64)$$

where

$$[f_m^k(x, y)]^T = [f_u(x, y) f_v(x, y) f_w(x, y)] \quad (5.65)$$

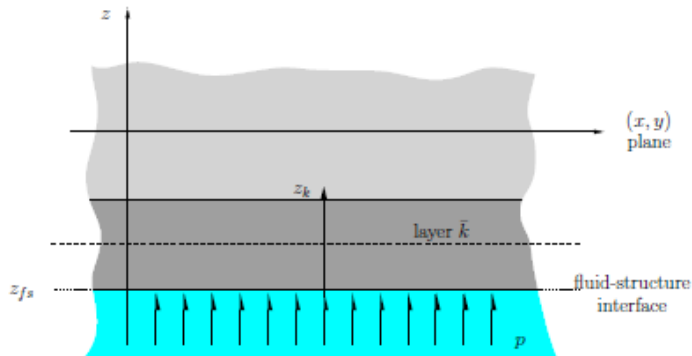
Then substituting the FE approximation of the UF variables, we can rewrite it as follows

$$\int_{\Gamma^k} [\partial U^k]^T f_m^k ds = [\partial Q_{sj}^k]^T F_\tau(z_l) \int_{A^k} N_i^s N_j^s ds = [\partial Q_{sj}^k]^T F_{si}^k \quad (5.66)$$

where A_k is the reference surface area for layer k and z_l is z -coordinate on which the load is applied. The matrix (previously introduced) F_{si}^k is fundamental 3×1 nuclei of the external loads.

5.9.3 Fluid-Structure Coupling Matrix

Let us consider the work done by the fluid



Introducing the Finite Element Approximation, we obtain

$$\int_{\Gamma_{fs}} [\partial U^k]^T f_{fs} ds = [\partial Q_{sj}^k]^T F_\tau(z_{fs}) \int_{A^k} N_i^s N_j^p ds [n \ 0]^T P_j = [\partial Q_{sj}^k]^T S^{k\tau ij} P_j \quad (5.67)$$

where the 4x1 fluid coupling nucleus $S^{k\tau ij}$ has been introduced.

5.9.4 Structural Mass Matrix

The virtual work done by the inertial loads of the k_{th} layer for the structural variables U_k can be rewritten as

$$\int_{\Omega_s^k} [\partial U^k]^T \rho_s^k I \frac{\partial^2 U^k}{\partial t^2} ds = [\partial Q_{sj}^k]^T M^{k\tau sij} \frac{\partial^2 Q_{\tau i}^k}{\partial t^2} \quad (5.68)$$

5.9.5 Fluid Stiffness and Mass Matrices

The fluid internal work and inertial load of fluid is obtained throughout the Finite Element interpolation of the fluid variable p ; obtaining the acoustic stiffness matrix and the acoustic mass matrix

$$\int_{\Omega_f} \partial p_{,i} p_{,i} dV = \partial P_i H^{ij} P_j \quad (5.69)$$

$$\frac{1}{c_f^2} \int_{\Omega_f} \partial p \frac{\partial^2 p}{\partial t^2} dV = \partial P_i Q^{ij} \frac{\partial^2 P_j}{\partial t^2} \quad (5.70)$$

5.10 Final Form of the Coupled Equations

After having derived the *fundamental nuclei* matrices, the assembly procedure will be obtained. It consists in substituting the matricial form in equation (5.61) for the structural and in equation (5.60) for the fluid.

$$\begin{bmatrix} \mathbf{M} & \mathbf{0} \\ -\rho_f \mathbf{S}^T & \mathbf{Q} \end{bmatrix} \begin{Bmatrix} \ddot{\mathbf{Q}} \\ \ddot{\mathbf{P}} \end{Bmatrix} + \begin{bmatrix} \mathbf{K} & \mathbf{S} \\ \mathbf{0} & \mathbf{H} \end{bmatrix} \begin{Bmatrix} \mathbf{Q} \\ \mathbf{P} \end{Bmatrix} = \begin{Bmatrix} \mathbf{F} \\ \mathbf{0} \end{Bmatrix}$$

This system has unknown in (s, p)

A FE code based on the formulation presented in this chapter has been implemented. In particular, even if a structural FE code based on the UF was available at the Department of Aerospace Engineering of Politecnico di Torino, named "**MUL2**". In the following, we present the comparing solutions (given by actran), and solutions (given by MUL2 software). As we are going to see, they work on different philosophy, but in the end they both converge to the same solution. For doing so, we will take a plate cavity coupled by fluid.

5.11 Acoustic Coupling

The aim of the following part is studying problems where the structure globally interacts with a surrounding fluid. The importance of this interaction depends on the fluid nature (in terms of density) on the structure of interest.

A simple criterion to *characterize* the amount of coupling for a plate-like structure is given by

$$\beta_c = \frac{\rho_0 c_0}{\rho_s h_s \omega_s} \quad (5.71)$$

where

- h_s represents the characteristic thickness of the structure
- ρ_s and ρ_0 represent the density of the structure and of the fluid respectively
- c_0 represents the sound speed in the fluid
- ω_c represents the first natural frequency of the structure.

For $\beta_c \ll 1$, the *coupling* is considered as **weak**. This is generally the case of a structure that is coupled to a **light fluid**.

Please keep in mind that in weak coupling, The calculation of the structural vibratory response is sufficient for the fully determining the coupled solution with the superposition of the modal fluid behaviour. [25]

For $\beta_c \gg 1$, the *coupling* is considered as **strong**. This is the case when the structure radiates in a **heavy fluid**. In this configuration, the fluid *modifies* the vibratory and acoustic response of the structure. In this case, it is necessary to account for the fluid loading in determining the coupled solution. In other words, the coupled equations governing the wave propagation in the fluid and in the structure must be solved simultaneously. [27]

In the following, we will consider two different cases. Cubic cavity coupled with air and according to the previous formula

$$\text{AIR} \quad \beta_c \simeq \frac{1.225 \, 340}{2700 \, 0.01 \, 50} \simeq 0.3085 \quad \textbf{Weak Coupling} \quad (5.72)$$

$$\text{WATER} \quad \beta_c \simeq \frac{1000 \, 1500}{2700 \, 0.01 \, 40} \simeq 1388.88 \quad \textbf{Strong Coupling} \quad (5.73)$$

These values can be considered *antipodes*. The major values that changes is fluid density.

5.12 Drawback: Limitations due to the patch size

The approximation of space-dependent physical or numerical functions by uniform patch averages reaches its limit when the fluctuation pattern within a patch cannot be captured by the coarse resolution of the patch grid. When the wavelength becomes smaller than two patches, the grid resolution is not sufficient small anymore to capture the wave shape and aliasing phenomenon will occur.

The main limitation of FEM-coupled method is that modes with a transverse wavelength below the dimension of two patches are missed. In this case, the patch grid is not able to represent the wave shape according to the Nyquist theorem and aliasing effects occur.

As sake of simplicity, the relative difference might be quite high between two solution, for instance, considering a parallelepiped cavity. The Mesh has an importance into the final solution. The coarse mesh is composed by [5x5x5], while the finest one by [20x20x10]

When frequency are low, the pressure peak are almost the same; while increasing the frequency, the pressure peak of the coarser one has *lost its fairness*, this because we are going to consider a wide range of frequency.

Remark *The missed modes in the higher frequency range lead to an underestimation of the system response.*

Chapter 6

Weak Coupling Interaction

This chapter deals with the validation of the structural-acoustic Finite Element code throughout the fluid-structure coupling in a plate cavity system coupled with fluid. First of all, the acoustic elements are validated for a simple geometry, where analytical solution is already known in literature; firstly in a cubic cavity, and later in parallelepiped one. The coupled fluid is also important, we will use two different fluid: *Air*, in order to analyse the **weak** coupling; and *water*, instead, for the **strong** coupling.

The *coupling solution method* is validated considering *two test cases*; the first is referred to a *weak coupled system*, while the second is a *strong coupled case* one. The validation is valid by comparing the solution of a commercial software, *Actran*. The main goal of this part is showing the differences between the two solution, and trying to find why.

This means that when structures vibrate against a fluid, the normal component of the vibration to the structural surface *must be identical* to the corresponding particle velocity in the coupled fluid. This concept must be kept on mind along this chapter. This simple equality allows us to **couple** the equations that define *structural* and *fluid motion* at the fluid-structure interface, as previously explained.

The *fluid-structure coupling* concept is that the **normal particle velocity** is *identical* onto the structure and fluid boundary, but the *tangential particle velocity* is **not** the same, defining the "*slip condition*" between the material wall and fluid, typical in Fluid dynamic.

This concept is implemented in Actran software through the using of *interfaces and coupling surfaces*. Remember that, as sake of simplicity, we are assuming the Fluid Linearity, so that fluid properties do not depend on the fluctuating pressure amplitude or phase.

The coupling surface is the exactly interface between the structural force applied onto the fluid, and in the same time, the pressure force applied onto the structure; we will see that this coupling concept will be implemented in a different way; but the solution will be comparable.

It is quite difficult to classify vibro-acoustic systems for their coupling behaviour, the following classification is valid just for simple geometries, like those considered in the following: Whenever an **heavy fluid**, like as *water*, is contact with a structure, a *strong coupling behaviour* is observed, while the cavity is filled by a **light fluid**, like air, a *weak coupling* is obtained.

The structure is composed as follows: *Structural plate, coupling surface* and the *acoustic volume*. First of all, we start with the validation of structural plate results **only**, comparing the results obtained with Actran. The Plate is modelled by the *Classical Plate Theory* (CLPT)

6.1 Classical Plate Theory (CLPT)

Considering a plate with dimension a (along x), width b (along y), thickness h (along z) and number of layers N_l which can be both isotropic or orthotropic is defined in the orthogonal coordinates $(x_1^k; x_2^k; x_3^k)$ of the k_{th} lamina oriented at an angle θ_k . Assuming the xy -plane of the problem in the undeformed mid-plane of the laminate. The k_{th} layer is located between the points $z = z_k$ and $z = z_{k+1}$ in the thickness direction. Consider the following assumptions

- Thickness of the plate is small compared to other dimensions.
- The displacement components of the mid surface of the plate are small compared to the thickness.
- Transverse shear deformation is neglected. Perpendicular surface to the mid surface before and after deformation remains normal.
- The transverse normal strain ϵ_{zz} under transverse loading can be neglected and also σ_{zz} is small and is negligible compared with the other stress components.
- Constant Displacement throughout the thickness direction.

Out-of-plane Displacement of Plates

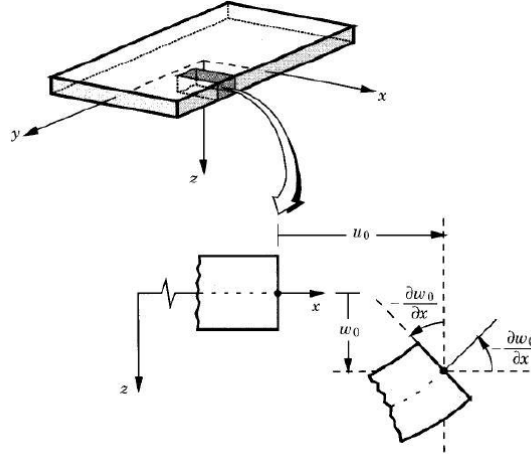


FIGURE 6.1: Undeformed and deformed geometry in thickness direction under Kirchhoff hypothesis

In the Kirchhoff hypothesis displacements (u, v, w) are assumed as follows

$$u(x, y, z, t) = u_0(x, y, t) - z \frac{\partial w_0}{\partial x} \quad (6.1)$$

$$v(x, y, z, t) = v_0(x, y, t) - z \frac{\partial w_0}{\partial y} \quad (6.2)$$

$$w(x, y, z, t) = w_0(x, y, t) \quad (6.3)$$

where u_0, v_0, w_0 are displacements of the mid-plane surface; and (x, y) are in-plane coordinates and z is the thickness direction, assumed as reference.

It is possible to define linear three-dimensional strain-displacement relations as follows

$$\begin{Bmatrix} \epsilon_{xx} \\ \epsilon_{yy} \\ \gamma_{xy} \end{Bmatrix} = \begin{Bmatrix} \epsilon_{xx}^{(0)} \\ \epsilon_{yy}^{(0)} \\ \gamma_{xy}^{(0)} \end{Bmatrix} + z \begin{Bmatrix} \epsilon_{xx}^{(1)} \\ \epsilon_{yy}^{(1)} \\ \gamma_{xy}^{(1)} \end{Bmatrix} = \begin{Bmatrix} \frac{\partial u_0}{\partial x} \\ \frac{\partial v_0}{\partial y} \\ \frac{\partial u_0}{\partial y} + \frac{\partial v_0}{\partial x} \end{Bmatrix} + \begin{Bmatrix} -\frac{\partial^2 w_0}{\partial x^2} \\ -\frac{\partial^2 w_0}{\partial y^2} \\ -2\frac{\partial^2 w_0}{\partial x \partial y} \end{Bmatrix}$$

where $\epsilon_{xx}^0, \epsilon_{yy}^0, \gamma_{xy}^0$ are the membrane strains and $\epsilon_{xx}^1, \epsilon_{yy}^1, \gamma_{xy}^1$ are the flexural (*bending*) strains which is known as the curvature.

We use the previous strain relation in order to calculate the force and momentum applied on the plate through the following relation

$$\begin{Bmatrix} N_{xx} \\ N_{yy} \\ N_{xy} \end{Bmatrix} = \begin{bmatrix} A_{11} & A_{12} & A_{16} \\ A_{12} & A_{22} & A_{26} \\ A_{16} & A_{26} & A_{66} \end{bmatrix} \begin{Bmatrix} \epsilon_{xx}^{(0)} \\ \epsilon_{yy}^{(0)} \\ \gamma_{xy}^{(0)} \end{Bmatrix} + \begin{bmatrix} B_{11} & B_{12} & B_{16} \\ B_{12} & B_{22} & B_{26} \\ B_{16} & B_{26} & B_{66} \end{bmatrix} \begin{Bmatrix} \epsilon_{xx}^{(1)} \\ \epsilon_{yy}^{(1)} \\ \gamma_{xy}^{(1)} \end{Bmatrix}$$

$$\begin{Bmatrix} M_{xx} \\ M_{yy} \\ M_{xy} \end{Bmatrix} = \begin{bmatrix} B_{11} & B_{12} & B_{16} \\ B_{12} & B_{22} & B_{26} \\ B_{16} & B_{26} & B_{66} \end{bmatrix} \begin{Bmatrix} \epsilon_{xx}^{(0)} \\ \epsilon_{yy}^{(0)} \\ \gamma_{xy}^{(0)} \end{Bmatrix} + \begin{bmatrix} D_{11} & D_{12} & D_{16} \\ D_{12} & D_{22} & D_{26} \\ D_{16} & D_{26} & D_{66} \end{bmatrix} \begin{Bmatrix} \epsilon_{xx}^{(1)} \\ \epsilon_{yy}^{(1)} \\ \gamma_{xy}^{(1)} \end{Bmatrix}$$

where M_{xx}, M_{yy}, M_{xy} are moments resultants and N_{xx}, N_{yy}, N_{xy} are force resultants are expressed in matricial form.

The coefficients A_{ij}, B_{ij}, D_{ij} are extensional stiffness, bending-extensional coupling stiffness and bending stiffness, respectively defined as

$$(A_{ij}, B_{ij}, D_{ij}) = \sum_{k=1}^N \int_{z_k}^{z_{k+1}} \tilde{C}_{ij}^{(k)}(1, z, z^2) dz \quad (i, j) = 1, 2, 6$$

Keep in mind that in our test case, *Just* a **Point Force** is applied on node of mesh constituting the plate; please remember that these matrices could change considering different leyers, for instance, in the case of the Orthotropic Material, as we will deal with them.

6.2 Boundary Condition

In the following, we will deal with *two different types* of Boundary Condition (BC).

Boundary Condition: Simply Supported

For a simply supported plate, it is prevented from deflecting but it results free to rotate about a line along the boundary edge.

For example, for a simply supported edge parallel to the y axis, they can be expressed by imposing the following condition

$$w = 0 \quad \text{and} \quad M_x = 0 \quad (6.4)$$

For practical ways, For thin shell elements in Actran, A *simple support* is modelled by restraining only the transverse translational degrees of freedom. This will be visualized as follows

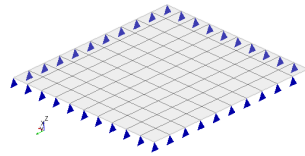


FIGURE 6.2: Actran Visualization of **Simply Supported edges** plate

Boundary Condition: Clamped

If a plate is clamped at the boundary, the deflection and the slope of the middle surface must vanish at the boundary itself.

For example, for a clamped edge parallel to the y axis, they can be expressed by imposing the following condition

$$w = 0 \quad \text{and} \quad \frac{\partial w}{\partial x} = 0 \quad (6.5)$$

For practical ways, For thin shell elements in Actran, a *clamped edge* is modelled by restraining the *translational* and *rotational* degrees of freedom of the external nodes. This will be visualized as follows

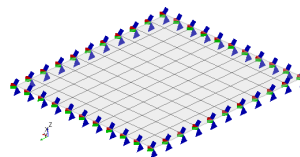


FIGURE 6.3: Actran Visualization of **Clamped edges** plate

6.3 Cubic Cavity

6.3.1 Structural Validation

First of all, we have to validate the structural behaviour in term of displacement. We will compare the displacement of the solution of MUL2 software, to the corresponding Actran solution, in order to eliminate any structural responsibility in the difference (shown in the following) valid for the coupled cavity.

In this Section, we will deal with a squared dimension $1 \times 1 [m^2]$ made by aluminium with thickness equal to $0.01 [m]$; through a structural mesh $[20 \times 20]$ elements. Firstly, we consider the following *mechanical properties* of the *isotropic plate* are as follows: Young's Modulus $E_s = 70 [GPa]$, mass density $\rho_s = 2700 [kg/m^3]$ and Poisson's ratio $\nu = 0.35$. A constant amplitude force excitation of $1 [N]$, over the frequency range from $0 - 300 [Hz]$, was applied at one of the off-center nodes of the structural FE mesh with coordinate $(0.25m, 0.35m)$, point at which the measurement of displacement is acted [20][21].

We will test this plate in these different condition

- *Isotropic Plate with Simply Supported edges boundary condition*
- *Isotropic Plate with Clamped edges boundary condition*
- *Orthotropic Plate with Simply Supported edges boundary condition*
- *Orthotropic Plate with Clamped edges boundary condition*

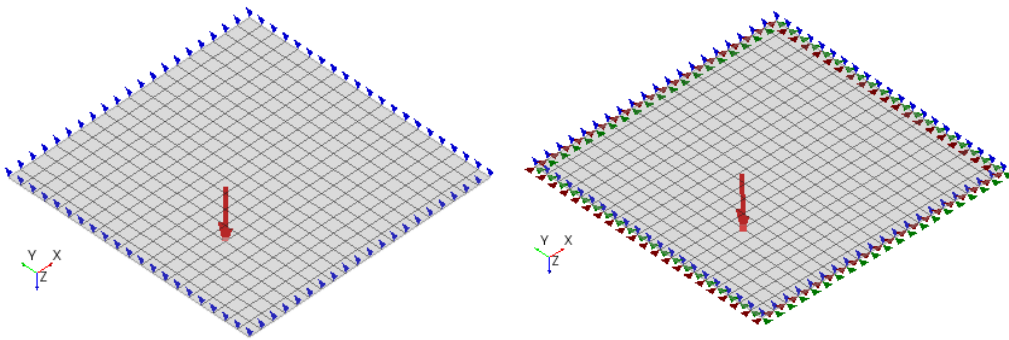


FIGURE 6.4: Simply Supported edges (at left); Clamped edges (at right)

We will graph the displacement considering different polynomial-grade displacement function through the thickness (Lawerwise), as previously explained; obtained in MUL2 and Actran in order to compare the response. The point load will oscillate with variable frequency in range $(0/300 [Hz])$.

The Point in which we will record the displacement results coincides with the excitation point, that is $(0.25m, 0.35m)$.

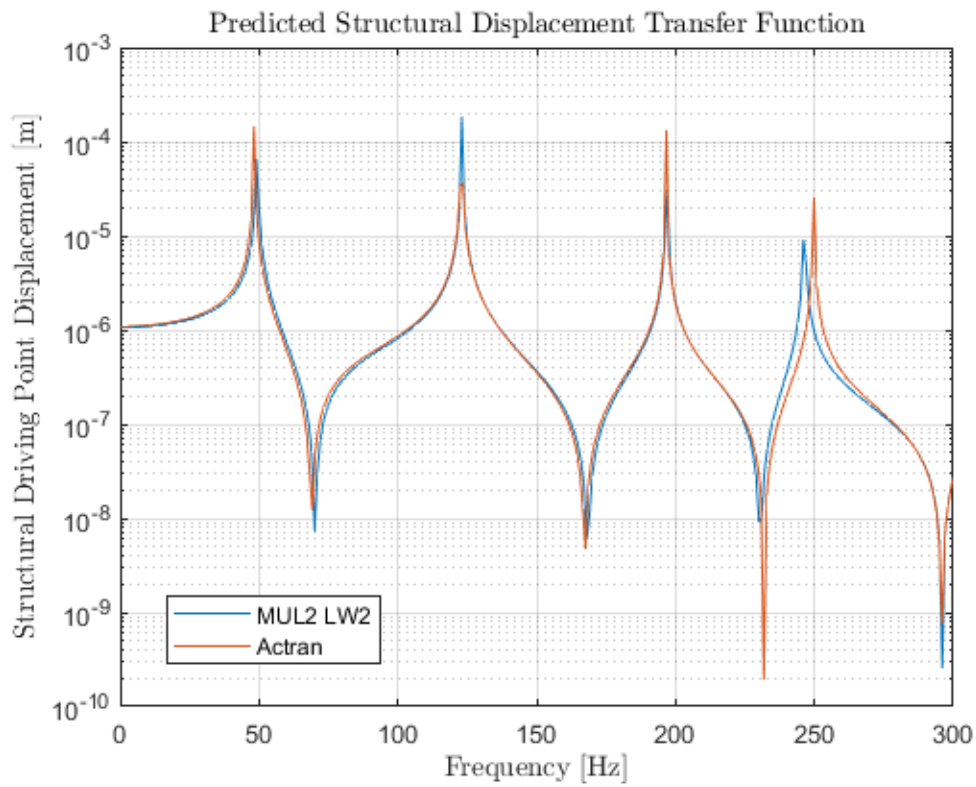


FIGURE 6.5: Displacement at $(0.25m, 0.35m)$ for *Isotropic* plate with layer-wise 2 considering *Simply Supported* edges

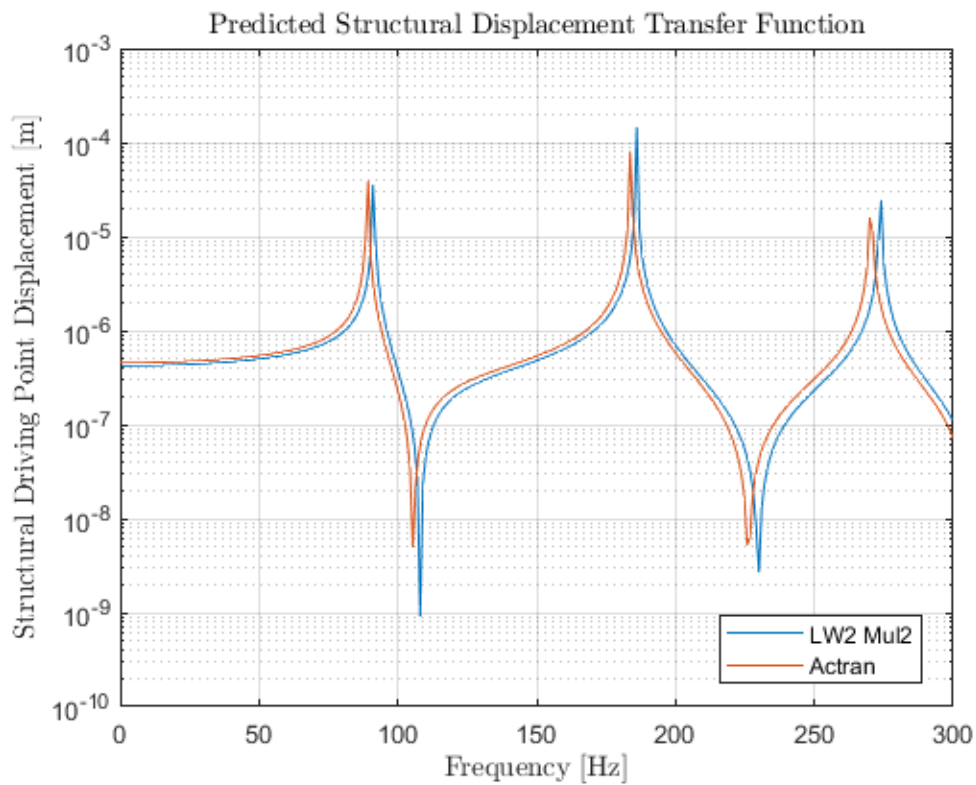


FIGURE 6.6: Displacement at $(0.25m, 0.35m)$ for *Isotropic* plate with different layer-wise considering *Clamped* edges

As we see MUL2 solutions are comparable for LW2 and LW3, despite in LW1 the shape is captured, but it presents valuable error (compared to the Actran solution), since it involves linear expansion through the thickness (Kinematics of displacement not fully expressed through linear), probably it's not sufficient grade to completely represent the displacement, we can also verify that LW1 predicts bigger resonance frequency, and the error (the distance between Actran peak and LW1 one) increases with the frequency itself. As a matter of fact, the LW2 solution can properly represent the structural point displacement in a correct way.

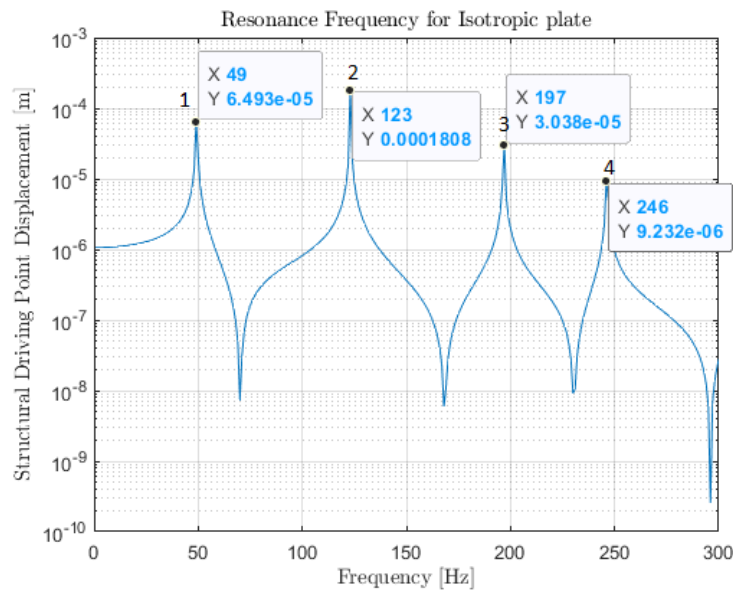
Both Simply supported and Clamped have comparable behaviour, but the Clamped solution error is bigger than simply supported one (for the same frequency range).

After the interpretation of the following results, we can assume that the structure part (just the plate)

Vibration Analysis

Vibration is time dependent displacements of a part of the structure from an equilibrium position; these displacements could be repetitive and their repetitions are executed at equal interval of time from the equilibrium position the resulting motion is said to be *periodic* in a particular frequency range.

In this case, a Point Load is excited in a particular point, the excitation point. One of the most important parameters associated about vibration is its natural frequency. Each structure has its own natural frequency for a series of different modes which control its dynamic behaviour of the plate, as sake of simplicity, for Isotropic plate (simply supporter edges) they can be visualize in following figures through its maximum local peak. [15]



Natural Frequency		
mode		Value
1	(1,1)	49 [Hz]
2	(2,1)	123 [Hz]
3	(2,2)	197 [Hz]
4	(3,2)	246 [Hz]

Each mode can be represented as follows

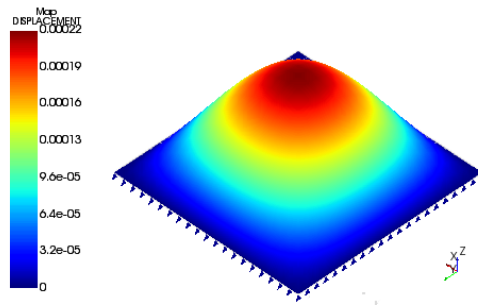


FIGURE 6.7:
49 [Hz]

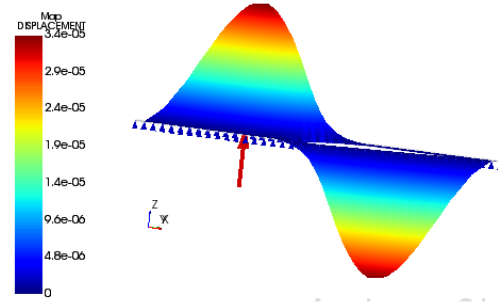


FIGURE 6.8:
123 [Hz]

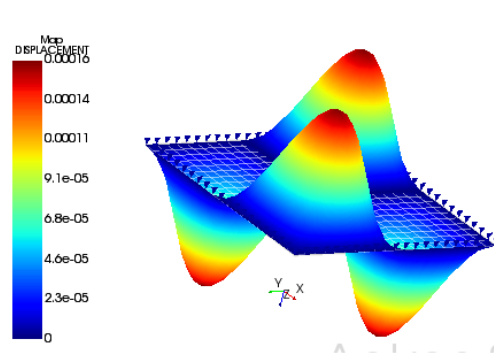


FIGURE 6.9:
197 [Hz]

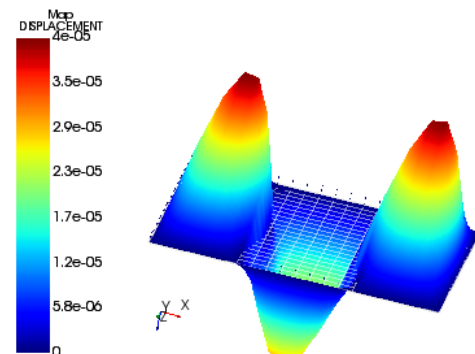


FIGURE 6.10:
246 [Hz]

Solution predicted by these theories can give us insight into the dynamic behaviour of plate and this includes the propagation of waves and the study standing waves and for the vibration modes [8][13].

When an oscillating force is applied at a resonant frequency of a dynamical system, the system will oscillate at higher amplitude than when the same force is applied at other non-resonant frequencies .

In the previous pictures, the peak are shown and they represent the **Resonance Frequency** of vibration plate, and we later verify that these points act the sound pressure level inside the cavity, in fact the peaks of SPL are influenced from the 'structural' natural plate frequency [19].

This analysis is made for many others condition: Clamped, Orthotropic (Clamped and Simply Supported) for $[0^\circ/90^\circ/0^\circ]$ and $[90^\circ/0^\circ/90^\circ]$ lamination, but the reasoning is all the same.

Orthotropic Material plate

We consider a multi-layered composite plate; three-layered composite, composed by the following mechanical constants $E_1 = 25 [GPa]$, $E_2 = E_3 = 1 [GPa]$, $G_{13} = G_{23} = 0.5 [GPa]$, $G_{12} = 0.2 [GPa]$ and $\nu_{13} = \nu_{23} = \nu_{12} = 0.25$ considering different lamination $[0^\circ/90^\circ/0^\circ]$ and $[90^\circ/0^\circ/90^\circ]$, despite we will not aspect any huge difference. We consider the same dimension $[1m \times 1m]$, and the same point of excitation.

The results are the following

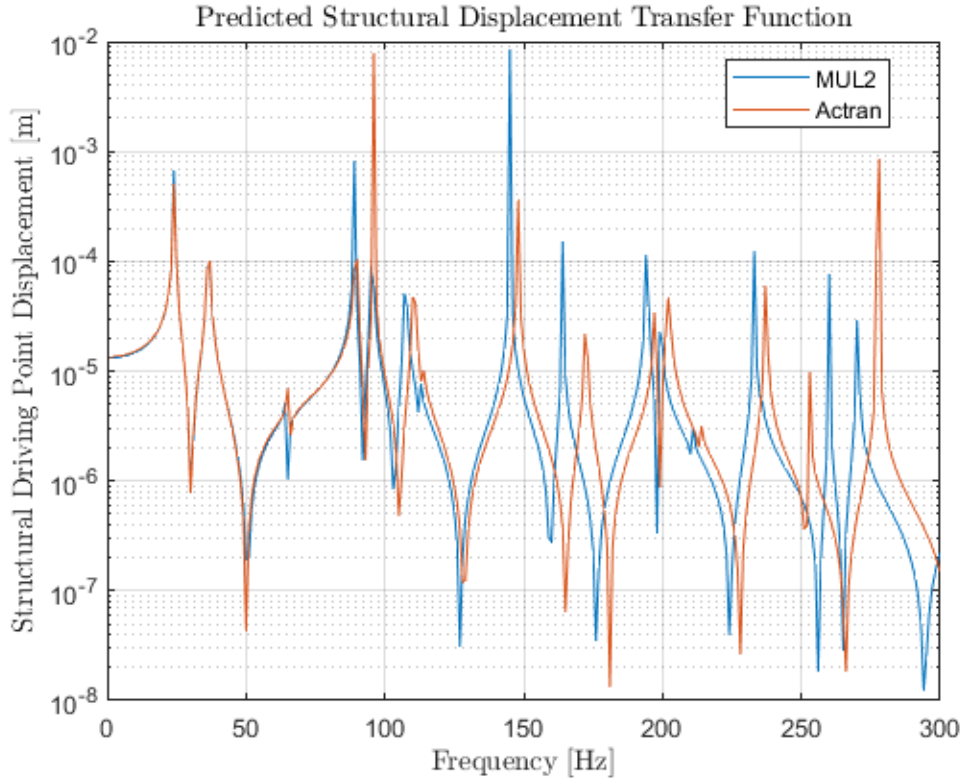


FIGURE 6.11: Displacement at $(0.25m, 0.35m)$ for *Orthotropic* plate **LW2**, lamination $[0^\circ/90^\circ/0^\circ]$, considering *Simply Supported edges*

Here we can verify that the differences become larger in the case of composite plate, where the layers effects are more pronounced. Indeed, the layer-wise model (implemented in MUL2) is able to capture the complex dynamic of the structure, while the Actran solution is made up considering an average of the properties in the multi-layer laminate. This may be create **huge** error between MUL2 and any commercial software based on finite element method [23][24].

Indeed the Orthotropic behaviour is largely different from the isotropic one, in fact if the latter presents a good estimate of displacement, the former is reduced in such a limited range of frequency (smaller ones), while considering higher frequency the error may increase since the average contribution presented in Actran solution [18].

This difference obviously will interfere with the coupling fluid, as we will deeply study [17].

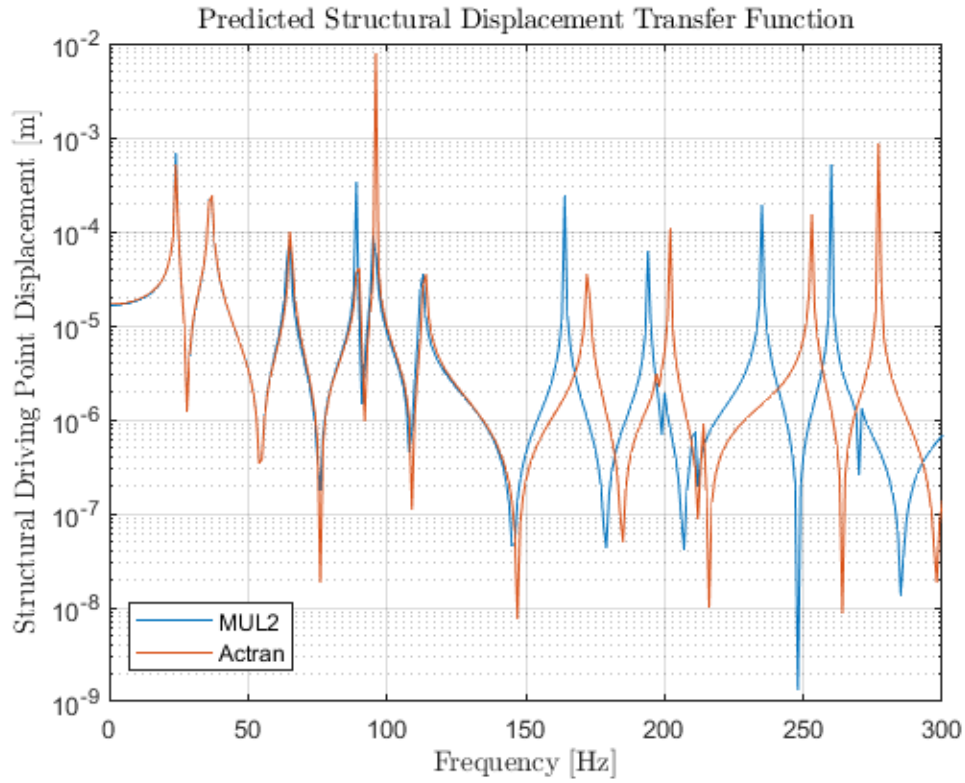


FIGURE 6.12: Displacement at $(0.25m, 0.35m)$ for *Orthotropic* plate **LW2**, lamination $[90^\circ/0^\circ/90^\circ]$, considering *Simply Supported* edges

As a sake of completeness, we are going to analyse the plate, changing the BC into 'Clamped' edges.

As we verified, in wish of obtaining the accurate prediction of displacement (and stress) distribution and consequently model the entire kinematics of laminated composites, the three dimensional state of displacement have to be analysed, in these case the usage of new family of layer-wise theories (**LW**) is crucial, in which the displacement field is defined for each layer, including discrete material layer [22].

Actran uses models based on the equivalent single layer (ESL), and in the case of ortotropic plates, it produces much error (mostly in higher frequencies), while in the isotropic plate case, the two solution Equivalent Single layer and Layer-wise theories coincides.

Layer-wise Theories provide more accurate solutions of the three dimensional states that are of primary importance in the structural behaviour, and subsequently, for the acoustic field behaviour inside the cavity, and as matter of facts, we aspected much error in ortotropic plates solutions at higher frequencies.

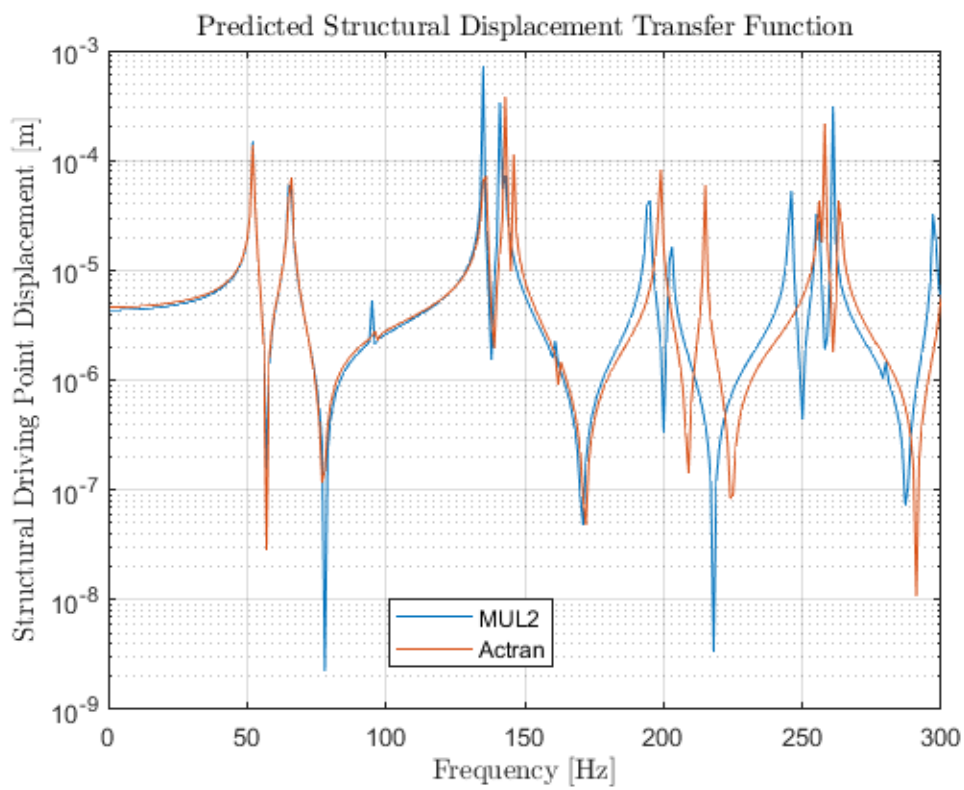


FIGURE 6.13: Displacement at $(0.25m, 0.35m)$ for Orthotropic plate LW2, lamination $[0^\circ/90^\circ/0^\circ]$, considering Clamped edges

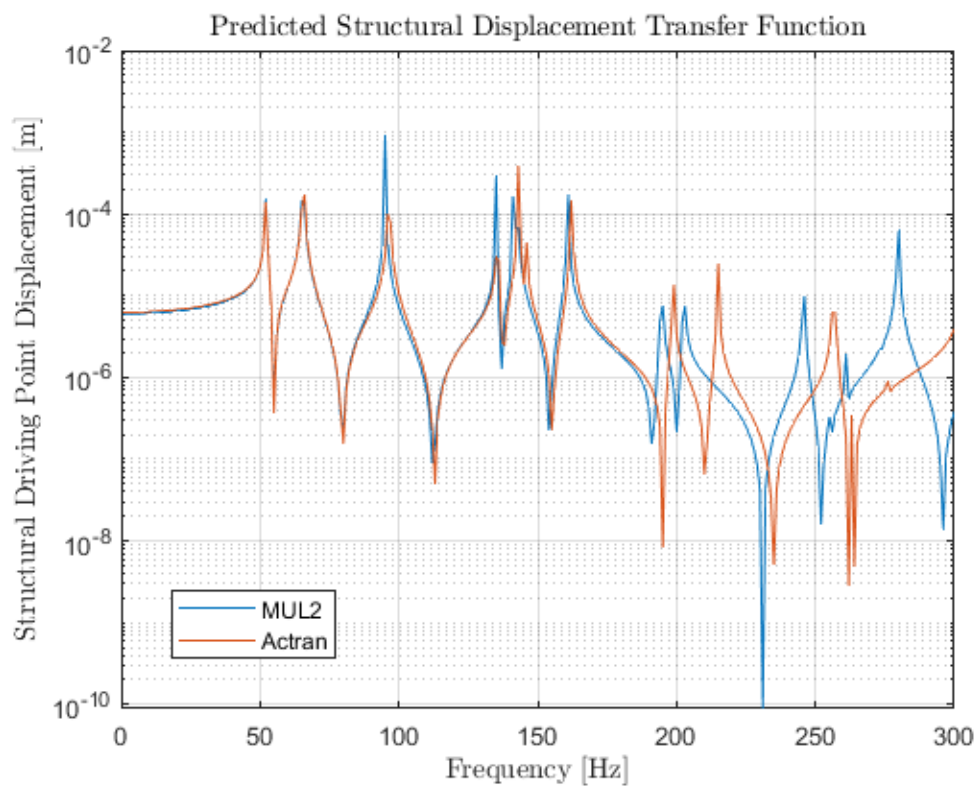


FIGURE 6.14: Displacement at $(0.25m, 0.35m)$ for Orthotropic plate LW2, lamination $[90^\circ/0^\circ/90^\circ]$, considering Clamped edges

6.3.2 Coupled Fluid-Structure Cavity

The test here considered in this work is a simplified structure, a *cubic* cavity composed by a rigid walled cubic cavity of dimensions $1 \times 1 \times 1$ [m³], over which a *square isotropic plate* is simply supported of dimension 1×1 [m²] made by aluminium with thickness equal to 0.01 [m], as shown in figure (6.15).

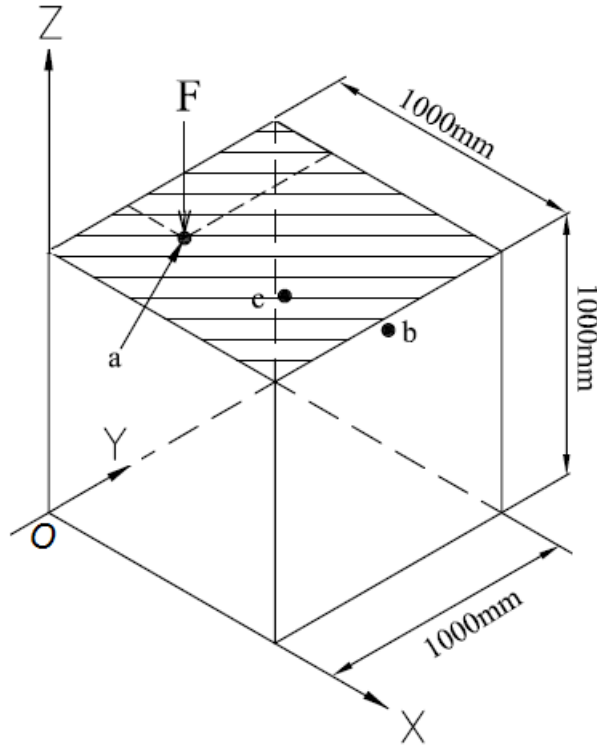


FIGURE 6.15: Plate backed *Cubic Cavity* system.

Excitation location: A = (0.25m, 0.35m, 1m);

Measurement locations: B = (0.75m, 0.75m, 0.75m), C = (0.35m, 0.70m, 0.65m);

The *mechanical properties* of the plate are as follows: Young's Modulus $E_s = 70$ [GPa], mass density $\rho_s = 2700$ [kg/m³] and Poisson's ratio $\nu = 0.35$. A constant amplitude force excitation of 1 [N], over the frequency range from $0 - 300$ [Hz], was applied at one of the off-center nodes of the structural FE mesh.

For Computational effect, a mesh composed by $10 \times 10 \times 10$ elements, through using H27 (Hexa) for the discretization of the fluid, and Q9 (QUAD) for the discretization of the plate.

The previous cavity will be analysed filled filled with air and water, respectively, in order to study the weak and strong coupling effect.

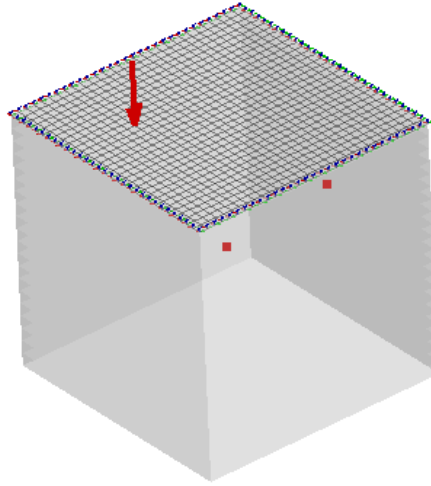


FIGURE 6.16: Coupled FE/FE model: Plate backed by a rigid walled cavity.

6.3.3 Weak Coupling Interaction

The cubic cavity is filled with **air** with the following properties: speed of sound $c_f = 343 [m]$ and mass density $\rho_f = 1.2 [Kg/m^3]$. In order to study, the Sound Pressure Level (SPL) in points B and C, we added two 'Virtual Microphones'.

Plotting the Results, the *frequency response functions* (FRF), obtained in *Actran*

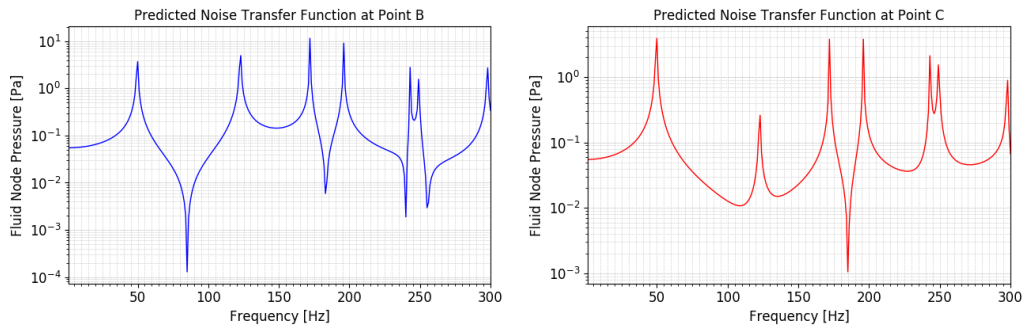


FIGURE 6.17: Actran Solution (FRF) in point B(0.75m, 0.75m, 0.75m)[left] and C(0.35m, 0.70m, 0.65m) [right] for **Isotropic** plates

Here we show the values of the **absolute** value of the fluid node pressure in pascal in point B and C; obtained in Actran. We have to *validate* the results from MUL2 program, in the same points and for the same condition. First of all, we have to decide the order of expansion we used to discretize the thickness of the plate itself. We later see how the MUL2 solution is modified by changing it [31].

Notation LDN is the notation adopted for LW models, where L define the use of a LW description and D and N indicates the PVD variational principle and the order of the expansion, respectively.

Plotting the Node Pressure for LDN for $N = 2, 3, 4$ we obtain

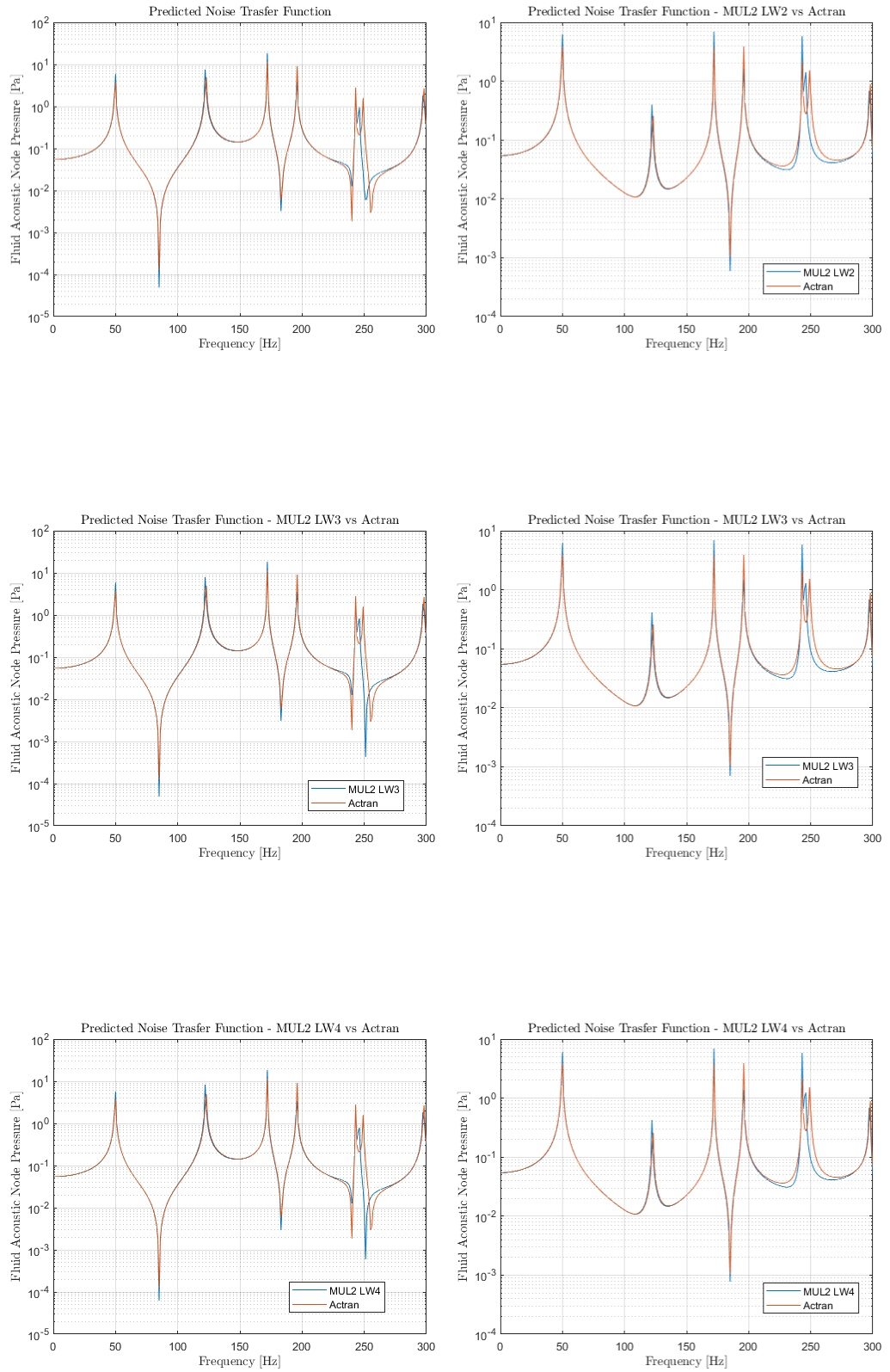


FIGURE 6.18: Fluid Node Pressure in point B(0.75m, 0.75m, 0.75m) [left] and C(0.35m, 0.70m, 0.65m) [right] for Isotropic plates

It can be observed that *there is no visible difference* in the respective noise transfer functions between the two softwares, despite the expansion order is increasing. More it increases, more time is necessary to compute the solution. The LD1 approximates the function as linear so it will produce much error than the others, but in the same time, if we add a double linear element through the thickness, we reach the results given by LD2. [3]

The different behaviour is caused because the linear approximation is not sufficient enough to represent the complete kinematics of the coupled system. That is valid for *Isotropic plates* and for *simply supported edges*.

In the following, a **Parametric study** is made to analyse how the solution is modified due to relative changes, with the comparison of Actran solution.

We will test this plate in these different condition

- *Isotropic* Plate weakly Coupled increasing the thickness plate
- *Isotropic* Plate weakly Coupled changing the boundary condition
- *Orthotropic* Plate weakly Coupled with *Simply Supported* and *Clamped* edges BC with different lamination $[0^\circ/90^\circ/0^\circ]$ and $[90^\circ/0^\circ/90^\circ]$.

Isotropic Plate Coupled increasing the thickness plate

The next key point is increasing the plate thickness, and analyse the resulting results. Please keep in mind that thickness (reference value) is based on $t_{ref} = 0.01 [m]$, whose results were previously displayed. Now, the object of this part is to point out how the solution is modified in the case of $10 t_{ref}$, $20 t_{ref}$, $30 t_{ref}$ respect to reference value. A LW3 model will be used.

The results are shown in the following

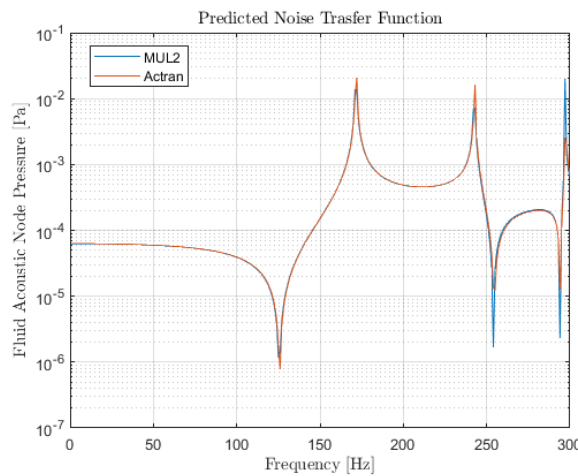
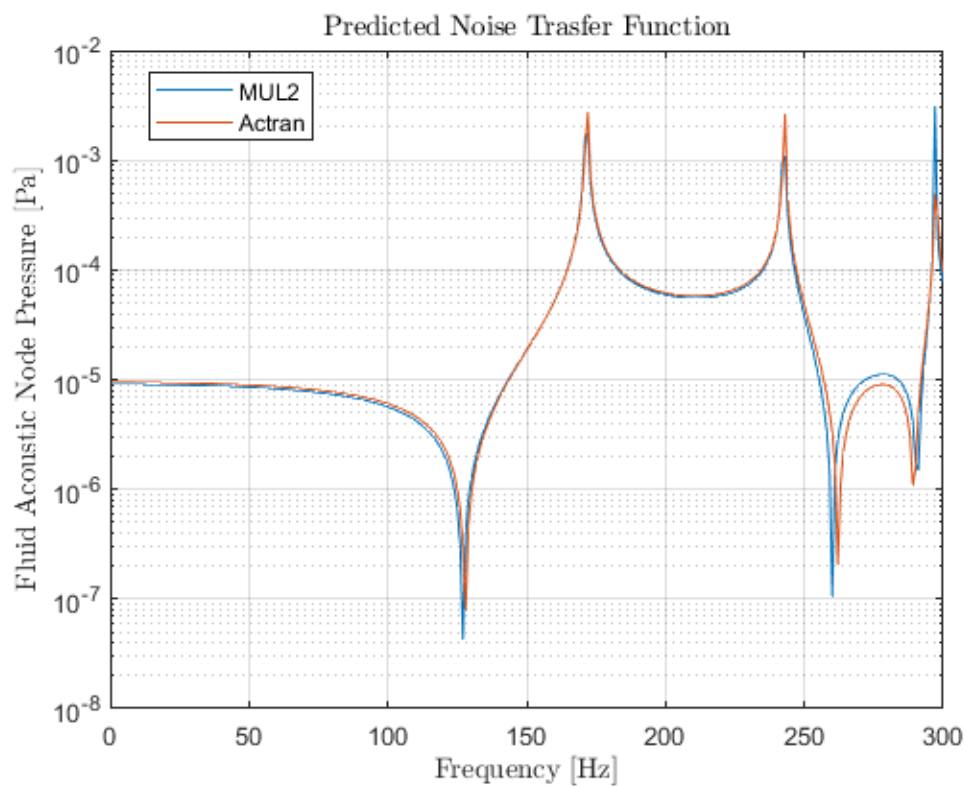
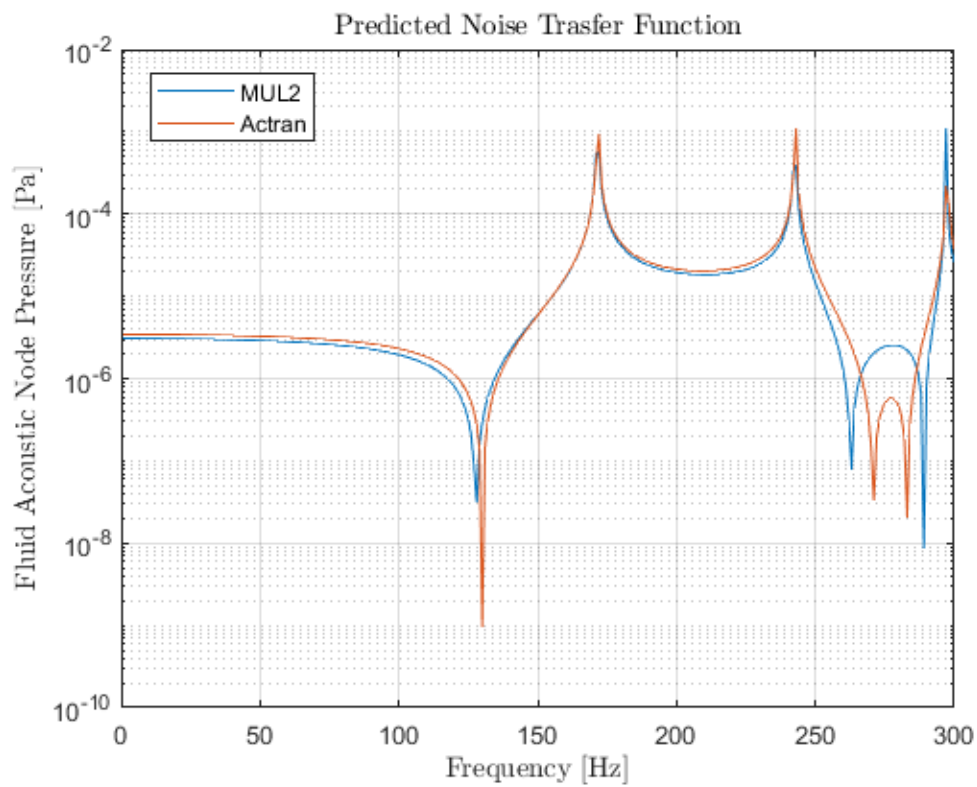


FIGURE 6.19: Coupled plate with $Thickness = 10 t_{ref}$ using LW3

FIGURE 6.20: Coupled plate with $Thickness = 20 t_{ref}$ using LW3FIGURE 6.21: Coupled plate with $Thickness = 30 t_{ref}$ using LW3

The Actran solution continues to converge to MUL2 one, despite the varying plate thickness, this means that there is no depending effect over the resulting results, so any future difference is independent from the thickness.

After having verified the fairness of the solution, we may notice that peaks are converging, useful in the project. The convergent values depend from the material properties like the mass density and as well as the geometry and BCs.

The resonance frequencies corresponding to the maximum peak on the SPL versus frequency curve decreases as plate thickness dimension is increased, which is expected because it produces a decrease of air cavity thickness which leads to increase equivalent air stiffness.

Overall, the curve is shifted toward downwards with increasing thicknesses, indicating that the sound transmission property is reduced due to the increase the stiffness bending $D = \frac{Et^3}{12(1-\nu^2)}$.

Isotropic Plate Coupled changing the boundary condition

Numerical studies are performed in this subsection to explore further the relationships between the two different boundary conditions and the significant influence of the boundary condition on the sound transmission properties of coupled panel structures in terms of frequency characteristic curves.

It can be expected that the natural frequency of the clamped system are distinctly higher than those of the simply supported system in the lower frequency range. This is attributed to the more rigorous constraint provided by the clamped condition than that by the simply supported condition, which is equivalent to increasing the panel stiffness.

An analytical approach has been developed to investigate the influence of boundary constraints (fully clamped versus fully simply supported) on the Fluid node pressure performance of a finite panel structure containing an air cavity. The theory is built upon the vibration responses of the panels coupled by the air cavity. Since Actran solution converges to MUL2 to validate the theoretical model, with good overall agreement achieved for both types of the boundary as in the following [5]

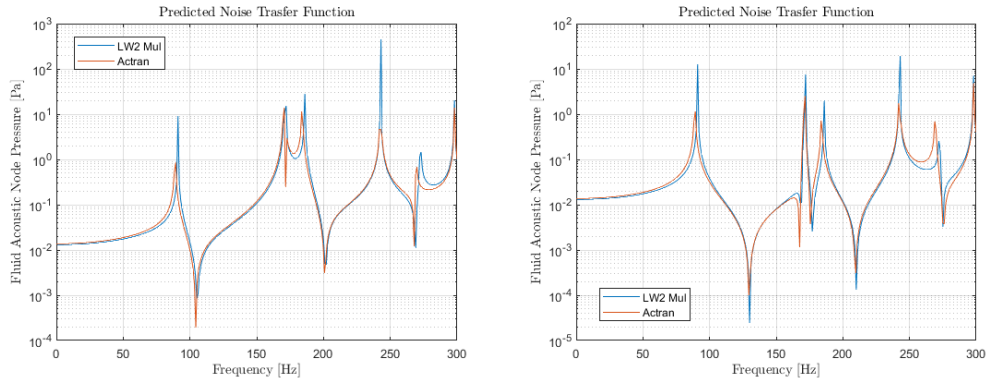


FIGURE 6.22: Clamped solution: Acoustic pressure in B (left); and Acoustic pressure in C (right)

The intense peaks and dips in the SPL versus frequency curve reflect the inherent modal behaviors of the panel system. The SPL dips in the simply supported case are shifted to *lower frequencies* in comparison with those ones of the clamped case, implying the fact that the natural frequencies of the simply supported system are lower than their counterparts of the clamped system, as a consequence the natural frequencies associated with the simply supported boundary condition are lower, as the clamped condition provides a *more rigorous constraint* on panel vibration [5]

To explore the boundary effects further, the typical (2, 2) mode behaviour of a fully clamped panel partition is compared in following figure with the relative of a simply supported one.

The (2, 2) mode natural frequency of the fully simply supported plate system occurs at $f_s^{(2,2)} = 197 [Hz]$, while in fully clamped system, it shifts to $f_s^{(2,2)} = 207 [Hz]$. Although the plate mode shapes at different boundary conditions exhibit similar forms, important discrepancies can be observed at panel edges, since these differences at the panel edges reflect the boundary effects, i.e., the requirement that $\frac{\partial w}{\partial z} = 0$ for the clamped condition and that $\frac{\partial^2 w}{\partial z^2} = 0$ for the simply supported condition.

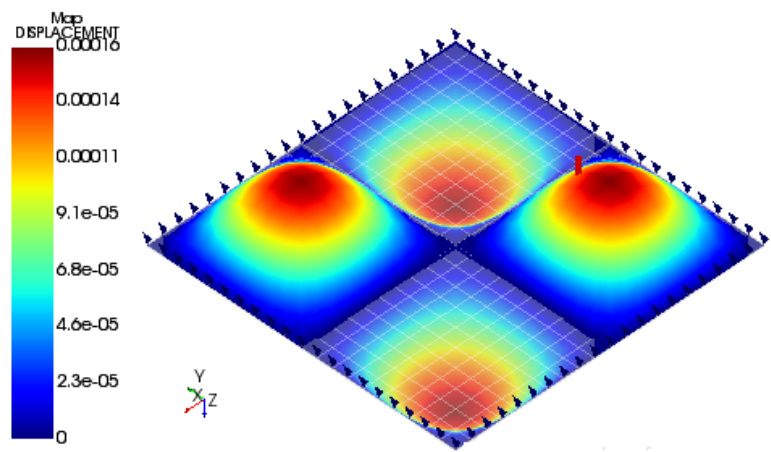


FIGURE 6.23: (2,2) mode Natural frequency comparison: Simply supported

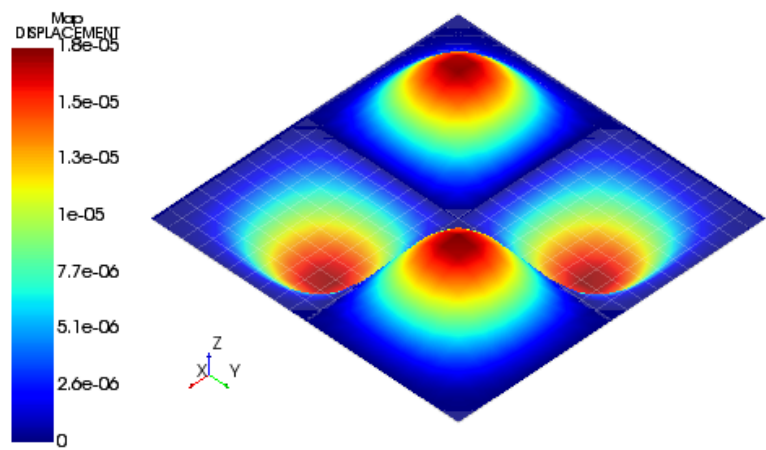


FIGURE 6.24: (2,2) mode Natural frequency comparison: Clamped

The consistency of the two models based separately on the *clamped* boundary condition and the *simply supported* boundary condition is confirmed when the panel dimensions become infinitely large; an excellent agreement is achieved between the two models, as the effect of boundary condition becomes negligible. In order to verify the last sentence, we are going to simulate a cubic cavity whose dimension reaches 1000 [m], if we register the acoustic pressure in clamped and simply supported, we **will not** note *any difference*.

The Boundary Condition influence strictly depends on the structural dimension of the considered plates, and it does not depend on the coupling influence.

Orthotropic Material plate

We consider a multi-layered composite plate; three-layered composite, composed by the following mechanical constants $E_1 = 25 [GPa]$, $E_2 = E_3 = 1 [GPa]$, $G_{13} = G_{23} = 0.5 [GPa]$, $G_{12} = 0.2 [GPa]$ and $\nu_{13} = \nu_{23} = \nu_{12} = 0.25$ considering different lamination $[0^\circ/90^\circ/0^\circ]$ and $[90^\circ/0^\circ/90^\circ]$, despite we will not aspect any huge difference. We consider the same dimension $[1m \times 1m]$, and the excitation is placed in the same point as the previous, coupled the acoustic cavity below. The following results are obtained though using **LW2** theory.

The results are the following

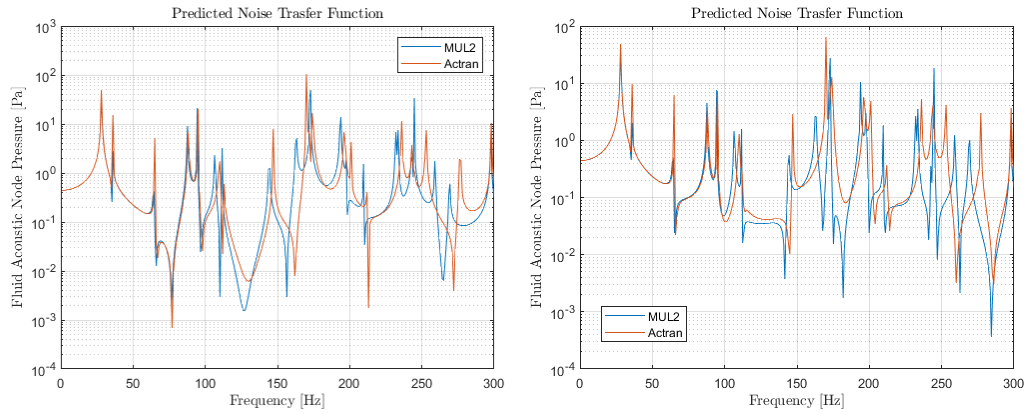


FIGURE 6.25: Fluid Node Pressure in point B(0.75m, 0.75m, 0.75m); [left] and C(0.35m, 0.70m, 0.65m) [right] for **Orthotropic** plates, *weakly* coupled, for the lamination $[0^\circ/90^\circ/0^\circ]$, **simply supported** edges

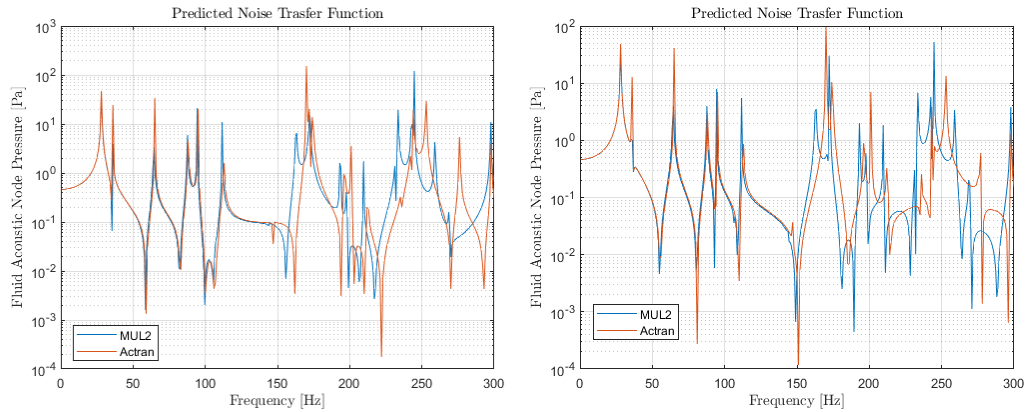


FIGURE 6.26: Fluid Node Pressure in point B(0.75m, 0.75m, 0.75m); [left] and C(0.35m, 0.70m, 0.65m) [right] for **Orthotropic** plates, *weakly* coupled, for the lamination $[90^\circ/0^\circ/90^\circ]$, **simply supported** edges

In the previous figures, we can verify the the difference between the Actran solution and the MUL2. As mostly explained before, in the case of ortotropic plates, the difference arises in higher frequency range due to the fundamental difference of structural behaviour.

The weak coupling may be influenced by the fluid density, in this case, low equal to $1.2 \left[\frac{Kg}{m^3} \right]$.

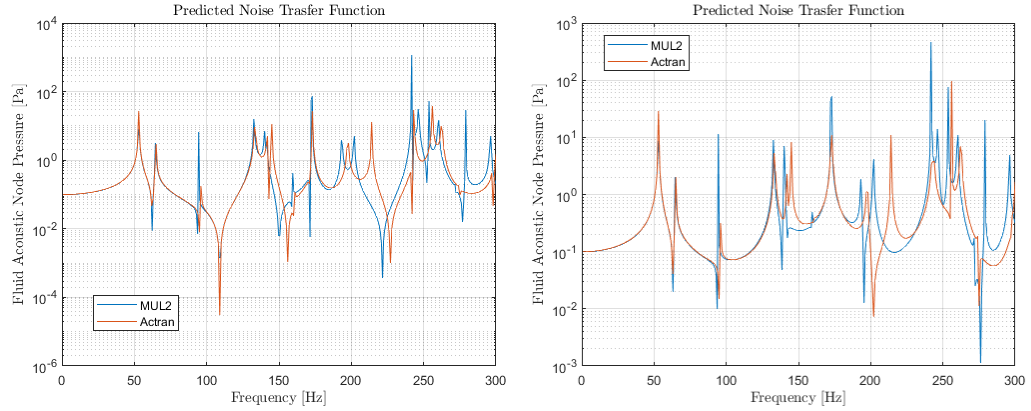


FIGURE 6.27: Fluid Node Pressure in point B(0.75m, 0.75m, 0.75m); [left] and C(0.35m, 0.70m, 0.65m) [right] for **Orthotropic** plates, *weakly* coupled, for the lamination $[0^\circ/90^\circ/0^\circ]$, **clamped** edges

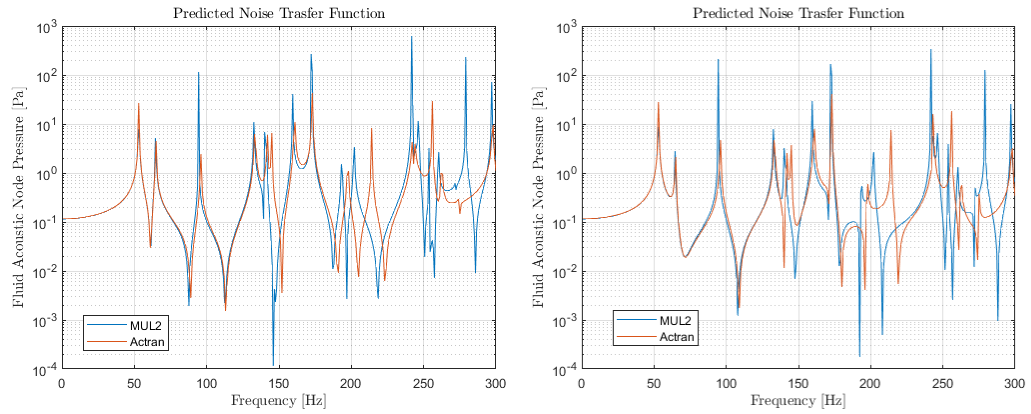


FIGURE 6.28: Fluid Node Pressure in point B(0.75m, 0.75m, 0.75m); [left] and C(0.35m, 0.70m, 0.65m) [right] for **Orthotropic** plates, *weakly* coupled, for the lamination $[90^\circ/0^\circ/90^\circ]$, **clamped** edges

As it clearly shows, the Actran solution, based on ESL approach is different from the MUL2 one which is based on layer-wise; in fact the ESL is defined where all the laminate layers are referred to the same degrees of freedom (DOFs), whose advantages are their inherent simplicity and low computational cost, due to the small number of dependent variable, but it results to fail in the dynamic response, since in the high frequency range, some differences are visible. The MUL2 solution is based on Layer-wise theory (LW), this approach provide the variables to be linked to a 'specific' layer.

In this work, a new high-order layer-wise plate formulation for vibration of laminated composite plate is used, whose performance of these LW models is better but it require high computational effort as the number of variables increases with the number of layer themselves.

These differences will be also distinguished in the node local pressure because the system is acted (throughout the initial displacement) in different way, because the displacement continuity condition between the plate structure and the adjacent fluid particle, the driving relation between the fluid particles and the plate dynamic response, changes considering the different model.

The previous results were obtained using LW2 theory, but in the following we are asking how the solution (and the relative difference in Actran) using LW1 theory.

Now Let us consider *LW1 Theory*.

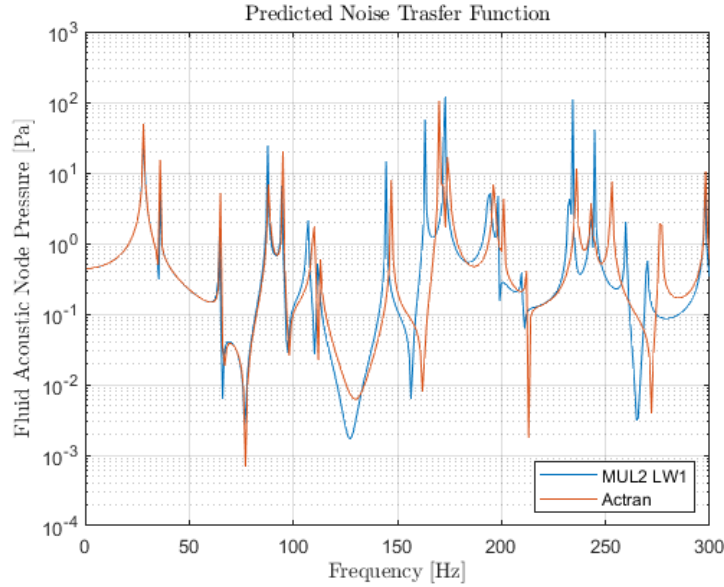


FIGURE 6.29: Fluid Node Pressure in point B(0.75m, 0.75m, 0.75m); [left] and C(0.35m, 0.70m, 0.65m) [right] for **Orthotropic** plates, *weakly* coupled, for the lamination $[0^\circ/90^\circ/0^\circ]$, **simply supported** edges

In the previous figure (6.29), the behaviour does *not* change (from the LW2 one), two different region are distinguished; **low frequency**, resulting the perfect match between two solution (LW1 *Mul2* and *Actran*), while the **higher frequency**, the relative difference will arise because of the theory used to describe the structural model.

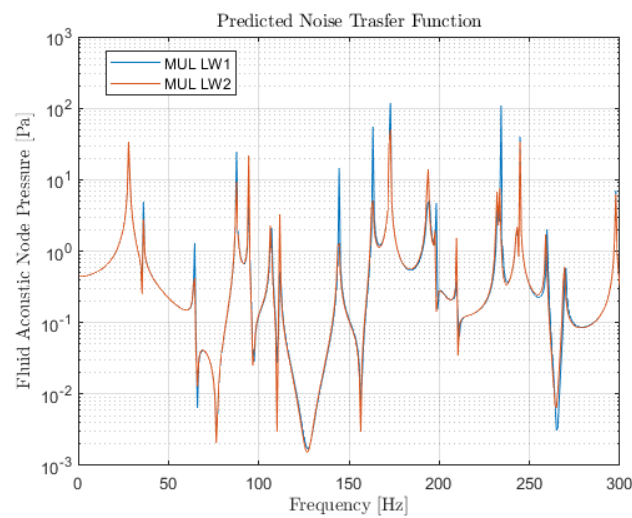


FIGURE 6.30: Relative Difference from LW1 and LW2 theories, the resulting solution are highly comparable

Appendix - Loss of Reality: Shifting Mode

As we stated previously, we must define the order of approximation throughout the thickness of the plate; this means that, if we define LD1, a first order approximation function is defined, that is two points are necessary; while if we define LD2, a second order approximation function is defined, that is three points are necessary, and so on.

These points are placed symmetrically throughout the thickness, so that, for the case LD1, one point is placed at the top ($+h/2$), and the other one is placed down in the bottom one ($-h/2$), where h is the entire thickness plate.

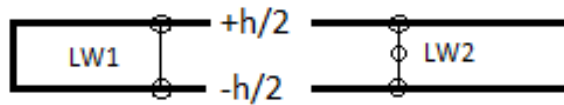


FIGURE 6.31: LD1 at the left **without** the central node, while LD2 at the right **with** the central node

Considering the mid-surface laying at $h = 0$. For Actran, it is necessary the presence of the nodes at the middle of thickness ($h = 0$), on which the fluid node pressure will work; without them, the solution will get be totally wrong. While in the case of LD2, down-half plate is placed inside the fluid volume, without numerical solution loss, because the nodes of fluid will work on the central nodes of the plate, although the loss of reality meaning.

In the case of LD1 since the missing of central nodes, the plate **up-shifting** for $h/2$ is necessary to re-obtain the solution as for LD2, considering errors due to low-order expansion.

In the shifted mode, down-half plate is placed at the coupling interface as in the reality: Fluid - Interface - Structure.

The Shifted mode is necessary for LDN with *odd* N ; while for *even* N it is not, the solution will converge to the same one as the not-shifted mode.

In this part, it is shown one of the most important difference between Industrial software, like Actran, and the MUL2 software. While the former waives the reality in order to use the finite element coupled method; the latter can produce the same outputs without the loss. That's a important key concept.

6.3.4 Resume: Weak coupling Effect

Thanks to the low modal density in the considered frequency range $0[\text{Hz}] - 300[\text{Hz}]$, every single modal contribution is clear visible to effect the node pressure response because of concerning the structural response, and here to the weak coupling between fluid and structure, the natural frequencies of the coupled system are controlled by the plate vibrations mode.

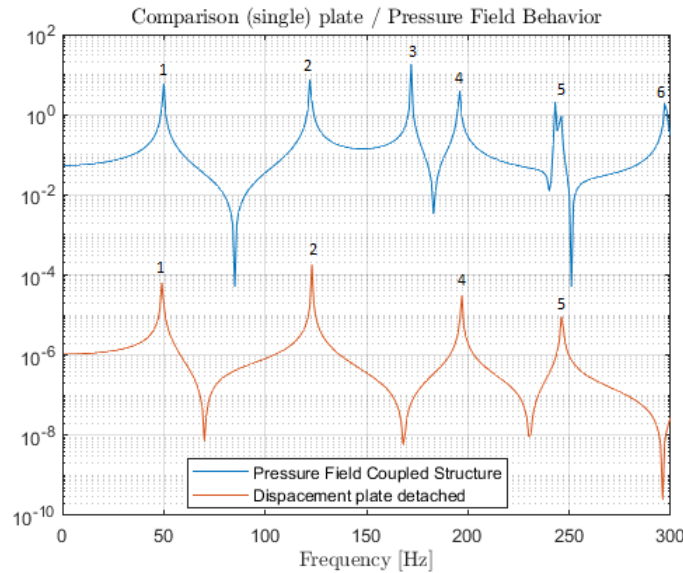


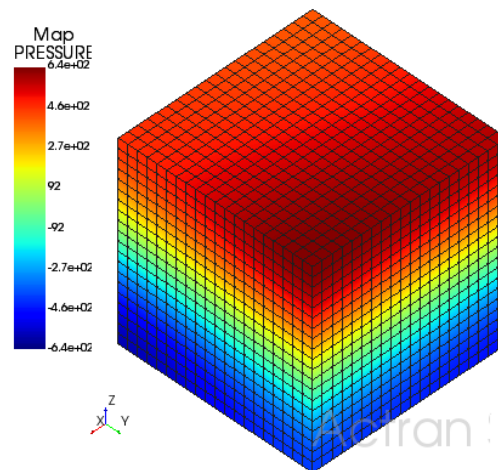
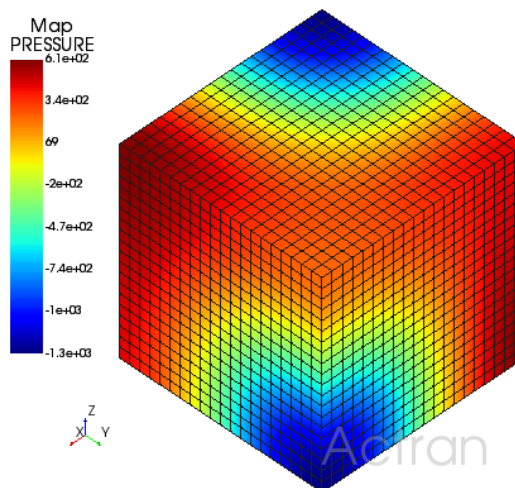
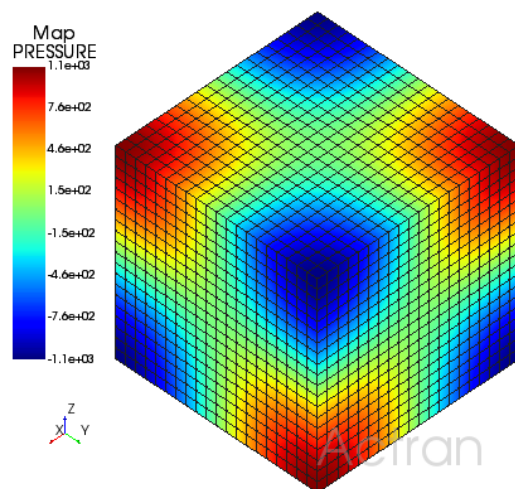
FIGURE 6.32: Comparison: FRF Pressure response (top) and Plate Dynamic Response (bottom)

The effect of using the refined LD2 model with respect to the EDN solution is evident for the plate displacement dynamic; in fact, figures show that the FRF response of the refined LW model appears shifted toward low frequencies, due to the over stiffness exhibited by the ED2 solution, except the LW1 whose behaviour is similar to EDN models. In figure (6.32), that the resonance peak of the coupled system is fully controlled by the modal vibration of plates, since the coupling fluid, in this case air, has low density and so low effect in sway the FRF solution. We can also verify that the resonance frequency, in the case of weak coupling, can be obtained through the **superposition** of the modal vibration of plates (peak 1,2,4,5) and the missing are given by the modal fluid cavity

In fact, through the modal extraction of the **uncoupled** fluid cavity, we obtain the missing peak in FRF solution (peak 3,6)

Modal Extraction of the <i>Uncoupled</i> Fluid Cavity	
Peak	Value
3	171 [Hz]
5	242 [Hz]
6	297 [Hz]

As sake of simplicity, the weak coupling solution (in term of frequency) may be obtained without the coupled resolution of the fluid structural system. This permits a rapid evaluation and low computation effort. This is **not** true in the case of strong coupling, in which the solution is reached just through the resolution of complete system of equation.

FIGURE 6.33: 1st Cavity Mode at 171 [Hz]FIGURE 6.34: 2nd Cavity Mode at 242 [Hz]FIGURE 6.35: 3rd Cavity Mode at 297 [Hz]

Chapter 7

Strong Coupling Interaction

To **fully** complete the *coupled problem*, the displacement continuity condition between the plate particle and the adjacent fluid particle and the driving relation between the fluid particles and the plate dynamic response.

It is usually complex to classify vibro-acoustic systems for their coupling behaviour, the following classification is valid *just* for simple geometries, like those considered in this thesis, it states that whenever an heavy fluid fluid, like as water, is contact with a structure, a strong coupling behaviour is observed.

In general, the continuity condition for the fluid-structure coupling is described through the condition of the velocity of the particles pertaining separately to the fluid medium and the solid plate when the fluid is at rest, closed within the surrounding cavity. Firstly, we have considered the coupling with air, and since its density is low, we have called the '*weak*' coupling. Now we are going to change the the coupled fluid with water, and since its density is quite high, we call the '**Strong**' effect. In this part, we are going to analyse the difference effect of the acoustic cavity in the the evaluation of the node pressure effect.

Please keep in mind that structure dimension will be **unchanged**, in order to compare similar structure, so the *dimension* will be the **same** as the previous case; later we are going to modify the plate dimension as a rectangular in order to evaluate its effect, considering parallelepiped structure cavity. Please keep in mind that the virtual microphones will be placed at the same as the weakly one. The only changing thing is fluid into *Water*.

It consists of a aluminium plate backed by a rigid-walled acoustic cavity in figure (6.15) and in the case of *Strong Coupling*, **Water**, with the following material properties $\rho_0 = 1000 [Kg/m^3]$, $c_0 = 1500 [m/s]$.

We will test this plate in these different condition

- *Isotropic* Plate with *Simply Supported* and *Clamped* edges boundary conditions
- *Isotropic* Plate strongly Coupled increasing the thickness plate
- *Orthotropic* Plate strongly Coupled with *Simply Supported* and *Clamped* edges BC with different lamination $[0^\circ/90^\circ/0^\circ]$ and $[90^\circ/0^\circ/90^\circ]$.

Notation LDN is the notation adopted for LW models, where L define the use of a LW description and D and N indicates the PVD variational principle and the order of the expansion, respectively.

Plotting the Node Pressure for LDN for $N = 2, 3$
For Simply Supported Edges (SS), we obtain

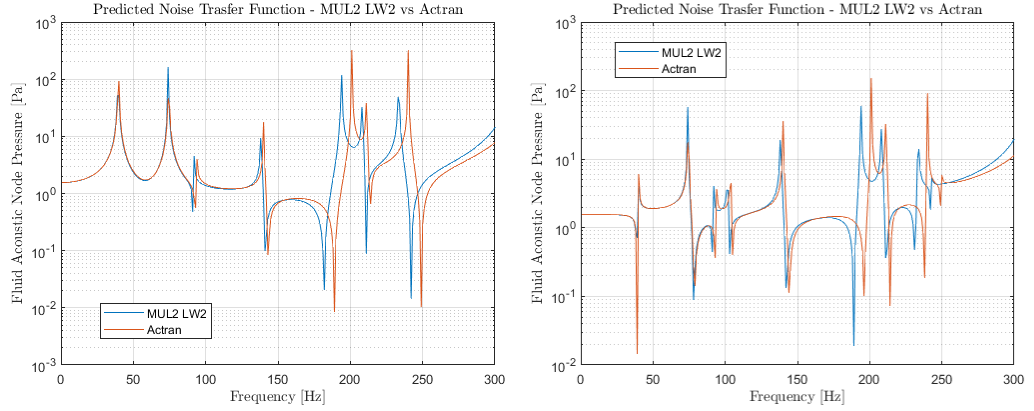


FIGURE 7.1: Fluid Node Pressure in point B(0.75m, 0.75m, 0.75m) [left] and C(0.35m, 0.70m, 0.65m) [right] for **Isotropic** plates for Simply supported edges, using LW2 Mul solution.

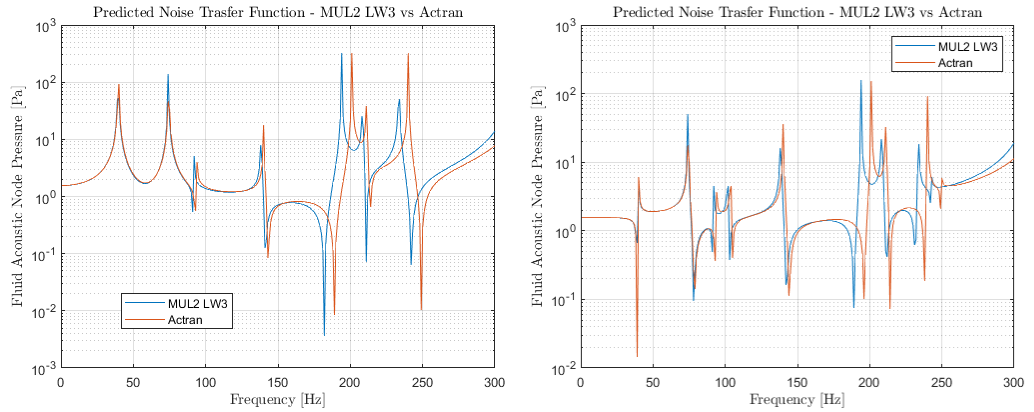


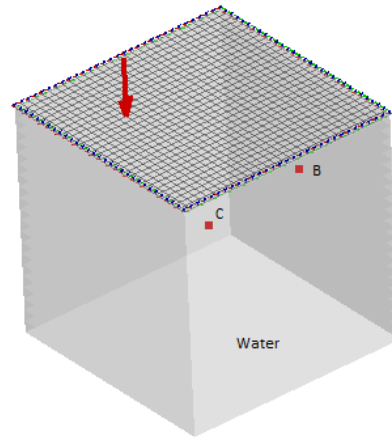
FIGURE 7.2: Fluid Node Pressure in point B(0.75m, 0.75m, 0.75m) [left] and C(0.35m, 0.70m, 0.65m) [right] for **Isotropic** plates for Simply supported edges, using LW3 Mul solution.

We observe, that in *high density* fluid like water, the mean pressure level are higher than the correspondence of air due to the high difference in density value. Nothing new about the behaviour of the relative solution Actran and MUL2 one. The MUL2 LW1 has the *usual* different behaviour as the weak coupling for the isotropic; This lets me assert that the coupling doesn't influence on the rightness of the solution at least for the the Isotropic case. That was valid for Simply supported edge.

In order to evaluate the effect of the boundary condition on the interaction fluid - structure, let us simulate imposing the null rotation around the edges, constituting

the *clamped solution* with isotropic plate (**Strong Coupling**).

Remembering the structure:



In the following, let us graph the comparison between the LWn ($n = 1,2,3$) and the actran solution:

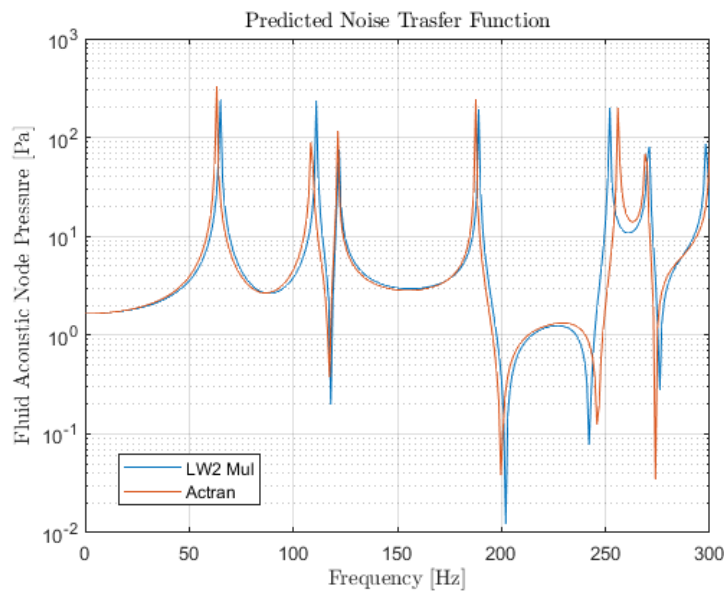


FIGURE 7.3: Fluid Node Pressure in point B(0.75m, 0.75m, 0.75m) for **Isotropic** plates for *Clamped edges* for LW2 and Actran for **Strong Coupling**

It can be seen that the natural frequency of the clamped system are distinctly higher than those of the simply supported system in the lower frequency range. This is attributed to the more rigorous constraint provided by the clamped condition than that by the simply supported condition, which is equivalent to increasing the panel stiffness. Finally, it can be noticed that increasing the edge does not provide any difference in solution, none effect could be attributed due to its constraint.

The difference between the MUL2 LW1 is due to **locking effect**.

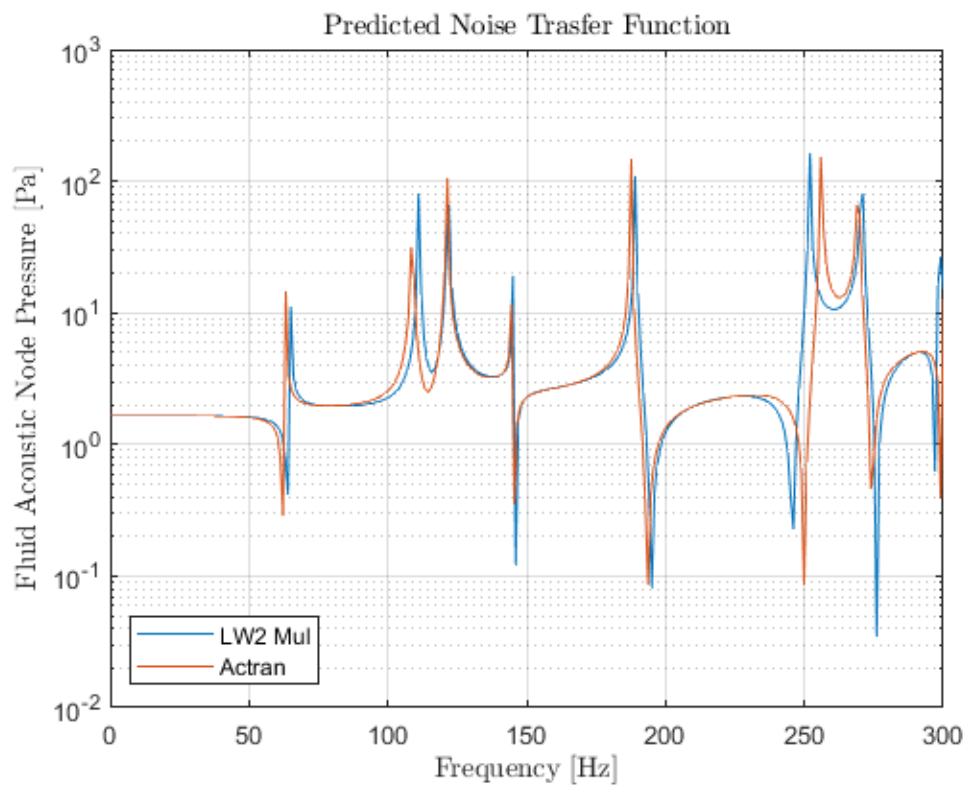


FIGURE 7.4: Fluid Node Pressure in point C(0.35m, 0.70m, 0.65m) for **Isotropic** plates for *Clamped edges* for LW2 and Actran for **Strong Coupling**

7.0.1 The Locking Phenomenon in finite element method

The *Locking Effect* is a term describing the **overestimation** of the stiffness in a structure or element, leading to poor prediction of the structural response in terms of displacement.

Solid elements with linear interpolation, as in the LW1 case, are especially susceptible to many locking phenomena. Special precautions to remedy these problems are therefore needed in order to obtain an element that is usable in analysis of shell like structures [29]. Common locking phenomena are due to the *Poisson and thickness locking* whose phenomena occurs in out-of-plane bending analyses using solid elements. The underlying reason for this effect is the approximation on the displacement field. A linear displacement approximation, will produce constant transverse normal strains through the thickness, which will couple with the linearly varying in-plane strains due to the Poisson's effect. This causes a discrepancy between the transverse and in-plane strains, leading to overestimation of the stiffness.

In order to avoid it, we will considering two elements constituting the whole plate thickness.

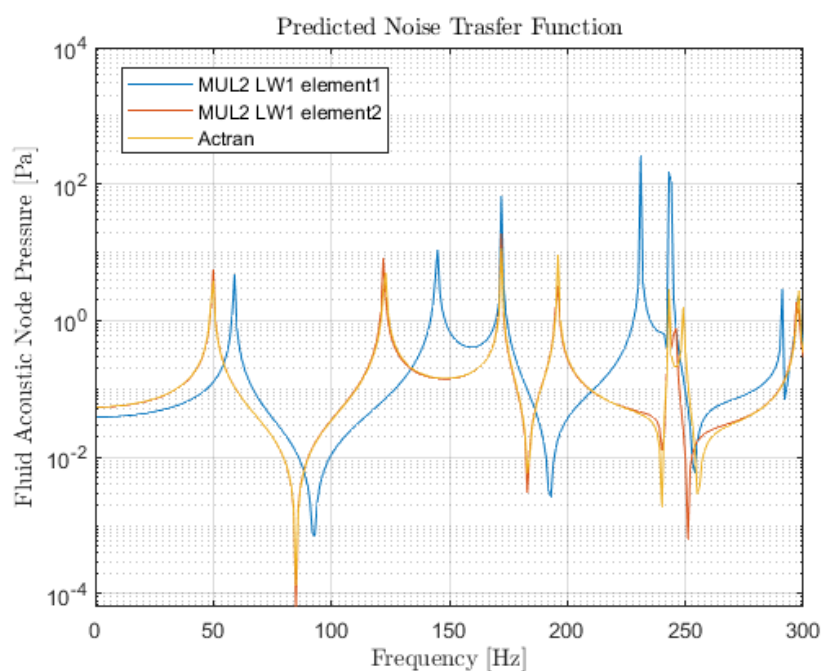


FIGURE 7.5: Fluid Node Pressure in point B(0.75m, 0.75m, 0.75m) for **Isotropic** plate, considering considering MUL2 LW1 with element 1 and 2 and Actran

This is symptom of the locking effect affecting the MUL2 solution.

7.0.2 Isotropic Plate strongly Coupled increasing the thickness plate

The influence of panel thickness, in the case of **water**, on SPL is particularly **strong** for finite systems at low frequencies, the significance of which should not be overlooked in the process of designing.

The Plate reference is fixed at $t_{ref} = 0.01 [m]$, it might be considered as thin shell strongly coupled. In order to study the influence of panel thickness, we are going to consider different thicknesses $\times 10$, $\times 20$, $\times 30$, so the panel plate may be considered as a thick.

The results are the following

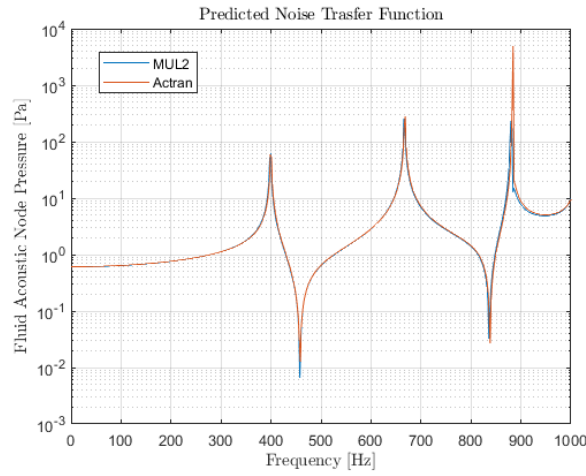


FIGURE 7.6: Fluid Node Pressure in point B(0.75m, 0.75m, 0.75m) for **Isotropic** plate, considering thickness $\times 10 t_{ref}$ for LW3 MUL2 and Actran for **Strong Coupling**

The solution seems not to be influenced by the coupling effect, and as in the previous of weak coupling, The MUL2 solution and Actran one are comparable also in this case.

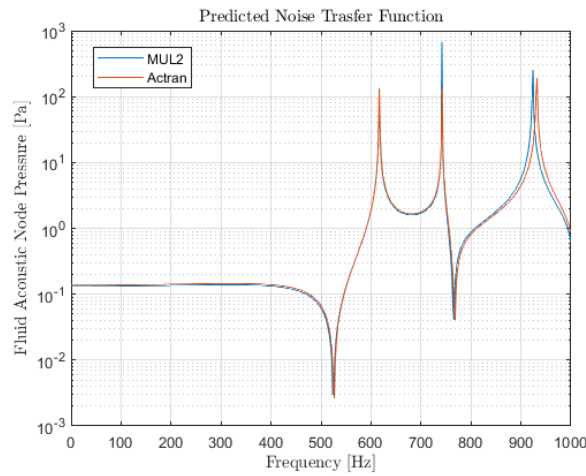


FIGURE 7.7: Fluid Node Pressure in point B(0.75m, 0.75m, 0.75m) for **Isotropic** plate, considering thickness $\times 20 t_{ref}$ for LW3 MUL2 and Actran for **Strong Coupling**

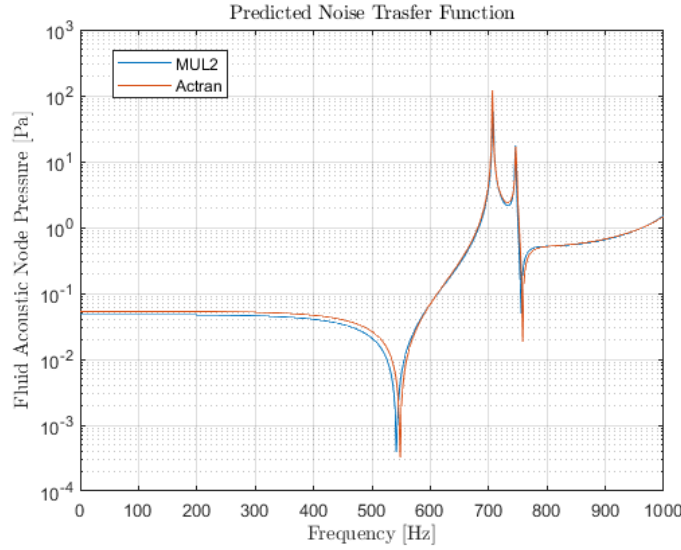


FIGURE 7.8: Fluid Node Pressure in point B(0.75m, 0.75m, 0.75m) for **Isotropic** plate, considering thickness $x30 t_{ref}$ for LW3 MUL2 and Actran for **Strong Coupling**

Finally, we can state that the thickness of the plate doesn't influence the relative error between the MUL2 and Actran solution.

7.0.3 Orthotropic Plate strongly Coupled with Simply Supported and Clamped edges BC with different lamination $[0^\circ/90^\circ/0^\circ]$ and $[90^\circ/0^\circ/90^\circ]$.

We consider a multi-layered composite plate, coupled to **water**; three-layered composite, composed by the following mechanical constants $E_1 = 25 [GPa]$, $E_2 = E_3 = 1 [GPa]$, $G_{13} = G_{23} = 0.5 [GPa]$, $G_{12} = 0.2 [GPa]$ and $\nu_{13} = \nu_{23} = \nu_{12} = 0.25$ considering different lamination $[0^\circ/90^\circ/0^\circ]$ and $[90^\circ/0^\circ/90^\circ]$, despite we will not aspect any huge difference.

We consider the same dimension $[1m \times 1m]$, and the excitation is placed in the same point as the previous, coupled the acoustic cavity below. The following results are obtained though using LW2 theory.

The results, using **LW2 theory**, are the following

In the previous figures, we can verify the the difference between the Actran solution and the MUL2. As mostly explained before, in the case of ortotropic plates, the difference arises in higher frequency range due to the fundamental difference of structural behaviour model used in the description.

The strong coupling may be influenced by the fluid density, in this case, high equal to $1000 \left[\frac{Kg}{m^3} \right]$.

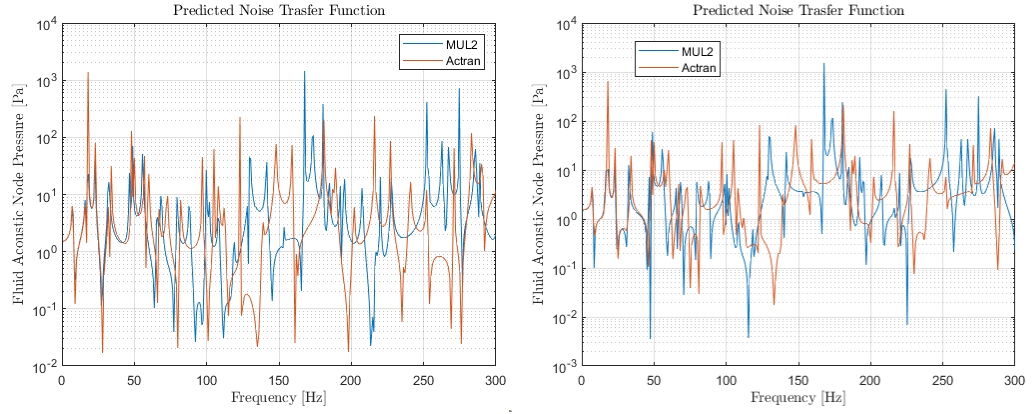


FIGURE 7.9: Fluid Node Pressure in point B(0.75m, 0.75m, 0.75m); [left] and C(0.35m, 0.70m, 0.65m) [right] for **Orthotropic** plates, *strongly* coupled, for the lamination $[0^\circ/90^\circ/0^\circ]$, **simply supported** edges

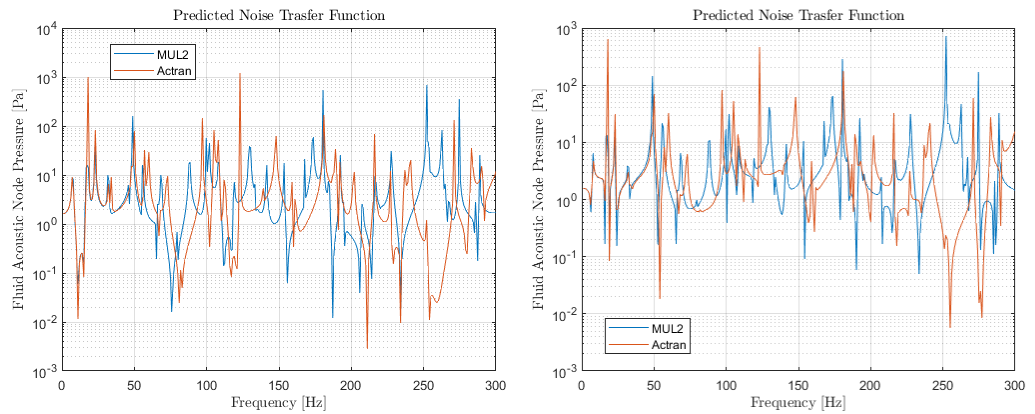


FIGURE 7.10: Fluid Node Pressure in point B(0.75m, 0.75m, 0.75m); [left] and C(0.35m, 0.70m, 0.65m) [right] for **Orthotropic** plates, *strongly* coupled, for the lamination $[90^\circ/0^\circ/90^\circ]$, **simply supported** edges

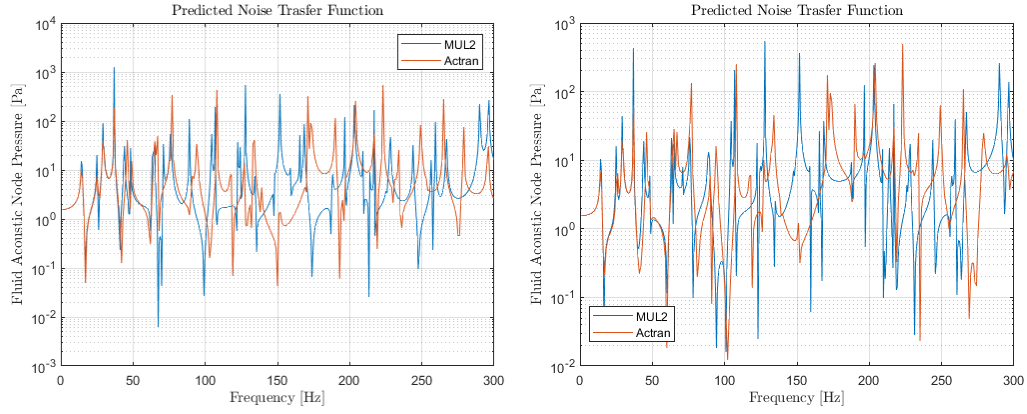


FIGURE 7.11: Fluid Node Pressure in point B(0.75m, 0.75m, 0.75m); [left] and C(0.35m, 0.70m, 0.65m) [right] for **Orthotropic** plates, *strongly coupled*, for the lamination $[0^\circ/90^\circ/0^\circ]$, **clamped edges**

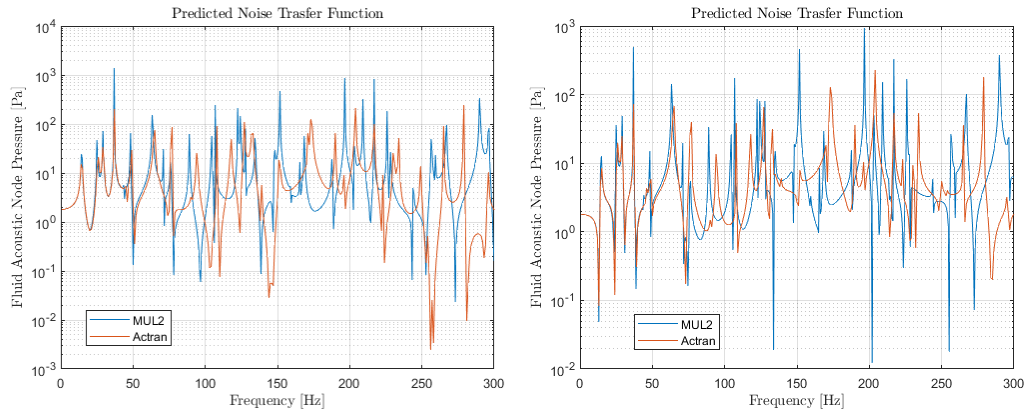


FIGURE 7.12: Fluid Node Pressure in point B(0.75m, 0.75m, 0.75m); [left] and C(0.35m, 0.70m, 0.65m) [right] for **Orthotropic** plates, *strongly coupled*, for the lamination $[90^\circ/0^\circ/90^\circ]$, **clamped edges**

As it clearly shows, the Actran solution, based on ESL approach is different from the MUL2 one which is based on layer-wise; in fact the ESL is defined where all the laminate layers are referred to the same degrees of freedom (DOFs), whose advantages are their inherent simplicity and low computational cost, due to the small number of dependent variable, but it results to fail in the dynamic response, since in the high frequency range, some differences are visible. The MUL2 solution is based on Layer-wise theory (LW), this approach provide the variables to be linked to a 'specific' layer.

In this work, a new high-order layer-wise plate formulation for vibration of laminated composite plate is used, whose performance of these LW models is better but it require high computational effort as the number of variables increases with the number of layer themselves.

These differences will be also distinguished in the node local pressure because the system is acted (throughout the initial displacement) in different way, because the displacement continuity condition between the plate structure and the adjacent fluid particle, the driving relation between the fluid particles and the plate dynamic response, changes considering the different model.

The previous results were obtained using LW2 theory, but in the following we are asking how the solution (and the relative difference in Actran) using LW1 theory.

7.0.4 Resume: Strong coupling Effect

Thanks to the high density in the considered frequency range $0[\text{Hz}] - 300[\text{Hz}]$, every single modal contribution is clear visible to effect the node pressure response because of concerning the structural response, and here to the strong coupling between fluid and structure, the natural frequencies of the coupled system are not just controlled by the plate vibrations mode, as happened in low density effect.

The peak given by the single structure will not create a corresponding peak for the coupled one, because the element associated due to the density is not negligible, but high; affecting itself on solution.

$$\begin{bmatrix} \mathbf{M} & 0 \\ -\rho_f \mathbf{S}^T & \mathbf{Q} \end{bmatrix} \begin{Bmatrix} \ddot{\mathbf{Q}} \\ \ddot{\mathbf{P}} \end{Bmatrix} + \begin{bmatrix} \mathbf{K} & \mathbf{S} \\ 0 & \mathbf{H} \end{bmatrix} \begin{Bmatrix} \mathbf{Q} \\ \mathbf{P} \end{Bmatrix} = \begin{Bmatrix} \mathbf{F} \\ 0 \end{Bmatrix}$$

In the following, We are going to deeply study another important geometry, *rectangular cavity* backed by a panel. This is important because it represents one of examples presented in vibroacoustic literature, in the thesis "*Krylov Subspace Based Direct Projection Techniques for Low Frequency, Fully Coupled, Structural Acoustic Analysis and Optimization.*" and in the book "Finite Element and Boundary Methods in Structural Acoustics and Vibration" by Sgard and Atalla.

In order to test the unknown validity of a program, MUL2; we are going to **compare** it a solution presented in literature. That represents a precious mine to pursuit our duty.

Chapter 8

Numerical Model Validation

In the following, We are going to deeply study another important geometry, *rectangular cavity* backed by a panel. This is important because it represents one of examples presented in vibroacoustic literature, in the thesis "*Krylov Subspace Based Direct Projection Techniques for Low Frequency, Fully Coupled, Structural Acoustic Analysis and Optimization.*" and in the book "Finite Element and Boundary Methods in Structural Acoustics and Vibration" by Sgard and Atalla [5].

In order to test the unknown validity of a program, MUL2; we are going to **compare** it a solution presented in literature. That represents a precious mine to pursuit our duty.

8.1 Vibro-Acoustic Response of a Rectangular Cavity (Water Filled) backed by a Isotropic panel

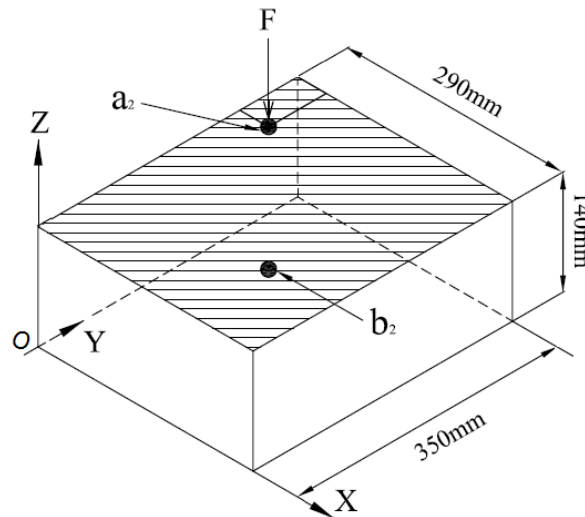


FIGURE 8.1: Plate backed rectangular cavity (water filled) system. Excitation location: $A = (0.0435 [m], 0.28 [m], 0.14075 [m])$; Measurement location(s): $A = (0.0435 [m], 0.28 [m], 0.14075 [m])$, $B = (0.1305 [m], 0.175 [m], 0.07 [m])$.

In order to exhibit the limitations (as previously introduced) of using modal basis let us consider the following example as in figure 8.1.

This consists of a simply supported aluminium plate backed by a rigid-walled acoustic cavity. The lateral dimensions of the plate are $a = 0.35 [m]$, $b = 0.29 [m]$ and its thickness is $1.5 [mm]$.

The lateral dimensions of the cavity are the same as the plate and its depth is $h_c = 14 [cm]$. The material properties are the following: $E = 72 [GPa]$, $\rho_{plate} = 2700 [Kg/m^3]$, $\nu = 0.33$. The fluid properties (**water**) are $\rho_0 = 1000 [Kg/m^3]$, $c_0 = 1500 [m/s]$. A harmonic unit point force (1N) is applied normally to the plate at point A = (0.0435 [m], 0.28 [m], 0.14075 [m]) over the entire frequency range of 0 – 600 [Hz]. The mesh used for the discretization is [10x10x10].

In the case of **air** (*weak coupling*), the use of uncoupled or coupled modal basis works well. However, in the case of **water** (*strong coupling*), the solution is not converged.

The desired output quantities considered for this test case are as follows; the structural displacement response at driving point at the unit structural point force location A = (0.0435 [m], 0.28 [m], 0.14075 [m]), and fluid pressure (quite close to the center of the rectangular domain) at B = (0.1305 [m], 0.175 [m], 0.07 [m]).

We are going to follow the same path (as in the previous chapter), but in this case we are going to visually compare to the solution in available literature. We have to validate the structural behaviour in term of displacement. We will compare the displacement of the solution of MUL2 software, to the corresponding Actran solution, in order to eliminate any structural responsibility in the difference (shown in the following) valid for the coupled cavity [1].

We will test this plate in these different condition

- *Isotropic Plate with Simply Supported edges boundary condition*
- *Isotropic Plate with Clamped edges boundary condition*

First of all, we are going to measure structural displacement in A, both in Simply-supported and Clamped condition considering **just** the *Plate Analysis*

From the previous pictures, we can state that the LW1 always present the '*different*' behaviour respect to high order theories (LW2, LW3), and changing the boundary condition (clamped) although more rigid, nothing new to be detected. The MUL2 solution and Actran are comparable.

8.1.1 Water Coupled Cavity

Let us lead to the coupled structure analysis using simply supported edges and let us compare it to the solution in literature

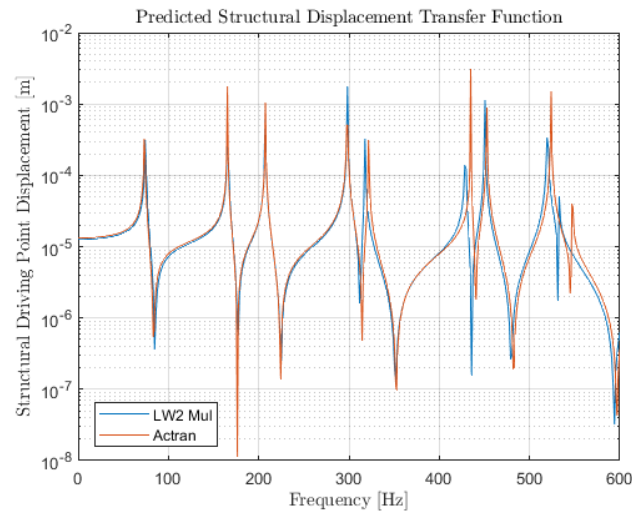


FIGURE 8.2: Displacement at $(4.35 [cm], 0.28 [m])$ for *Isotropic* plate **LW2** considering *Simply Supported* edges

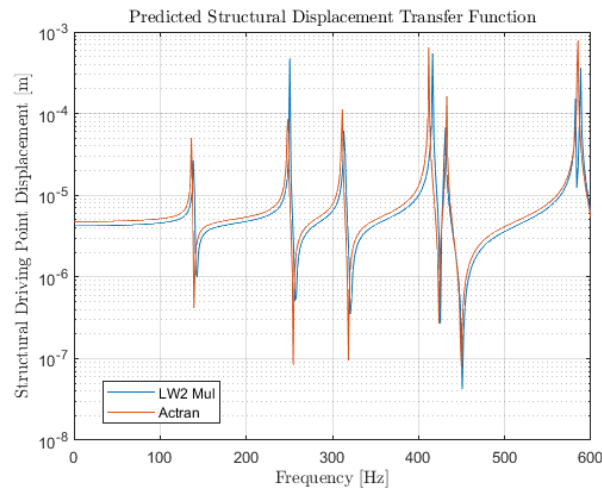


FIGURE 8.3: Displacement at $(4.35 [cm], 0.28 [m])$ for *Isotropic* plate **LW2** considering *Clamped*

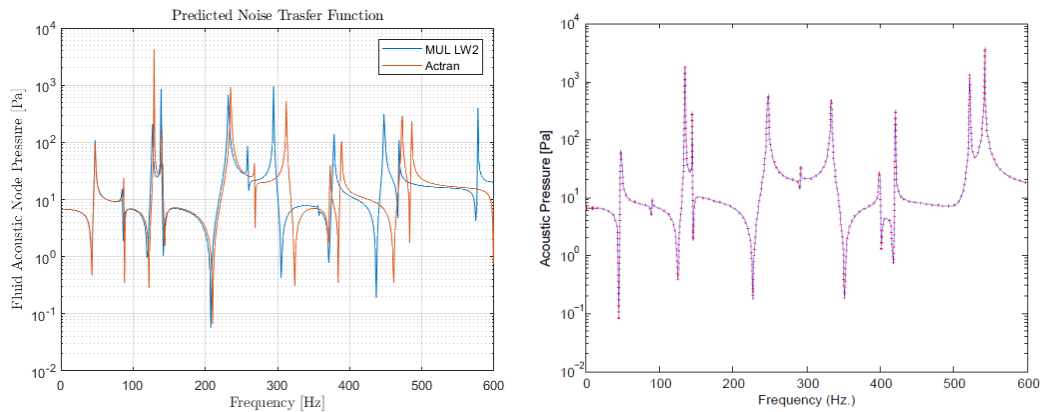


FIGURE 8.4: Fluid Node Pressure in point B; (left) Actran and Mul2 (LW2) solution, (right) literature

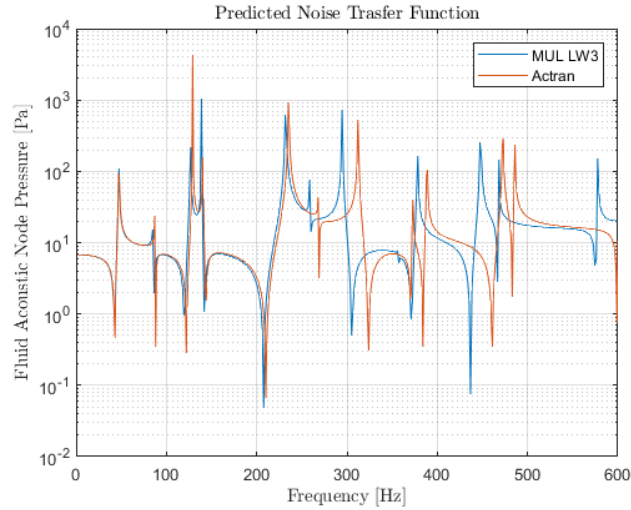


FIGURE 8.5: Fluid Node Pressure in point B using Actran and Mul2 (LW3)

In the previous figure, something important happens. The MUL2 solution highly comparable to a solution in literature obtained with other ways. **The validating process has been passed.** The main peak of the solution process highly coincide the the solution in literature, and this is enough important for the validating process design.

The displacement in A is the following desired feature.

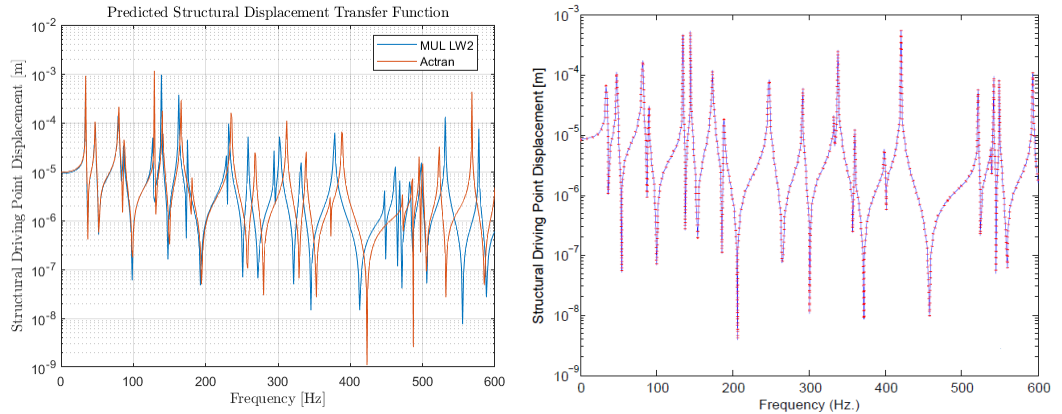


FIGURE 8.6: Plate (coupled) Displacement in point A; (left) Actran and Mul2 (LW2) solution, (right) literature

The displacement function follows the same directives explained in the previous section. Finally, we are changing the boundary condition from *Simply Supported* to *Clamped*. The resulting pressure in B for clamped edges is the following

We can observe the same difference in LW1 as in any other previous graph due to the low kinematics parameters used for describing it, while the LW2 and LW3 are almost comparable.

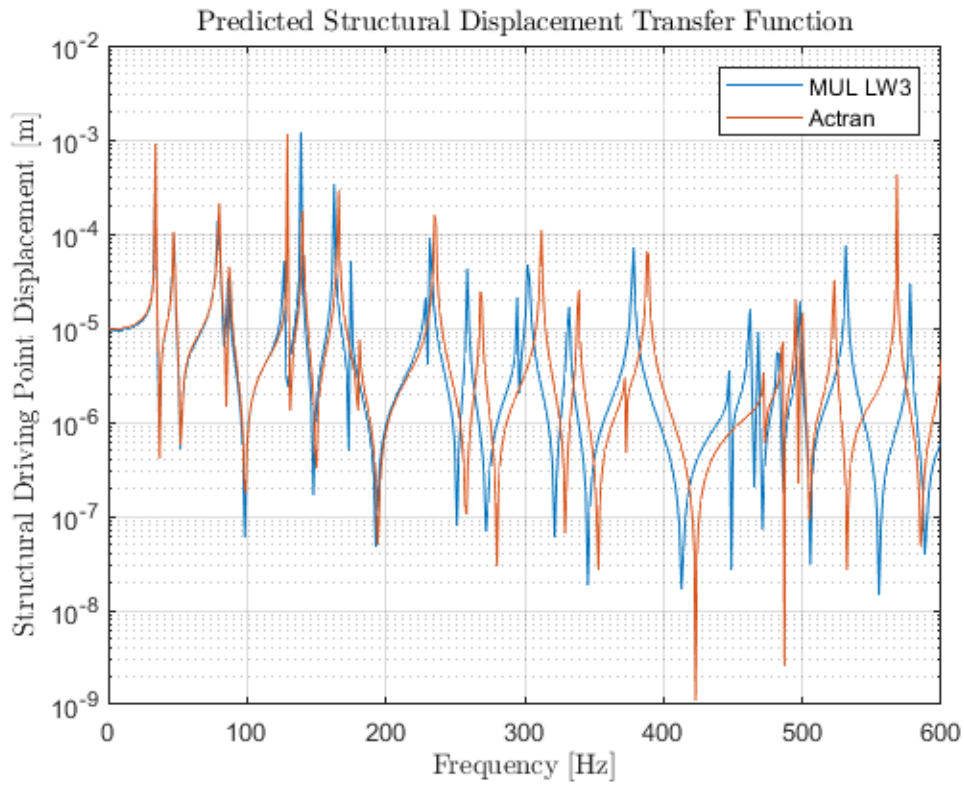


FIGURE 8.7: Plate (coupled) Displacement in point A; Actran and Mul2 (LW3) solution

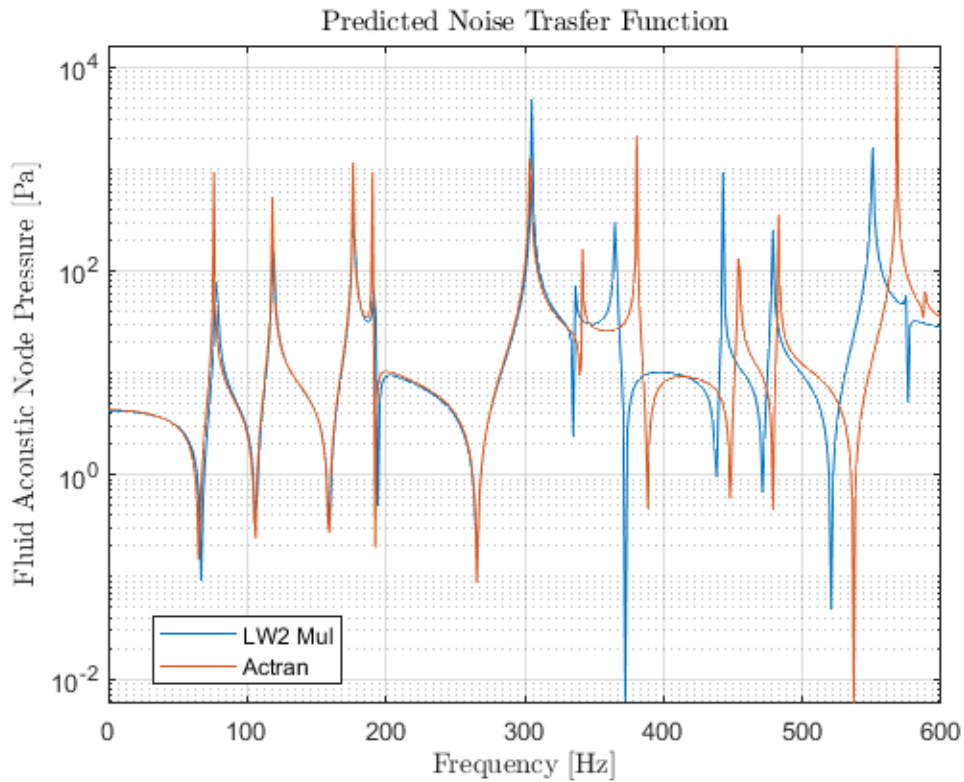


FIGURE 8.8: Fluid Node Pressure at B for *Isotropic* plate **LW2** considering *Clamped*

MUL2 solutions are comparable for LW2 and LW3, despite LW1 shape presents valuable error (compared to the Actran solution), since it evolves linear expansion through the thickness (Kinematics of displacement **not** fully expressed through linear expansion), probably it's not sufficient grade to completely represent the displacement, we can also verify that LW1 predicts bigger resonance frequency, and the error (the distance between Actran peak and LW1 one) increases with the frequency itself.

As a matter of fact, the LW2 solution can properly represent the structural point displacement in a correct way. Both Simply supported and Clamped have comparable behaviour, but the Clamped solution error is bigger than simply supported one (for the same frequency range).

Indeed, The solution in MUL2 seems to present the same trend as the solution in literature, that behaviour encourage over the strong validity of MUL2, thanks to the advance finite element (*through the Carrera Unified Element*), we can obtain better solution over the composite plate applying the **Layer-Wise Theory** (LW).

8.2 Sandwich Composite Plate

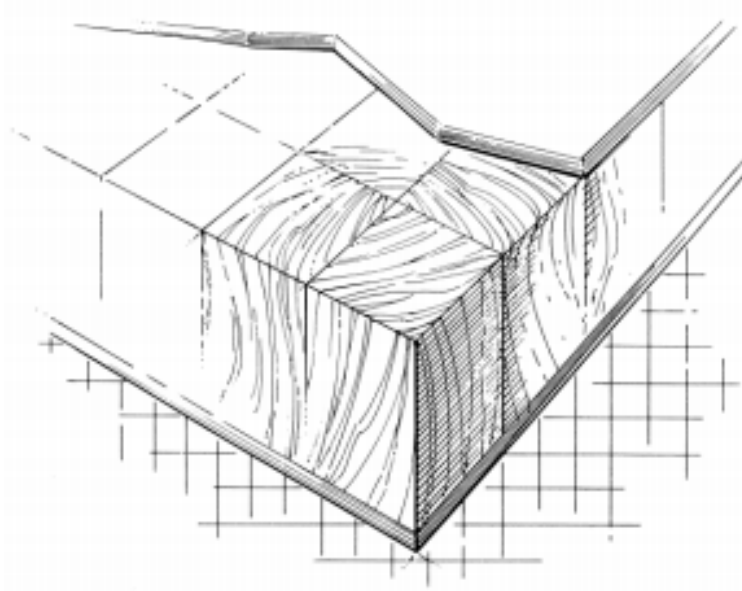


FIGURE 8.9: Example of Sandwich plate: **Face Sheet** and **Core**

We will deal with a squared dimension 1×1 [m^2] made by aluminium with thickness equal to 0.01 [m]; through a structural mesh [10×10 elements]. Firstly, we consider the following multi-layered composite plate composed by the following mechanical constants **Graphite-Epoxy**: $E_1 = 132.38$ [GPa], $E_2 = E_3 = 10.76$ [GPa], $G_{13} = G_{12} = 5.65$ [GPa], $G_{23} = 3.61$ [GPa] and $\nu_{13} = \nu_{12} = 0.24$ $\nu_{23} = 0.49$ for the face sheets (superior and inferior); while we are considering a Isotropic material for the core, whose mechanical constants are Young's Modulus $E_s = 0.00689$ [GPa], mass density $\rho_s = 0.097$ [kg/m^3] and Poisson's ratio $\nu = 0.0$.

The composite structure is made of two-layered *Gr - Ep* skins with lamination scheme $[90 / 0]$ and a soft core as above. The overall plate thickness is $h = 12$ [mm], so divided: the face skins layers are 0.5 [mm] each; and the core thickness is 10 [mm]. A constant amplitude force excitation of 1 [N], over the frequency range from $0 - 300$ [Hz], was applied at one of the off-center nodes of the structural 10×10 Finite Element mesh with coordinate $(0.25m, 0.35m)$, point at which the measurement of displacement is acted.

Excitation location: $A = (0.25m, 0.35m, 1m)$;

Measurement locations: $B = (0.75m, 0.75m, 0.75m)$, $C = (0.35m, 0.70m, 0.65m)$;

The fluid constants are $(343.0$ [m/s], 1.2 [Kg/m^3]) for Air, while $(1500.0$ [m/s], 1000.0 [Kg/m^3]) for water, indicating the speed of the sound and density respectively [1]. The solution are as follows

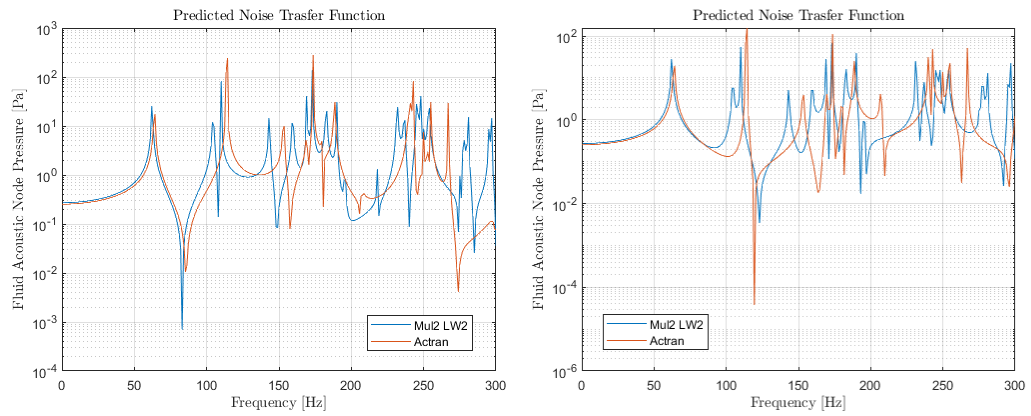


FIGURE 8.10: Sandwich Plate (**Air** coupled); Fluid node pressure in B (left); Fluid node pressure in C (right) with the relative Actran solution

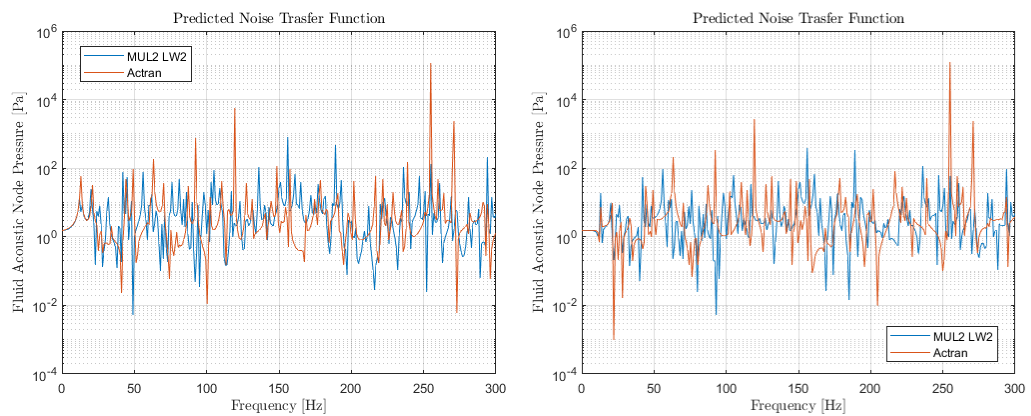


FIGURE 8.11: Sandwich Plate (**Water** coupled); Fluid node pressure in B (left); Fluid node pressure in C (right) with the relative Actran solution

As we can see that two solution are quite different. In *Weak* coupling, modal solution due to the lower modal density in the frequency interval $0 - 300$ [Hz]; that is in contrast considering the *Strong* coupling, because of high modal density, makes the solution unpredictable.

Dealing with *sandwich structures*, they usually present two main components: thin *face sheets* and a *thick core*. These layers are made to fulfill different functions. The former, [*thin face sheets*], give the part of the structural resistance and bending stiffness to the overall structure; while the latter, [*core*], is usually thicker than the skins and performs different functions, as acoustic and thermal insulation purpose, carrying the whole shear load acting on the structure itself. This fundamental characteristic increases the vibration damping capability of the material, thus leads to a more complex modelling, due to the frequency dependence of the material parameters. [28][30]

On the other hand, we can observe a difference in the relative behaviour of the solution. For **Weak Coupling**, A fully converged solution is reached considering an uncoupled modal basis obtained with the acoustic and structural modes below $2.5 f_{max}$, which means that below almost 100 [Hz] the Mul2 and Actran solution are quite the same; while in exactly the same condition, but considering **Strong Coupling**.

A fully converged solution is reached below $12 f_{max}$, which represents that larger difference between the two set of solutions is expected as the frequency increases, and when larger wavelengths appear, tend to highlight this effect. It can be pointed out that a poor description of the structural behaviour can potentially lead to significant error at high frequencies range. [10]

In *weak coupling*, thanks to the *low modal density* in the frequency range, every single modal contribution is clear visible in the final solution, mostly for what concern the structural response; here, due to the weak coupling between fluid and structure, the final solution is represented by a simply over position of the modal problem solution for both sandwich-plate and volume of fluid.

This is not true for the *strong coupling*. This results are *in agreement* with the analysis reported in chapter 7, where it has been shown that for thin multi-layered laminated plates. Although, the higher order effects get **more important** in the high frequency range and affect the resultant acoustic field pressure measurement.



FIGURE 8.12: Sandwich Plate: **Face Sheet** and **Core**

8.3 Vibro-Acoustic Response of a Cubic Cavity backed by a Multi-layered panel

This test case consists of a simply supported orthotropic multi-layered cubic plate backed by a rigid-walled acoustic cavity. The lateral dimension of the cubic plate are $l = 1 [m]$. The lateral dimensions of the cavity are the same as the plate and its depth is equal to the lateral side $l_{cubic} = 1 [m]$.

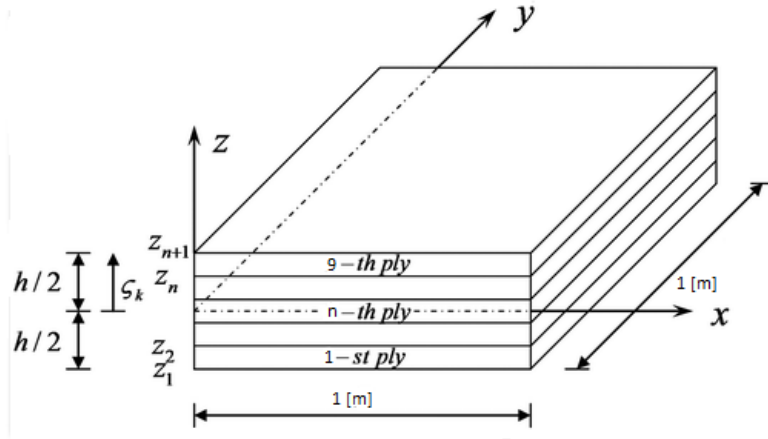


FIGURE 8.13: Multi-layered Plate

The multi-layered structure consists of **nine layers** in symmetric cross-ply configuration with sequent lamination scheme $[0/90, 0/90, 0/90/0, 90/0]$. The plate thickness is $h = 3 [mm]$, and each lamina is $0.3333 [mm]$ thick. In order to deeply analyse the behaviour of the orthotropic material, we are going to consider the following composite - mechanical constants: $E_1 = 132.38 [GPa]$, $E_2 = E_3 = 10.76 [GPa]$, $G_{13} = G_{12} = 5.65 [GPa]$, $G_{23} = 3.61 [GPa]$ and $\nu_{13} = \nu_{12} = 0.24$, $\nu_{23} = 0.49$ [9].

A harmonic unit point force is applied normally to the plate at point over the frequency range from $0 - 300 [Hz]$, was applied at one of the off-center nodes of the structural 10×10 Finite Element mesh with coordinate $(0.25m, 0.35m)$, point at which the measurement of displacement is acted [6].

Excitation location: $A = (0.25m, 0.35m, 1m)$;

Measurement locations: $B = (0.75m, 0.75m, 0.75m)$;

The fluid constants are $(343.0 [m/s], 1.2 [Kg/m^3])$ for Air, while $(1500.0 [m/s], 1000.0 [Kg/m^3])$ for water, indicating the speed of the sound and density respectively. [1]

The results are the following

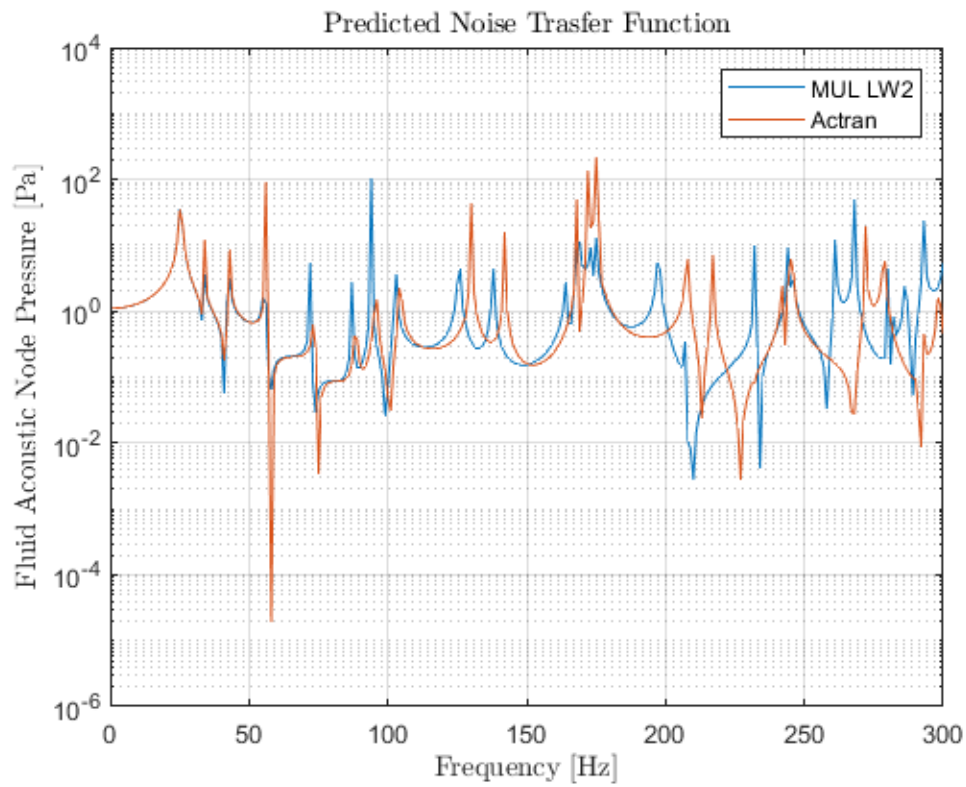


FIGURE 8.14: Multi-layered (nine-ply) Plate (**Air** coupled): Fluid node pressure in B with the relative Actran solution

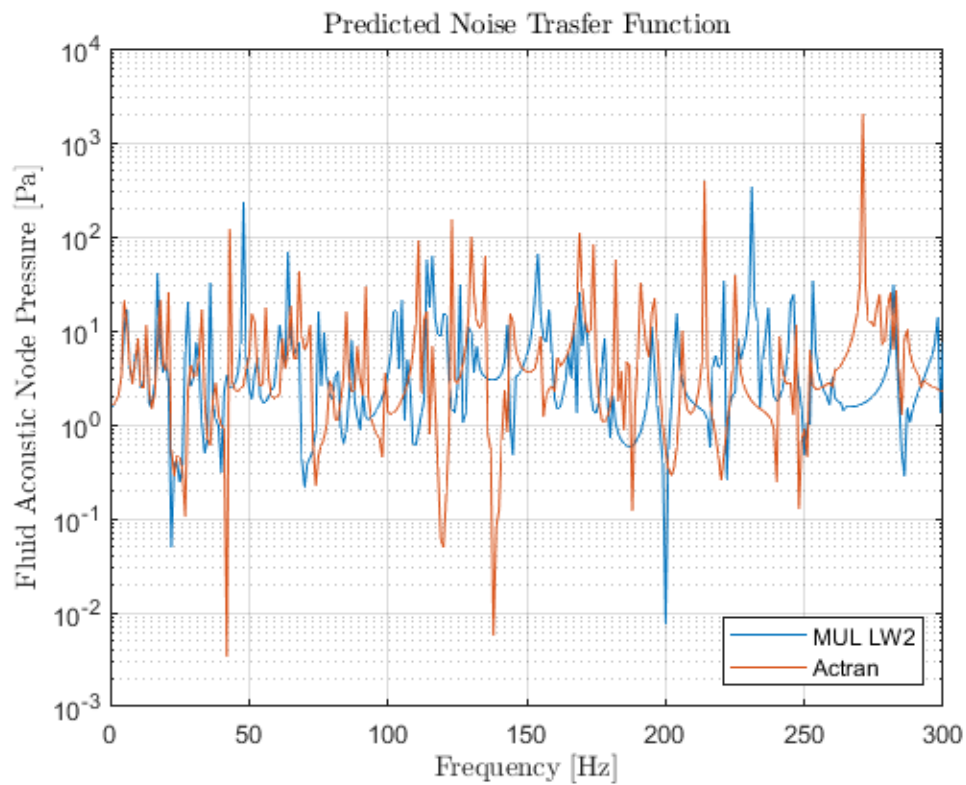


FIGURE 8.15: Multi-layered (nine-ply) Plate (**Water** coupled): Fluid node pressure in B with the relative Actran solution

8.4 Mesh Variation Effect

The approximation of space-dependent physical or numerical functions by uniform patch averages reaches its limit when the fluctuation pattern within a patch cannot be captured by the coarse resolution of the patch grid. When the wavelength becomes smaller than two patches, the grid resolution is not sufficient small anymore to capture the wave shape and aliasing phenomenon will occur.

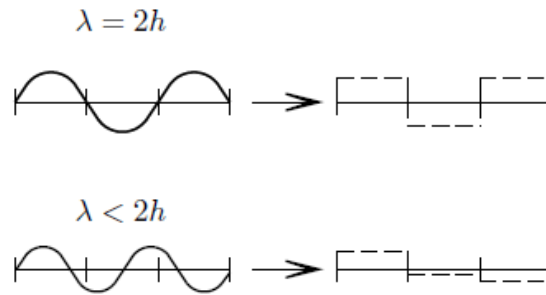


FIGURE 8.16: Patch size limit at the spatial wavelength frequency

The main limitation of FEM-coupled method is that modes with a transverse wavelength below the dimension of two patches are missed. In this case, the patch grid is not able to represent the wave shape according to the Nyquist theorem and aliasing effects occur.

As sake of simplicity, the relative difference might be quite high between two solution, for instance, considering a parallelepiped cavity. The Mesh has an importance into the final solution. The coarse mesh is composed by $[5 \times 5 \times 5]$, while the finest one by $[20 \times 20 \times 10]$ When frequency are low, the pressure peak are almost the

same; while increasing the frequency, the pressure peak of the coarser one has *lost its fairness*, this because we are going to consider a wide range of frequency.

Remark *The missed modes in the higher frequency range lead to an underestimation of the system response.*

In fact the dimension of mesh size in relation of the frequency may affect the resulting solution of the problem. As sake of clarity, we are going compare solutions at different resulting meshes, as we started using a 10×10 [elements] (*coarser mesh*); while we are approaching handling a 20×20 [elements] (*finer mesh*); obviously the resulting solution ws going to change; but the computational time is increasing as well too.

In this part, A simple laptop was not sufficient to achieve results, but Server was necessary. We are going to analyse the variation of both solution (Mul2 and Actran) for both situation (weak and strong coupling). We are using a simple Cubic Cavity, with Ortotropic material $[0^\circ/90^\circ/0^\circ]$, using the same material property as in reference (6).

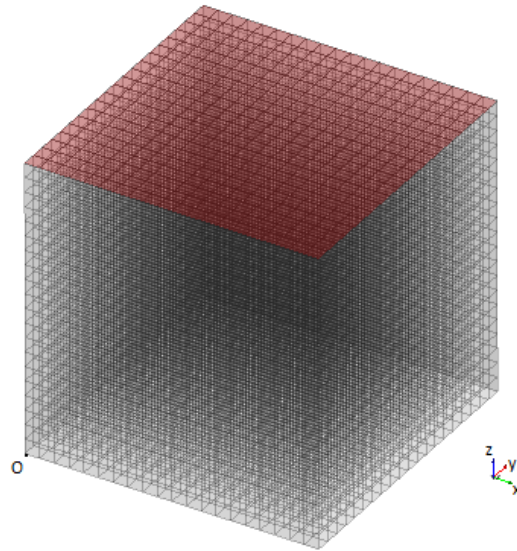


FIGURE 8.17: Mesh 20x20 elements, Cubic Cavity, Orthotropic Material Excitation Location in $A = (0.25, 0.35m, 1m)$; Measurement Location in $B = (0.35m, 0.7m, 0.65m)$

Air Cavity

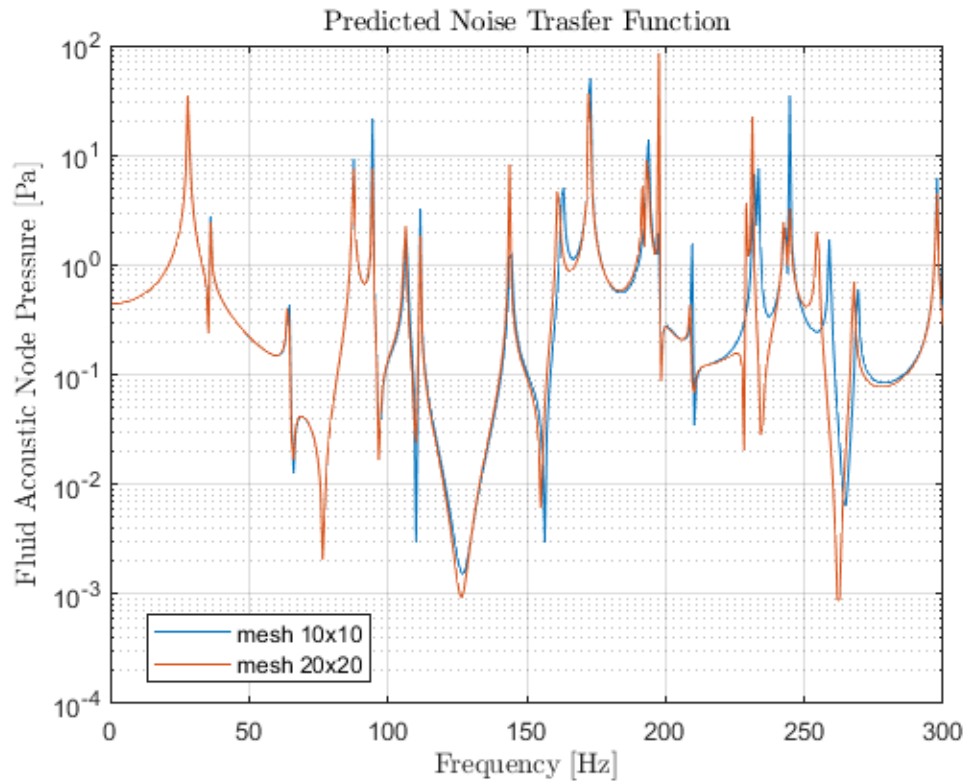


FIGURE 8.18: Fluid Node Pressure at B for *Orthotropic* plate **LW2** considering *Simply Supported* for **Air** filled cavity

As we expected, at **lower** frequency [0 – 200 Hz] within two solutions (mesh10 and mesh20), Nothing different may be noticed, thus the mesh10 (10x10 elements) solution is even better for the low computational effort; while in **higher** frequency range, mesh20 solution must be considered due to the high error for the previous one.

Water Cavity

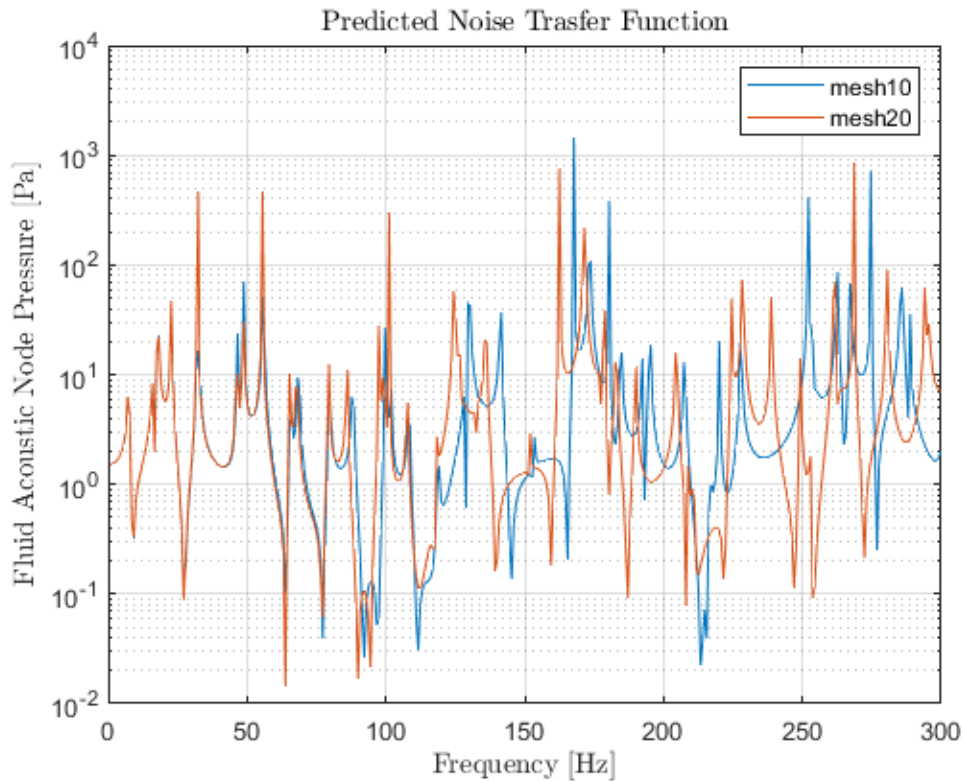


FIGURE 8.19: Fluid Node Pressure at B for *Orthotropic* plate **LW2** considering *Simply Supported* for **Air** filled cavity

Due to the **Strong coupling**, the difference (mesh10 e mesh20) starts at lower frequency (respect the weak coupling). In this case, at **lower** frequency [0 – 100 Hz] within two solutions (mesh10 and mesh20), Nothing different may be noticed, thus the mesh10 (10x10 elements) solution is even better for the low computational effort; but this range is even smaller, so the model may be validated for lower frequency, or in the same case, more elements (sharper mesh) are required to validate the solution at higher frequency.

8.5 Numerical Model Validation

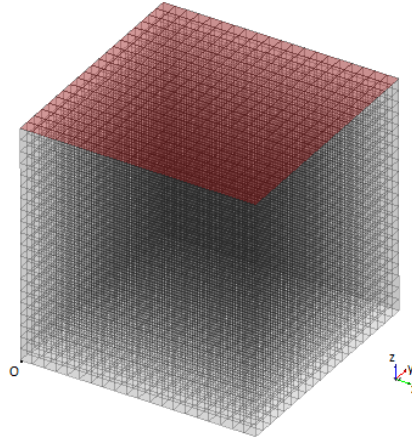
Previously, we have presented different numerical tests in both couplings comparing the MUL LW2 and Actran each other, but their solutions seem to be different and completely independent. In the following, we are going to **show** that *these solution are exactly the same*.

In fact, *Actran solution* is based on linear representation of structure deformation, essentially models based on Equivalent Single Layer (ESL). ESL gives sufficiently accurate global laminate response but they are inadequate, as seen in the previous chapter, at higher frequency.

On the other hand, *MUL2 solutions* are based on a more developed theory (LW); where the composite structure is thought as an different aggregate of independent layers, introducing much less error than the one introduced by ESL theories, originating upon the precise construction of a overall kinematic model of the entire layers within the thickness.

We might expect that the MUL2 result, based on its advanced theory, represent the correct solution and represent a limit solution towards which the actran itself tends to, under the same boundary condition.

As a sake of simplicity, we will deal with the most adverse example shown in chapter 7; so that Strong coupling (Water filled) with Cubic Orthotropic material plate.



In order to exhibit the correspondence between their solutions let us consider the following example.

The plate is composed by three layers $[0^\circ, 90^\circ, 0^\circ]$, whose following mechanical constants **Graphite-Epoxy**: $E_1 = 25.0 [GPa]$, $E_2 = E_3 = 1.0 [GPa]$, $G_{13} = G_{12} = 0.5 [GPa]$, $G_{23} = 0.2 [GPa]$ and $\nu_{13} = \nu_{12} = \nu_{23} = 0.25$.

We will keep the mesh used in MUL2 unchanged, fixed in 10x10.

In order to show our statement, we are going to modify the Mesh used to discretize the structure in Actran, to show that it represents a limit solution reached by Actran.

Firstly, **in Actran**, Let us use 10x10 mesh with quadratic interpolation for the fluid; while we keep 20x20 mesh linear for the representation of structure. We Obtain this

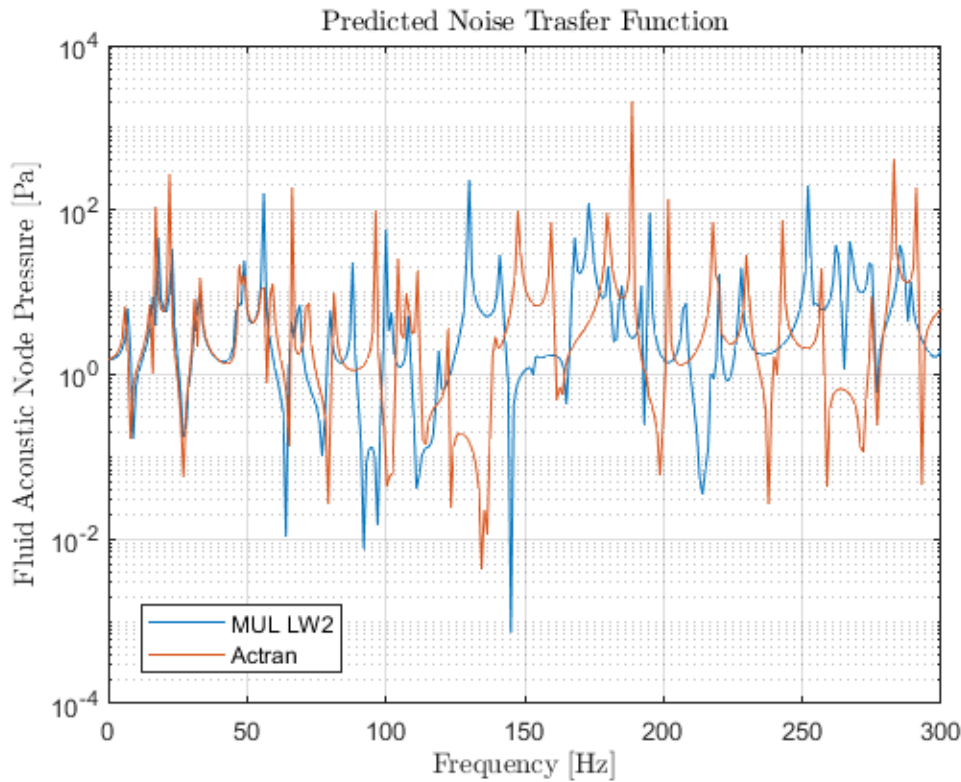


FIGURE 8.20: Test case: MUL2 LW2 vs 20x20 mesh structure in Actran

In the previous graph, a small part of the solutions are exactly the same, completely over position in the frequency 0 – 50 [Hz]; while in high frequency range, difference may be encountered, since in Actran the structural behaviour is poorer because the mutual interaction between acoustic and vibration activates a exciting mechanism through the structural displacement by sound waves and induces waves in the surrounding fluid. The numerical model of the problem should be able to handle this phenomenon in order to obtain reliable results, so a poor representation (as happens in Actran) can lead to rising errors, specially in high frequency range.

In order to avoid it, and to overcome these deficiencies in actran, let us highly increase **just** the structural mesh.

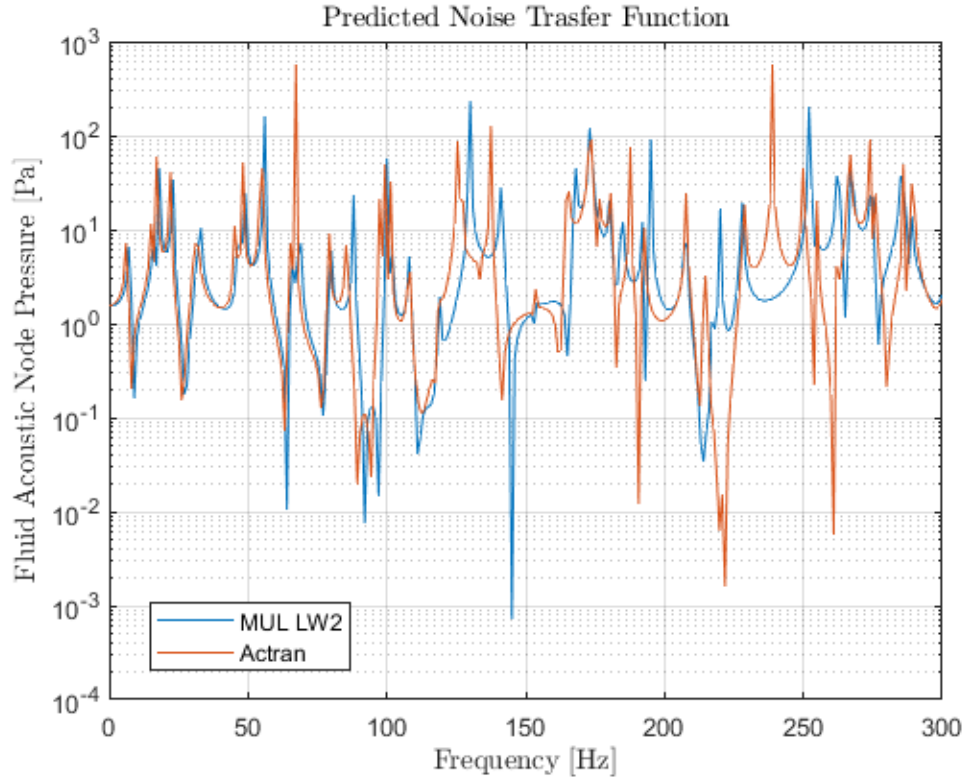


FIGURE 8.21: Test case: MUL2 LW2 vs 80x80 mesh structure in Actran

In Actran, We can verify the fact, that increasing the structural mesh, the solution tends over the MUL2 one, since its advance representation of the latter. The over position part (where the solutions are almost the same), increases in the frequency reaching 0 – 200 [Hz], just modifying the actran structural mesh without modifying the mul2 one, although the high adverse case (Strong coupling with Orthotropic plate).

We can extend our thought by reaching the whole frequency interval 0 – 300 [Hz] by increasing more and more the resultant mesh in Actran.

Finally, We have to highlight not just the fairness and the completeness of the MUL2 solution at fixed frequency; but MUL2 can also reach results, affected by less error, using larger dimension of the element. A good recovery in the solution is therefore reached, so the structural representation is more important than the surrounding fluid discretization. Behind these aspects, MUL2 program is a **very powerful** tool for representing the mean pressure value even at coarse mesh grid (as we seen Actran has more work to make).

Chapter 9

Conclusion and Further Developments

This final part sums up the whole research work.

Conclusions are drawn considering the achieved results and to conclude, some possible further developments are proposed in the field of fluid-structure coupling and vibroacoustics response.

9.0.1 Conclusion

The current work is focused on the development of advanced numerical procedure to predict vibroacoustic behavior (isotropic and orthotropic) structures.

A unified predicted model is needed to deeply explain the coupling between fluid/structure. Nowadays, we are constantly looking for new numerical tools which deal with fluid pressure in order to evaluate the surrounding noise.

The *objective of this work* aims at validate the MUL2 software, developed by MUL2 research group in the Polytechnic of Turin by comparing the results through commercial software, like Actran; and also we have also pointed out the powerful of the former.

The obtained results validate the model based CUF, that is their solution is comparable with Actran solution, but their behavior is also frequency dependant; indeed, for higher ranges of frequencies, this discrepancy is observed mainly in the case of Strong coupling, due to reduced wavelenght. This shows that the model based on the definition of Layer ways can take into account thickness effects that are not covered by Actran element method.

The differences become *larger* in the case of composite plate, mainly for the water-filled cavity where the coupling effects are more pronounced because the Actran solution is based on a general mixing of properties (*mesh-up properties*), resulting in overall average; while this difference may be considered negligible in the case of Isotropic material.

Layer ways model may predict the structural dynamic response of multi-layered composites which will influence the pressure level inside the cavity.

At the current state of the art, few works are available reporting a Layer ways (LW) methodology that considers all the relevant aspects for vibroacoustic - structural coupling behavior. In literature, most of research works are typically focused in numerical modelling more in Equivalent Single Layer (ESL). Conversely, the current research work considers the whole process required for a validation and reliable vibroacoustic coupling prediction: numerical modeling and comparison with available solution in currently literature about vibroacoustic structures. The innovative features of the presented work is the integration of CUF inside the discretization for the plate displacement.

On the other hand, few works are presented in literature that reports an extended model validation of both dynamic and acoustic numerical model throughout the coupling. This aspect has instead been considered fundamental in the current purpose alongside this dissertation. Reliability and Comparison are requirements for a numerical procedure to validate.

In this thesis, the FE dynamic (frequency dependant) model numerical correlation has been reported in terms of fluid node pressure, mode shapes and Frequency Response Function. In addition, different boundary conditions have been considered for the validation of the dynamic model.

9.0.2 Further Developments

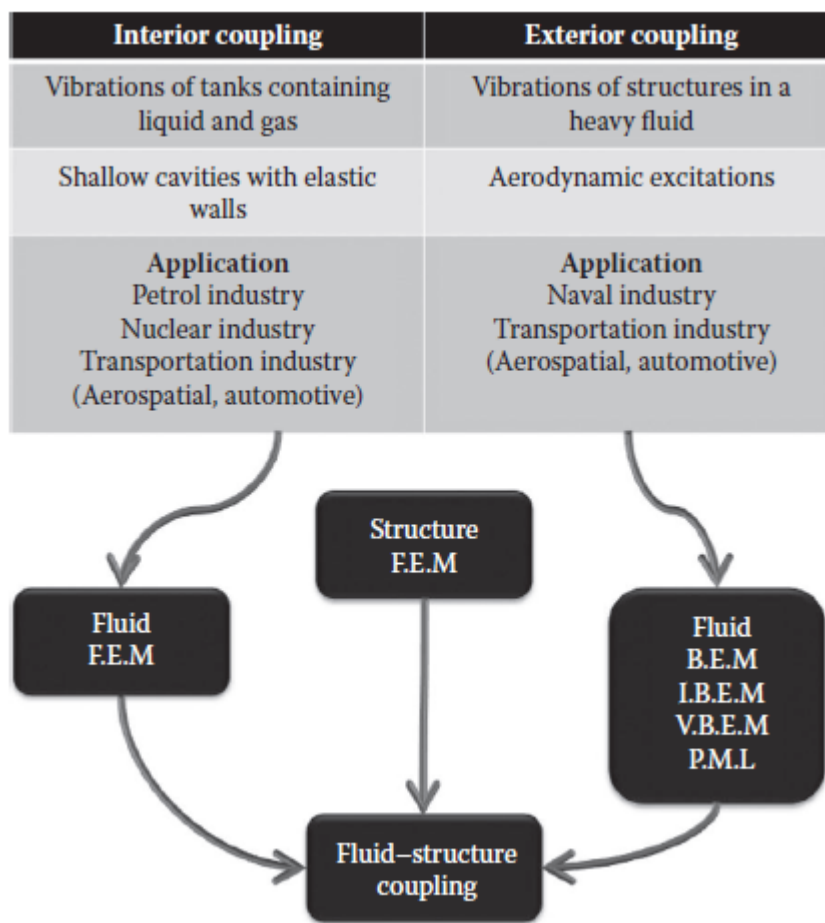
Different aspects need to be further investigated. The main purpose is to accurately represent the coupled interaction between the fluid and the structural behavior, whose possible developments are mainly related to the structure design parameter shape (like circle) and tuning in order to optimize the vibroacoustic performances, due to the high computational effort.

Furthermore, Vibroacoustic represent a frequency dependant problem; it is so useful to investigate the domain behavior in high frequency, reducing the high fitting meshes and enhances computational time, in the same way, thus combining the FE approach for the structural modeling with the efficient technique for the acoustic field, will surely obtain satisfactory results for the coupled problem.

It may be interesting also to extend of the numerically investigated frequency range to the ultra high frequency range, using suitable numerical techniques, to give a more complete acoustic characterization of the problem.

Finally, A constrained composite plate - rectangular cavity system was modeled and the lamination angles of the composite structure, assuming one *flexible wall* may be used to demonstrate the feasibility of reducing interior noise levels through optimal lamination angles of the superior plate, making an perfect tool for noise prediction within a chamber; these effects might not be ignored by any manufacturer and in general, automotive and aerospace designers place structural integrity higher up in priority than acoustic comfort.

In this case, we dealt an *Interior problem*, where the fluid domain is bounded within the cavity. The formulations used to solve the coupled problem are generally based on the finite element method (Advanced FEM) for both fluid and structure. A possible generalization is considering *Interior/exterior problems*, in which the structure couples two different fluid domains. The interior domain is bounded and the exterior one is unbounded; for instance the sound radiation of a structure coupled to an internal cavity and radiating in a heavy fluid, may represent a possible generalization



This represents the starting point for a large variety of problems in different fields.

Chapter 10

Matlab® Sources Used

To calculate the Frequency Response Function (FRF), we used the following Matlab® function that works with the files containing the solution for both MUL^2 and Actran in Matlab® tool, for the following elaboration. There we had the visualization of predicted Noise function and the displacement, where required, as are showed in this dissertation.

```
%% Data Acquisition Module

flag = 1; % 1 -> Pressure 0 -> Displacement
% Depending on the required Output
%

fid = fopen('C:\Users\Raf95\Downloads\INPUT_Air_LW2\DYNAMIC\POST_POINT_FREQ_01.dat ');
for i = 1:43
    fscanf(fid, '%s', [1 1]);
end

numDATA = fscanf(fid, '%f%f%f%f%f%f%f%f%f%f%f%f%f%f%f%f%f%f%f%f%f%f%f%f%f%f%f%f%f%f', [43 inf]);
fclose(fid);

figure(1)
frequency = numDATA(:,2);

if flag == 1
    pressure = abs(numDATA(:,end)); plotting = pressure;
else
    displacement = abs(numDATA(:,15)); plotting = displacement;
end
```

```

semilogy(frequency,plotting)
xlabel('Frequency [Hz]','interpreter','latex');

if flag == 1
    ylabel('Fluid Acoustic Node Pressure [Pa]','interpreter','latex');
    title('Predicted Noise Trasfer Function','interpreter','latex');
else
    ylabel('Structural Driving Point Displacement [m]','interpreter','latex');
    title('Predicted Structural Displacement Transfer Function','interpreter','latex');
end

grid on
hold on

%% Thickness Generator MUL2

clc; format longg
element = 1;
LW = 2;

%High
h = 1          % Cubic Cavity
h = 0.14       % Parallelepiped Cavity

% Thickness
t = 1.0e-2;    % Cubic Cavity
t = 1.5e-3;    % Parallelepiped Cavity

nodes = linspace(-t/2,t/2,LW*element+1);
node = h + nodes;          % senza Shift
node = h + t/2 + nodes;    % con Shift

% Thickness
t = 1.0e-2;    % Cubic Cavity
t = 1.5e-3;    % Parallelepiped Cavity

nodes = linspace(-t/2,t/2,LW*element+1);
node = h + nodes;          % senza Shift
node = h + t/2 + nodes;    % con Shift

length(nodes)
nodes
node

clear all
clc

```

```

Tool Connectivity 3D

fileID = fopen('results.dat','w');
for i=1:1e3
    fprintf(fileID,'%d%d%d%d%d%d%d%d%d%d%d%d%d%d%d%d%d%d 1\r\n',x(i,:));
end
fclose(fileID)

%%
% Thickness Variable Toolbox
%

clc; clear all;

Thickness
t_0 = 1.0e-2;    h = 1;           % Cubic Cavity
t_0 = 1.5e-3;    h = 0.14;        % Parallelepiped Cavity
caso = 1;

element = 1;
LW = 2;
t = 30*t_0;

nodes = linspace(-t/2,t/2,LW*element+1)
node = h + t/2 + nodes           % con Shift
(h+t/2)/10

%% Grafici di confronto con Actran - PARALLELEPIPEDO

load('C:\Users\Raf95\Downloads\Parallelepiped_Cavity\Parallelepiped_Actran.mat')
hold on
semilogy(f,spost_actran_par)

legend('MUL2 LW4','Actran')
title('Predicted Noise Trasfer Function - MUL2 LW4 vs Actran','interpreter','latex');

%% Grafici di confronto con Actran - Cubo con Aria

load('C:\Users\Raf95\Downloads\Cubic_Cavity\Actran_cub_air.mat')
hold on
semilogy(f,x_b)

legend('MUL2 LW4','Actran')
title('Predicted Noise Trasfer Function - MUL2 LW4 vs Actran','interpreter','latex');

%% Grafici di confronto con Actran - Cubo con Aria

load('C:\Users\Raf95\Downloads\Cubic_Cavity\Actran_cub_water.mat')
hold on
semilogy(f,x_b)

legend('MUL2 LW4','Actran')
title('Predicted Noise Trasfer Function - MUL2 LW4 vs Actran','interpreter','latex');

```


Chapter 11

Bibliography

- [1] *Alimonti*. Refined finite element structural models for the vibro-acoustic response of plate-cavity systems. Thesis.
- [2] *M. Cinefra, E. Zappino, E. Carrera and S. De Rosa*. Fully Coupled Vibro-acoustic analysis of multi-layered plates by CUF finite element. 3rd Euro-Mediterranean Conference on Structural Dynamics.
- [3] *R. Srinivasan Puri*. Krylov Subspace Based Direct Projection Techniques for Low Frequency, Fully Coupled, Structural Acoustic Analysis and Optimization.
- [4] *E. Carrera*. Multilayered shell theories that account for a layer-wise mixed description. part i. governing equations.
- [5] *N. Atalla and R.J. Bernhard*. Review of numerical solutions for low-frequency structural-acoustic problems. Applied Acoustics. Structural Acoustics and Vibrations.
- [6] *A. Benjeddou, J. F. De, and S. Letombe*. Free vibrations of simply-supported piezoelectric adaptive plates: an exact sandwich formulation. Thin-Walled Structures.
- [7] *C.H. Lin, and M.R. Jen*, Analysis of a laminated anisotropic plates By Chebyshev collocation method, Composites Part A e B: Engineering field.
- [8] *D. Zhou, Y.K. Cheung, S.H. Lo and F.T.K Au*, Three dimensional vibration analysis of rectangular thick plates on Pasternak foundation, International Journal for numerical methods in Engineering.
- [9] *A.J.M Ferreira and G.E. Fasshauer*, Analysis of natural frequencies of composite plates by an FRF-spectral method, Composite Structures.
- [10] *J. Thomas and B.A.H. Abbas*, Finite element model for dynamic analysis of composite plate, Journal of Sound and Vibration.
- [11] *M.A. Sprague and T.L. Geers*, Legendre spectral finite elements for structural dynamics analysis, Communications in numerical methods in engineering.
- [12] *S. B. Cokun, M. T. Atay and B. ztrk*, Transverse vibration analysis of plates using analytical approximate techniques, Advances in Vibration Analysis Research.
- [13] *A.W. Leissa*, The free vibration of rectangular plates, Journal of Sound and Vibration.
- [14] *S.M. Dickinson and E.K.H. Li*, On the use of simply supported plate functions in the Rayleigh-Ritz method applied to the vibration of rectangular plates, Journal of Sound and Vibration.

- [15] W.L. Li, X. Zhang, J. Du and Z. Liu, An exact series solution for the transverse vibration of rectangular plates with general elastic boundary supports, *Journal of Sound and Vibration*.
- [16] L. Dozio, On the use of the trigonometric Ritz method for general vibration analysis of rectangular Kirchhoff plates, *Thin-Walled Structures*.
- [17] R.F.S. Hearmon, The frequency of flexural vibration of rectangular orthotropic plates with clamped or supported edges, *Journal of Applied Mechanics*.
- [18] R.E. Rossi, D.V. Bambill and P.A.A. Laura, Vibrations of a rectangular orthotropic plate with a free edge a comparison of analytical and numerical results, *Ocean Eng.*
- [19] D.J. Gorman, Accurate free vibration analysis of clamped orthotropic plates by the method of superposition, *Journal of Sound and Vibration*.
- [20] D.J. Gorman, Accurate free vibration analysis of the completely free orthotropic rectangular plate by the method of superposition, *Journal of Sound and Vibration*.
- [21] D.J. Gorman and W. Ding, Accurate free vibration analysis of completely free symmetric cross-ply rectangular laminated plates, *Composite Structures*.
- [22] S. Yu and W. Cleghorn, Generic free vibration of orthotropic rectangular plates with clamped and simply supported edges, *Journal of Sound and Vibration*.
- [23] M. Dalaei and A.D. Kerr, Natural vibration analysis of clamped rectangular orthotropic plates, *Journal of Sound and Vibration*.
- [24] R.L. Ramkumar, P.C. Chen and W.J. Sanders, Free vibration solution for clamped orthotropic plates using Lagrangian multiplier technique, *Am Inst Aeronaut Astronaut*.
- [25] Sgard. Etude numérique du comportement vibro-acoustique d'un système plaque-cavité rayonnant dans un écoulement uniforme, pour différents types d'excitation.
- [26] Morand, H.J.-P. and R. Ohayon. *Fluid Structure Interaction*. Chichester, UK: Wiley-Blackwell.
- [27] Lesueur, C. *Rayonnement Acoustique Des Structures Vibroacoustique, Interactions Fluide-Structure*. 1st ed. Direction des études et recherches d'Electricité de France.
- [28] C. Dym and M. Lang. Transmission of sound through sandwich panels. *Journal of acoustical society of America*, vol. 56.
- [29] Erasmo Carrera and Salvatore Brischetto. Analysis of thickness locking in classical, refined and mixed multilayered plate theories. *Composite Structures*.
- [30] Tianjian Lu, Fengxian Xin. *Vibro-Acoustics of Lightweight Sandwich Structures*. Science Press Beijing. Springer Tracts in Mechanical Engineering.
- [31] Xin FX, Lu TJ, Chen CQ. Sound transmission through simply supported finite panel within enclosed air cavity. *J Vib Acoust*.
- [32] Yin XW, Gu XJ, Cui HF et al. Acoustic radiation from a laminated composite plate reinforced. *Journal of Sound Vibration*.
- [33] S. Brischetto, E. Carrera and L. Demasi. Improved bending analysis of sandwich plates using a zig-zag function. *Composite Structures*.
- [34] F. Fahy, *Sound and structural vibration*, Academic Press, 1985.